DYNAMICS OF ALLOSTERIC REGULATION OF THE PHOSPHOLIPASE C-γ ISOZYMES

Edhriz Siraliev-Perez

A dissertation submitted to the faculty at the University of North Carolina at Chapel Hill in partial fulfillment of the requirements for the degree of Doctor of Philosophy in the Department of Biochemistry and Biophysics.

Chapel Hill
2020

Approved by:

Saskia B. Neher

James E. Bear

Andrew L. Lee

Charles Carter Jr.

Brian A. Kuhlman

ABSTRACT

Edhriz Siraliev-Perez: DYNAMICS OF ALLOSTERIC REGULATION OF THE PHOSPHOLIPASE C-γ ISOZYMES
(Under the direction of John Sondek)

The phospholipase C (PLC)-γ isozymes (-γ1 and -γ2) are activated by phosphorylation downstream of numerous tyrosine kinases including receptor tyrosine kinases for growth factors. Once phosphorylated, PLC-γ isozymes catalyze the hydrolysis of the membrane phospholipid, phosphatidylinositol 4,5-bisphosphate (PIP_2) into the second messengers 1,2-diacyglycerol (DAG) and inositol 1,4,5-trisphosphate (IP_3). The regulated activation of this signaling pathway controls diverse biological processes including vasculature, chemotaxis, and immunity. Conversely, aberrant PLC-γ isozyme signaling leads to human diseases including cancer and immune disorders. The work presented in this dissertation describes a protocol for the quantification of PLC activity *in vitro*, the crystal structure of autoinhibited PLC-γ1, and a model of allosteric control of PLC-γ isozyme activation based on hydrogen deuterium exchange coupled to mass spectrometry (HDX-MS).

First, we developed a protocol for the quantification of PLC activity *in vitro* using a fluorogenic substrate that partitions into membranes. This assay permits the continuous monitoring of PLC activity at a pH of 7.4 ± 0.2 and at a concentration of free calcium of approximately 400 nM. This assay can be modified to include small molecules, peptides, and effectors.

Second, we describe the crystal structure of PLC-γ1 in the autoinhibited state. The structure illustrates the arrangement of the regulatory domains relative to the catalytic core

to form two interfaces that effectively block access to the active site. Simultaneously, the regulatory domains are arranged to integrate inputs from adaptor and signaling proteins.

Finally, the dynamics of PLC-γ isozyme activation were assessed with a 1:1 complex of PLC-γ1 bound to phosphorylated kinase domain of the fibroblast growth factor receptor 1 (FGFR1K). According to HDX-MS, binding of PLC-γ1 to the kinase causes widespread changes in deuterium incorporation that suggest a loosening of the interfaces between the regulatory domains and the catalytic core. These results suggest that kinase engagement shifts the dynamic equilibrium of PLC-γ isozymes from an autoinhibited conformation to a more active conformation. In addition, oncogenic substitution of PLC-γ1 mimics the effects of kinase engagement and uncovers functional cooperativity of kinases and lipid bilayers.

This work is dedicated to my parents, who instilled in me the importance of education, responsibility, and dedication.

ACKNOWLEDGEMENTS

First, I want to acknowledge our funding sources. The laboratory was consistently funded by the National Institutes of Health and I was personally funded by a Graduate Research Fellowship from the National Science Foundation. Continued funding for scientific research is essential for the training of aspiring scientists like me.

Next, I must thank John Sondek for accepting me in his laboratory and guiding me in the process of scientific inquire. One of the most memorable lessons from John was the difference between work that is done for the sake of completion versus work completed with the highest respect, detail, and quality. I aim to keep this lesson with me for the rest of my professional career.

I want to express my gratitude to Nicole N. Hajicek. Her hard-work, and pristine work ethic motivated me in the darkest of moments. Likewise, I want to praise the rest of the laboratory members in the Sondek lab and our faithful collaborators in the laboratory of Qisheng Zhang for their feedback and scientific expertise. In addition, my dissertation project provided new avenues to establish collaboration with the laboratory of John Burke at the University of Victoria in Canada. I am grateful for their willingness and timeliness.

Finally, I want to acknowledge the unconditional love and support from family and friends including my parents, Aida L. Perez-Ramos and Ismael A. Siraliev-Jimenez, as well as Dillon O. Smith, J. Felix Olivares, Raquel Martinez, and Hayden Dawes.

Thank you.

PREFACE

The work presented in this dissertation were completed in collaboration with other scientists. Chapter 2 represents a book chapter written in collaboration with Adam J. Carr. This work outlines a protocol to measure phospholipase C isozyme activity using lipid vesicles and a fluorogenic substrate. My contributions to this work are the expression and purification of all PLC-γ1 variants used in the study, and the experiments shown in Fig. 1. Adam J. Carr performed the experiments shown in Fig. 2-3 and Weigang Huang provided the fluorogenic substrate. John E. Sondek and Qisheng Zhang were responsible for conceptualization and supervision. This book chapter was accepted in *Methods in Molecular Biology* but is yet to be published at the time of this writing. The work has the following citation:

Carr, A. J., Siraliev-Perez, E., Huang, W., Sondek, J., Zhang, Q. (2020) Measurement of phospholipase C activity in lipid vesicles using the fluorogenic reporter XY-69. *Methods in Molecular Biology.* (In press)

Permission to include the article in its entirety in a Ph.D. dissertation was retained from Springer Nature Group (publisher of *Methods in Molecular Biology*) as explained at https://www.springer.com/authors/book+authors/helpdesk?SGWID=0-1723113-12-799504-0.

Chapter 3 represents work led by Nicole N. Hajicek. My contributions to this work are the expression and purification of all PLC-γ1 variants, and the experiments shown in Fig. 3b and 7b-c. Nicholas C. Keith performed *in cell* activity assays, Brenda R. S. Temple performed and analyzed molecular dynamic simulations, Weigang Huang provided the fluorogenic substrate. Qisheng Zhang, T. Kendall Harden, and John Sondek were

responsible for conceptualization and supervision. All authors contributed to the writing of the manuscript. This work is published with the following citation:

Hajicek, N., Keith, N., Siraliev-Perez, E., Temple, B. R. S., Huang, W,, Zhang, Q., Harden, T. K., Sondek, J. (2019) Structural basis for the activation of PLC-γ isozymes by phosphorylation and cancer-associated mutations. *eLife* 2019;8:e51700 (10.7554/eLife.51700)

Permission to include the article in its entirety in a PhD dissertation was retained from eLife Sciences Publications Ltd. (publisher of *eLife*) as explained at https://elifesciences.org/terms

Chapter 4 is the bulk of my dissertation project. This work was done in collaboration with the laboratory of John E. Burke at the University of Victoria, Canada. My contributions to this work are the expression and purification of all PLC-γ1 and FGFR1K variants, *in vitro* phosphorylation of the kinase, formation and validation of the protein complex, as well as all biochemical experiments preceding the HDX-MS experiments. In addition, I was responsible for formal data analysis, figures, writing, and editing the manuscript. The HDX-MS experiments were conducted by Reece Hoffmann. Jordan Stariha completed preliminary analysis and Qisheng Zhang provided fluorogenic substrate for activity assays. John E. Burke and John Sondek were responsible for conceptualization and supervision. A version of this chapter was submitted as an article for publication in *Journal of Biological Chemistry* with the following citation:

Siraliev-Perez, E., Hoffman, R., Stariha, J., Zhang, Q., Hajicek, N., Burke, J., and Sondek, J. (2020) “Dynamics of allosteric regulation of the PLC-γ isozymes”

All copyrighted material included in this dissertation is used with permission from the relevant copyright holders.

TABLE OF CONTENTS

LIST OF FIGURES xi

LIST OF ABBREVIATIONS xiii

CHAPTER I: PHOSPHOLIPASE C-γ ISOZYME SIGNALING 1

Cell signaling 1

PLC isozyme signaling 1

PLC isozyme domain architecture 2

PLC-γ isozymes 6

PLC-γ isozymes in normal physiology 13

PLC-γ isozymes in human diseases 16

Concluding remarks 22

References 30

CHAPTER II: FLUOROGENIC XY-69 TO MEASURE PLC ACTIVTIY[1] 39

Background 39

Materials 41

Methods 43

References 53

CHAPTER III: STRUCTURAL BASIS FOR ACTIVATION OF PLC-γ ISOZYMES[2] 56

Background 56

Materials and Methods 60

Results 71

Discussion 80

References 100

CHAPTER IV: ALLOSTERIC REGULATION OF THE PLC-γ ISOZYMES[3] 109

Background 109

Materials and Methods 112

Results 120

Discussion 129

References 145

CHAPTER V: CONCLUSIONS AND FUTURE DIRECTIONS 148

Conclusions 148

Future directions 149

References 152

LIST OF FIGURES

Figure 1.1 – The thirteen mammalian phospholipase C (PLC) isozymes 23

Figure 1.2 – General and versatile activation of the PLC isozymes 24

Figure 1.3 – Structure of PLC-δ1 highlights conserved domain architecture 25

Figure 1.4 – Isozyme-specific modes of activation 26

Figure 1.5 – Additional regulatory domains in the PLC-γ isozymes 27

Figure 1.6 – Crystal structure of PLC-γ1 28

Figure 1.7 – PLC-γ isozymes as gatekeepers of health and disease 29

Figure 2.1 – Effects of pH and free Ca^{2+} concentration on XY-69 hydrolysis 50

Figure 2.2 – Phospholipase activity of PLC-γ1 (D1165H) in lipid vesicles 51

Figure 2.3 – Size of lipid vesicle affects the relative rate of XY-69 hydrolysis 52

Figure 3.1 – Crystal structure of autoinhibited PLC-γ1 83

Figure 3.2 – Primary sequence alignment of PLC-γ isozymes 84

Figure 3.3 – Crystallographic-grade PLC-γ1(21-1215) Δ25 is fully autoinhibited 85

Figure 3.4 – Surface of autoinhibited PLC-γ1 is electronegative 86

Figure 3.5 – Structural comparisons of autoinhibited PLC-γ1 and fragments 87

Figure 3.6 – The regulatory domains are organized to integrate multiple inputs 88

Figure 3.7 – Interfacial regulation of purified forms of PLC-γ1 89

Figure 3.8 – The regulatory domains of PLC-γ1 are dynamic in aMD simulations 90

Figure 3.9 – Activated forms of PLC-γ1 have highly mobile regulatory domains 91

Figure 3.10 – Substitutions of PLC-γ1 analyzed in aMD simulations 92

Figure 3.11 – Point mutations in the cSH2 domain recapitulate dynamics 93

Figure 3.12 – Substitutions of PLC-γ1 found in cancers activate the enzyme 94

Figure 3.13 – Constitutive activation of PLC-γ2 in cancers 95

Figure 3.14 – Oncogenic substitutions within the SH3 domain activate PLC-γ1 96

Figure 3.15 – Oncogenic substitutions prime PLC-γ1 for activation by EGFR 97

Figure 3.16 – Model for phosphorylation-induced activation of PLC-γ1 98

Figure 3.17 – Proposed mechanism for priming of PLC-γ1 by FGFR1 99

Figure 4.1 – PLC-γ1 forms a stable complex with phosphorylated FGFR1K 132

Figure 4.2 – PLC-γ1 (H335A) is catalytically inactive and binds liposomes 133

Figure 4.3 – FGFR1K is phosphorylated only on Tyr766 134

Figure 4.4 – PLC-γ1 and phosphorylated FGFR1K form stable complexes 135

Figure 4.5 – FGFR1K potentially disrupts autoinhibition 136

Figure 4.6 – FGFR1K and liposomes act independently 137

Figure 4.7 – Priming of PLC-γ1 by FGFR1K 138

Figure 4.8 – Oncogenic substitution of PLC-γ1 mimics kinase engagement 139

Figure 4.9 – Oncogenic substitution uncovers functional cooperativity 140

Figure 4.10 – FGFR1K and liposomes affect the deuterium exchange 141

Figure 4.11 – Functional cooperativity in PLC-γ1 (D1165H) 142

Figure 4.12 – Phosphorylated FGFR1K increases PLC-γ1 specific activity 143

Figure 4.13 – Dynamical activation of PLC-γ1 144

LIST OF ABBREVIATIONS

A	Alanine
Å	angstrom (1Å = $1x10^{-10}$ meters)
AD	Alzheimer's disease
aMD	accelerated molecular dynamics
ApoE	apolipoprotein E
ATL	adult T cell leukemia/lymphoma
ATP	adenosine triphosphate
BCR	B-cell antigen receptor
BSA	bovine serum albumin
BTK	Bruton's tyrosine kinase
C2	calcium binding domain
Ca^{2+}	calcium ion
$CaCl_2$	calcium chloride
cAMP	cyclic adenosine monophosphate
Cbl	Casitas B-lineage lymphoma
CD3	cluster of differentiation 3
CD79	cluster of differentiation 79
CLL	chronic lymphocytic leukemia
cMD	conventional molecular dynamics
CHAPS	3-[(3-cholamidopropyl)dimethylammonio]-1-propanesulfonate
CHAPSO	3-[(3-cholamidopropyl)dimethylammonio]-2-hydroxy-1-propanesulfonate
$CHCl_3$	Chloroform
cSH2	C-terminal SH2
CTCL	cutaneous T cell lymphoma

C-terminal	carboxy-terminus
CV	column volume
Cys	Cysteine
D	aspartic acid
DABCYL	4-(dimethylaminoazo)benzene-4-carboxylic
DAG	1,2-diacylglycerol
DLS	dynamic light scattering
DNA	deoxyribonucleic acid
DTT	1,4-dithiothreitol
E	glutamic acid
Ed	average dihedral energy
EDTA	ethylenediamine tetra-acetic acid
EF hand	calcium binding domain
EGF	epidermal growth factor
EGFR	EGF receptor
EGTA	ethylene glycol tetra-acetic acid
Ep	total potential energy
ER	endoplasmic reticulum
ERK	extracellular signal-regulated kinase
F	Phenylalanine
F_c	fragment crystallizable region
FAF BSA	fatty acid-free bovine serum albumin
FGFR	fibroblast growth factor receptor
FGFR1K	kinase domain of FGFR1
FGFR2K	kinase domain of FGFR2

FITC	fluorescein isothiocyanate
G	Glycine
$GdCl_3$	gadolinium chloride
Glu	glutamic acid
Gly	Glycine
GPCR	G protein coupled receptor
GTPase	guanosine triphosphatase
H	Histidine
H_2O	Water
HA	Hemagglutinin
HDX-MS	hydrogen deuterium exchange-mass spectrometry
HEK293	human embryonic kidney 293 cell line
HEPES	4-(2-hydroxyethyl)piperazine-1-ethanesulfonic acid
His	Histidine
HPLC	high performance liquid chromatography
I	Isoleucine
IMAC	immobilized metal affinity chromatography
IP_3	inositol 1,4,5-trisphosphate
IPTG	isopropyl β-D-1-thiogalactopyranoside
K	Lysine
KCl	potassium chloride
K_d	dissociation constant, binding affinity
kDa	Kilodalton
L	Leucine
LAT	linker for activation of T cells

LC	liquid chromatography
LiCl	lithium chloride
LVAB	lipid vesicle assay buffer
LVS	lipid vesicle solution
Lys	Lysine
M	Methionine
MD	molecular dynamics
MeOH	methanol
$MgCl_2$	magnesium chloride
MS/MS	tandem mass spectrometry
MWCO	molecular weight cut-off
N	Asparagine
N_2	Nitrogen
Na^+	sodium ion
NaOH	sodium hydroxide
NFAT	nuclear factor of activated T-cells
NF-κB	nuclear factor kappa-light-chain-enhancer of activated B cells
NGF	nerve growth factor
NMR	nuclear magnetic resonance
nSH2	N-terminal SH2
N-terminus	amino-terminus
OD_{600}	optical density at 600 nm
P	Proline
PAGE	polyacrylamide gel electrophoresis
PCR	polymerase chain reaction

PDB	protein data bank
PE	phosphatidylinositol ethanolamine
PEG	poly (ethylene glycol)
PES	polyether sulfone
pH	power of hydrogen
PH	pleckstrin homology
PIP_2	phosphatidylinositol 4,5-bisphosphate
PIP_3	phosphatidylinositol 3,4,5-trisphosphate
PKC	protein kinase C
PLC	phospholipase C
PLCDB	PLC dilution buffer
pTyr	phosphorylated tyrosine, phosphotyrosine
Q	Glutamine
R	Arginine
RMSD	root mean square deviation
RMSF	root mean square fluctuation
RTK	receptor tyrosine kinase
S	Serine
SAD	single-wavelength anomalous diffraction
SAXS	small-angle X-ray scattering
SDS-PAGE	sodium dodecyl sulfate-polyacrylamide gel electrophoresis
SEC-MALS	size exclusion chromatography-multiple angle light scattering
SEM	standard error of the mean
Ser	Serine
SH2	Src homology 2

SH3	Src homology 3
SLP-76	SH2 domain-containing leukocyte protein of 76kDa
sPH	split pleckstrin homology
Src	sarcoma viral oncogene homologue
Syk	spleen tyrosine kinase
TB	terrific broth medium
TCR	T-cell antigen receptor
TEV	tobacco etch virus protease
TIM	triosephosphate isomerase
TREM2	triggering receptor expression on myeloid cell-2
Trk	tropomyosin receptor kinase
Tyr	Tyrosine
UV	Ultraviolet
V	Valine
VEGF	vascular endothelial growth factor
W	Tryptophan
WT	wild type
Y	Tyrosine
z_{av}	z-average particle size

CHAPTER I: PHOSPHOLIPASE C-γ ISOZYME SIGNALING

Cell signaling

Cells maintain homeostasis by responding to numerous extracellular signals. These signals bind and activate cell-surface receptors to elicit intracellular responses. The conglomerate of proteins that receive, interpret, and relay this information is known as a signaling pathway or axis. In addition, signaling pathways amplify the incoming signal and modulate the time and duration of the response. A key step in the amplification of a signal is the creation of second messengers (1). One such example is the formation of 1,2-diacylglycerol (DAG) and inositol 1,4,5-trisphosphate (IP_3) produced from the hydrolysis of phosphatidylinositol 4,5-bisphosphate (PIP_2) by phospholipase C (PLC) isozymes (2).

PLC isozyme signaling

A multitude of extracellular signals including neurotransmitters, hormones, and growth factors stimulate the activation of the thirteen mammalian PLC isozymes (3). These isozymes are divided into six subgroups (-β, -γ, -δ, -ε, -ζ, -η) based on sequence similarity and share a conserved catalytic core (Fig. 1.1) (4). Upon release of autoinhibition, all PLC isozymes hydrolyze the minor membrane phospholipid PIP_2 at the inner leaflet of the plasma membrane. Hydrolysis of the phosphodiester bond between the inositol head group and the glycerol backbone generates the second messengers DAG and IP_3. DAG remains at the inner leaflet of the plasma membrane and activates conventional protein kinase C (PKC) isozymes while IP_3 diffuses throughout the cytosol and binds IP_3 receptors to liberate calcium ions sequestered inside the endoplasmic reticulum (Fig. 1.2) (2, 3, 4).

In addition, the consumption of PIP_2 modulates the function of membrane proteins including ion channels and phosphoinositide-binding proteins (3, 4). This bifurcated signaling axis initiates and amplifies numerous biological processes including cell division, differentiation, and migration (2, 3, 4).

PLC isozyme domain architecture

The structure of the ancestral homolog PLC-δ1 highlights the conserved domain architecture shared among all PLC isozymes, which consists of an N-terminal pleckstrin homology (PH) domain, two pairs of EF hands, a catalytic triosephosphate isomerase (TIM) barrel, and a C-terminal C2 domain (Fig. 1.3A) (5). The following subsections aim to briefly describe the structure and function of these domains.

PH domain

PH domains were first described in pleckstrin, a protein in platelets, and later found in a wide variety of proteins including kinases, small G protein regulators, and cytoskeletal proteins (6, 7). The domain is approximately 120 residues and comprised of perpendicular β strands centered between a C-terminal amphipathic α helix and three unstructured loops of varying length and amino acid composition at the amino terminus (4, 7).

Typically, PH domains bind membrane-embedded phosphoinositides with high affinity (low μM to nM range) (8) and high specificity thus enabling the recruitment of cytosolic proteins to membranes, cellular compartments, and signaling hubs. For example, structural and biochemical studies have shown that the PH domain of PLC-δ1 preferentially binds to PIP_2 with high affinity (~1μM) (9) and is responsible for membrane recruitment of full-length PLC-δ1 (Fig. 1.4A) (10). Interestingly, the residues responsible for coordinating the inositol head group are not conserved among the PLC isozymes suggesting that the N-terminal PH domain is not functionally redundant. In fact, the PH

domain of PLC-β isozymes do not bind phosphoinositides, instead it binds Rac isozymes in the GTP-bound form (4). This high affinity interaction (K_d = 5-10 μM for PLC-β2 and >25 μM for PLC-β3) (11) is proposed to stabilize PLC-β isozymes at the membrane after recruitment by G proteins (Fig. 4, center). A similar scenario is present in PLC-γ1 where the PH domain is proposed to bind PIP_3 instead of PIP_2 (4) although the crystal structure of essentially full-length PLC-γ1 contradicts this idea (12).

EF hands

Most EF hands are calcium-binding motifs comprised of two α helices, helix E and helix F, connected through an unstructured loop (13). Conserved acidic residues within these loops bind calcium ions with high affinity eliciting structural changes first described in parvalbumin (14). There is little evidence to suggest calcium-dependent activation or regulation of the PLC isozymes mediated through their EF hands. This notion is further supported by the structures of several PLCs. The structure of PLC-δ1 highlights a lack of electron density in the loop regions of the EF hands, suggesting that the loops are highly mobile (5). Moreover, there is no calcium bound in the structures of PLC-δ1 (5), PLC-β2 (15), PLC-β3 (16), or PLC-γ1 (12). However, a new function of the EF hands was highlighted by the structure of active PLC-β3 in complex with $G\alpha_q$. The structure describes an insertion of eight amino acids between the third and fourth EF hands that have GTPase activating protein (GAP) function (16). This insertion is unique in the PLC-β isozymes and robustly stimulate hydrolysis of GTP by the $G\alpha_q$ subunit. Hydrolysis of GTP results in the simultaneous shut-off of $G\alpha_q$ signaling and alters the dynamics of PLC-β signaling (17).

C2 domain

The C-terminal C2 domain is a β-sandwich consisting of eight antiparallel β strands that are capped by three loops (18). Together, the loops form calcium binding sites that,

upon binding, elicit conformational changes of the loops. Generally, these conformational changes are described as jaws that open in the presence of calcium ions (19). In PLC-δ1, residues responsible for calcium binding are required for plasma membrane association (20). This mechanism of membrane recruitment has not been proved for PLC-β2 and PLC-γ1. Another putative function of the C2 domain is maintenance of structural integrity of the catalytic core. This idea is supported by the structures of PLC-δ1 (5, 19), PLC-β2 (16), and PLC-γ1 (12) where the C2 domain is tightly packed against the catalytic TIM barrel.

TIM barrel

The TIM barrel is the most common protein fold found in nature (21). This fold consists of eight β strands and α helices that form a cylinder where numerous and biologically unrelated chemical reactions are catalyzed (21). In the PLC isozymes, the TIM barrel constitutes the active site where hydrolysis of membrane-bound PIP_2 is catalyzed (Fig. 1.3B) (3). Of note, the TIM barrel is split into two halves, the X and Y boxes, by a linker of varying length known as the X-Y linker (4).

The structure of PLC-δ1 illustrates the organization of the TIM barrel and describes a mechanism for the hydrolysis of PIP_2 (5). The active site is formed as a solvent-accessible cavity with several residues responsible for ligation of the substrate, coordination of the essential calcium cofactor, and orientation of the nucleophile (Fig. 1.3D). First, substrate binding is achieved by an extensive network of hydrogen bonds between the side chains of Lys438, Lys440, Ser522, and Arg549 with the 4' and 5' phosphorylated hydroxyl groups of the inositol head group. In addition, the aromatic ring of Tyr551 forms numerous van der Waals contacts with the parallel inositol ring. Second, hydrolysis of PIP_2 requires a calcium cofactor that is ligated by surrounding acidic residues Asn312, Glu341, Asp343, and Glu390.

Finally, hydrolysis of PIP_2 follows a general acid-base catalysis where the 2'-hydroxyl group of the inositol group is deprotonated by a general base (Glu341). The 2'-hydroxyl group then carries out a nucleophilic attack on the 1'-phosphate leading to the formation of DAG and a cyclic intermediate that is stabilized by His311 and the calcium ion. Subsequently, His356 coordinates an incoming water molecule that carries out a nucleophilic attack on the cyclic intermediate thus forming IP_3. Mutation of any of the residues involved in substrate binding, calcium coordination, or catalysis, lead to a spectrum of catalytically-deficient enzymes as measured by hydrolysis of [^{3}H]-PIP_2 embedded in phospholipid vesicles (22). These residues are strictly conserved across all PLCs indicating that the mechanism for substrate hydrolysis is conserved.

The PLC isozymes are basally cytosolic whereas their substrate, PIP_2 is membrane bound. Therefore, access to PIP_2 requires membrane association and partial insertion of the TIM barrel into lipid bilayers This is attained by a ridge of hydrophobic residues (Leu320, Tyr358, Phe360, Leu529, and Trp555 in PLC-δ1) that surround the active site (Fig. 1.3C). These residues are highly conserved across all PLCs and their orientation is the same in the structures of PLC-β2 and PLC-β3. Alanine substitutions of these bulky nonpolar residues decreased PIP_2 hydrolysis only in the context of phospholipid vesicles (22).

X-Y linker

As mentioned above, the catalytic TIM barrel is bisected by a linker of varying length known as the X-Y linker. In most PLCs the X-Y linker basally autoinhibits phospholipase activity and its removal leads to a significant increase in phospholipase activity both *in vitro* and in cells (4). The chemical and physical properties of the X-Y linker diverge across PLCs and thus, engender unique regulatory mechanisms to individual isozymes (Fig. 1.4A-C, lower panels).

The PLC-δ isozymes share a negatively charged linker that precludes membrane association via electrostatic repulsion (Fig. 1.4A). The crystal structure of PLC-δ1 highlights a lack of electron density in this region suggesting that the linker is disordered and highly mobile (5). The X-Y linker of the PLC-β isozymes is also negatively charged and largely unstructured except at the C-terminus where a single α helix physically occludes access to the active site (Fig. 1.4B) (16, 23). In contrast, the PLC-ζ possess a positively-charged linker that associates with membranes and drives elevation of phospholipase activity (5). Finally, the PLC-γ isozymes are unique as the X-Y linker contains an array of additional regulatory domains poised to basally autoinhibit phospholipase activity and to simultaneously bind additional scaffolding proteins (Fig. 1.4C) (12, 24). The PLC-γ isozymes are the focus of this dissertation and are discussed in more detail in the following sections.

PLC-γ isozymes

The PLC-γ isozymes, PLC-γ1 and PLC-γ2, are unique among the PLCs in that they are directly activated by tyrosine phosphorylation and possess an array of additional regulatory domains comprised of a split PH domain (sPH), an N-terminal SH2 (nSH2) domain, a C-terminal (cSH2) domain, and an SH3 domain (3) (Fig. 1.5). The following section describes how these regulatory domains mediate autoinhibition, and the interplay between phosphorylation-dependent activation and the scaffolding properties of the regulatory domains. Next, a mechanistic model of PLC-γ isozyme activation is proposed.

Autoinhibition

The array of additional regulatory domains unique to the PLC-γ isozymes autoinhibit phospholipase activity as removal of the entire array leads to a robust increase in PLC-γ1 activity (24). Subsequent systematic deletion of the regulatory domains

implicated the cSH2 domain as the major determinant mediating autoinhibition of phospholipase activity since removal or mutation of this domain also leads to a robust elevation of PLC-γ isozyme activity *in vitro* and in cells (24).

The crystal structure of the isolated cSH2 of PLC-γ1 describes a patch of positively charged residues that comprise the BG and EF loops (25) suggesting that the cSH2 domain may mediate autoinhibition through interactions with a complementary surface within PLC-γ1 of negative charge. Consequently, charge swap mutations within the catalytic core resulted in an increase in phospholipase activity suggesting that disruption of interactions between the cSH2 domain and the catalytic core release autoinhibition (25). In fact, the isolated cSH2 domain binds with approximately 0.36μM binding affinity to a peptide encompassing phosphorylated Tyr783 (pY783) of PLC-γ1 (24). A crystal structure of the isolated cSH2 domain bound to this peptide illustrates that the peptide-binding surface is the same electropositive surface that mediates autoinhibition (25). Together, these data suggest that autoinhibitory contacts between the cSH2 domain and the catalytic core are disrupted by binding of phosphorylated tyrosines of PLC-γ1 to the cSH2 domain.

The recent crystal structure of essentially full-length PLC-γ1 provides a premier look into two major interfaces that position the regulatory domains on top of the catalytic core to mediate autoinhibition (Fig. 1.6) (12). One interface is formed by the cSH2 domain and the catalytic core. Specifically, the structure illustrates how the BG and EF loops of the cSH2 domain clasp prominent turns of the C2 domain of the catalytic core (Fig. 1.6D). Importantly, these turns serve as anchor points to membranes in PLC-δ1, where calcium ions mediate interaction with negatively-charged membranes and the C2 domain (20) (Fig. 1.3A-B). The second interface is formed between the sPH domain which lies directly on top of the catalytic TIM barrel (Fig. 1.6C). Here, residues of the sPH domain interdigitate

with residues of the hydrophobic ridge thus sterically occluding access to the active site. Although these interfaces do not overlap, a C-terminal portion of the SH3 domain supports and maintains the cSH2 and sPH domain together.

Prior to the advent of the crystal structure of PLC-γ1, Bunney et al. described a structure of PLC-γ1 using small-angle X-ray scattering (SAXS) (26). The model describes the regulatory domains in a completely different arrangement relative to the crystal structure. The authors propose that the sPH and cSH2 domain occupy the central volume of the SAXS envelope with the nSH2 and SH3 domains occupying flanking positions. This arrangement of the regulatory domains would require a different mode of autoinhibition as the sPH domain does not contact the TIM barrel implicating only the cSH2 domain in mediating autoinhibition.

Phosphorylation-dependent activation

The activation of the PLC-γ isozymes requires phosphorylation of tyrosine residues within the regulatory domains. Several classes of tyrosine kinases phosphorylate and activate PLC-γ isozymes including both soluble and receptor tyrosine kinases (RTKs) (2, 4). Depending on the cell context, the PLC-γ isozymes are activated by soluble kinases coupled to immune receptors as well as by receptors for fibroblast growth factor (FGF), epidermal growth factor (EGF), platelet-derived growth factor (PDGF), and nerve growth factor (NGF) (3).

Activation of PLC-γ isozymes downstream of RTKs is initiated in the presence of an extracellular stimuli. The receptors dimerize and autophosphorylate tyrosine residues C-terminal to the kinase domain, e.g. Tyr766 in FGFR1 (27). These phosphorylated tyrosines serve as docking sites for the nSH2 domain within the regulatory domains to recruit PLC-γ isozymes from the cytosol to membranes (28). Subsequently, active kinases phosphorylate tyrosine residues within the regulatory domains of PLC-γ isozymes

including positions 186, 472, 481, 771, 775, 783, 959, 977, and 1254 (29, 30). Of these, only Tyr775 and Tyr783 are conserved in PLC-γ2 (equivalent positions Tyr753 and Tyr759) (3). Additional tyrosines in PLC-γ2 (positions 1197 and 1217) are also phosphorylated and implicated in regulation although these sites are not conserved in PLC-γ1 (31).

Phosphorylation of Tyr783 in PLC-γ1 is required for phosphorylation-dependent elevation of phospholipase activity (32). This model is further supported by biochemical studies in which Tyr783 was mutated to phenylalanine. This PLC-γ1 variant had a reduction in total phosphorylation and is refractory to kinase-stimulated elevation of phospholipase activity (24). Phosphorylation of Tyr775 in PLC-γ1 has also been shown to be essential for PLC-γ isozyme activation downstream of the B-cell receptor (30) and RTKs (32). Surprisingly, mutation of Tyr775 in PLC-γ1 did not substantially affect total phosphorylation or kinase-stimulated activity with purified components (24). The non-essential function of Tyr775 is further supported by mutation of this site along with six other tyrosines, which did not affect phospholipase activation and appear to be dispensable for FGF-dependent stimulation of endothelial cells (26).

Dual phosphorylation of Tyr775 and Tyr783 in PLC-γ1 and the equivalent positions in PLC-γ2 are required downstream of soluble tyrosine kinases associated to immune receptors (30). How dual phosphorylation drives elevation of phospholipase activity in this context remains to be understood. However, binding affinity experiments with the isolated cSH2 domain of PLC-γ1 and peptides encompassing phosphorylated tyrosines revealed that phosphorylation of Tyr775 decreased binding affinity of pY783 toward the cSH2 domain suggesting that phosphorylation at this site may modulate the magnitude of activation upon binding of pY783 to the cSH2 domain (24).

Scaffolding properties of the regulatory domains

The regulatory domains confer unique properties for the regulated activation of the PLC-γ isozymes. First, the sPH domain binds the small GTPase Rac2 (33). This is supported by a nuclear magnetic resonance (NMR) structure of the sPH domain of PLC-γ2 bound to active Rac2 (34). Subsequent biochemical studies showed that this interaction elevates PLC-γ2 activity in cells and with purified components. This interaction is thought to stabilize the active ensemble of membrane-bound PLC-γ2 instead of disrupting the overall structure of autoinhibited PLC-γ2.

Adjacent to the sPH domain are two SH2 domains in tandem, the nSH2 and the cSH2 domains. The nSH2 domain is required for binding to active tyrosine kinases (28) and binds with high affinity (K_d = 0.40μM) to a peptide encompassing phosphorylated Tyr769 of FGFR2 (24). The role of the nSH2 domain as the site for association with active tyrosine kinases is further supported by a structure of the tandem SH2 domains in complex with the kinase domain of FGFR1 (FGFR1K) (35). In this structure, phosphorylated Tyr766 (pY766) of FGFR1K is bound to the nSH2 domain – not the cSH2 domain. However, this study also shows that isolated cSH2 domain can bind phosphorylated FGFR1K albeit with approximately 15-fold lower binding affinity than the isolated nSH2 domain. The authors also describe a secondary binding site outside of the canonical phosphotyrosine (pTyr)-binding pocket of the nSH2 domain. Residues within this secondary binding site are implicated in binding FGFR1K as mutation of these residues decreased binding affinity approximately 4-fold.

Although the pTyr-binding pocket of the cSH2 domain is buried in the structure of PLC-γ1, the isolated cSH2 domain binds with nanomolar affinity to a peptide encompassing phosphorylated Tyr783 (pY783) of PLC-γ1 (24). As mentioned above, a crystal structure of the isolated cSH2 domain bound to this peptide (25) illustrates that the

pTyr-binding surface of the cSH2 domain is the same surface that clasps prominent turns of the C2 domain in full-length PLC-γ1 (12). Together, these data suggest that autoinhibition is disrupted, in part, by the intramolecular interactions between phosphorylated tyrosines of PLC-γ1, e.g. Tyr783, and the cSH2 domain.

The SH2 domains may work in concert upon engagement of kinases to facilitate intramolecular interactions between pY783 of PLC-γ1 to the cSH2 domain. This idea is supported by comparison of the structure of full-length PLC-γ1 (12) to the aforementioned structure of the tandemSH2 domain bound to phosphorylated FGFR1K (35). This comparison illustrates that the βA/αA loop of the nSH2 domain is rearranged to accommodate pY766 of FGFR1K and that this rearrangement leads to additional movements of the cSH2 domain. If true, equivalent movements in full-length PLC-γ1 would partially expose the pTyr-binding surface of the cSH2 domain, thus priming the cSH2 domain to accept phosphorylated tyrosines, e.g. pY783. Engagement of pY783 by the cSH2 domain is presumed to disrupt interactions between the cSH2 domain and the C2 domain of the catalytic core to initiate rearrangements of the regulatory domains relative to the catalytic core effectively releasing autoinhibition.

A competing model for the roles of the SH2 domains in PLC-γ isozymes was proposed by Huang et al. (36). This study postulates that the cSH2 domain – not the nSH2 domain – is responsible for association with tyrosine kinases downstream of a panel of growth factors. Moreover, the study shows that mutation of the cSH2 domain is sufficient to abrogate binding to the phosphorylated kinase domain of FGFR2. The study also describes a crystal structure of the isolated cSH2 domain of PLC-γ1 bound to two kinase domains of FGFR2. The authors suggest that this interaction is biologically relevant and propose that one kinase is responsible for recruiting PLC-γ isozymes to signaling hubs whereas a second kinase phosphorylates PLC-γ1. In contrast, in the structure of PLC-γ1,

the nSH2 has unfettered access to the solvent whereas the pTyr-binding surface of the cSH2 domain is buried and contacts prominent turns of the C2 domain, effectively mediating autoinhibition (12).

The array of regulatory domains is completed by an SH3 domain. Typical SH3 domains engage various proteins via the canonical polyproline binding site (37). In the PLC-γ isozymes, the SH3 domain serves as a scaffolding module that engages proteins of T cell signaling including Vav1 (38) and SH2 domain-containing leukocyte protein of 76kDa (SLP-76) (39). A comparison of the unbound structure of the isolated SH3 domain of PLC-γ1 and this domain bound to a peptide encompassing SLP-76 reveals that several residues within the SH3 domain shift toward SLP-76 to optimize shape complementarity and hydrophobic contacts (40).

Model of activation

The biochemical and structural studies described above evoke a mechanism for the regulated activation for the PLC-γ isozymes. The model posits that the regulatory domains sit atop the highly conserved catalytic core to prevent the core from accessing membranes and spuriously hydrolyzing PIP_2. Moreover, the regulatory domains are poised to integrate numerous inputs that control phospholipase activity and serve as scaffolding modules for adaptor proteins.

In general, PLC-γ isozyme activation is initiated by an extracellular signal that activate cell-surface receptors, e.g. RTKs. These receptors recruit PLC-γ isozymes via interaction with the nSH2 domain which is optimally arranged to engage phosphorylated kinases. This interaction brings PLC-γ isozymes in close vicinity to kinases and other adaptor proteins that consequently promote the phosphorylation of tyrosine residues within the regulatory domains of PLC-γ1, e.g. Tyr783. These phosphorylated tyrosines bind to the cSH2 domain and unlatch the cSH2 domain from the C2 domain in the catalytic

core. Presumably, this interaction initiates an ill-defined rearrangement of the regulatory domains relative to the catalytic core. Consequently, the TIM barrel inserts into lipid bilayers to hydrolyze the membrane-embedded PIP_2.

Understanding the arrangement of the regulatory domains in active PLC-γ isozymes will provide mechanistic details into their regulated activation. The dissertation research presented here aims to fill this gap by quantifying deuterium incorporation in PLC-γ1 in three different states: bound to phosphorylated FGFR1K, in the presence of PIP_2-containing liposomes, and with both, kinase and liposomes. The studies also include a constitutively active variant, PLC-γ1 (D1165H), to describe the effect of oncogenic substitution on the structure of PLC-γ isozymes. This information will be useful during drug discovery efforts that aim to target aberrant PLC-γ isozyme signaling in human diseases.

PLC-γ isozymes in normal physiology

PLC-γ1 plays a pivotal role in many physiological processes due to its ubiquitous expression (2, 3). In contrast, PLC-γ2 is primarily expressed in cells of the hematopoietic system indicative of its role in immunity (3). This section seeks to provide a brief overview of the diverse physiological processes that the PLC-γ isozymes mediate (Fig. 1.7). Many of the cited studies use genetically modified organisms with conventional or conditional knock-outs, as well as knocking-in mutant forms of PLC-γ isozymes and their regulators.

Vascular development

Vasculogenesis is the formation of new blood vessels and occurs throughout embryonic development and adulthood (41). Mouse embryos lacking PLC-γ1 fail to grow and die approximately 9 days after fertilization due to an impairment in endothelial cell maturation and in the formation of blood vessels (42). A similar phenotype is observed in mutant zebrafish with impaired PLC-γ1 function. These embryos displayed defects in the

formation of arteries, but not veins (43). Consistent with these observations, PLC-γ1 is directly activated by vascular endothelial growth factor (VEGF) further implicating PLC-γ1 in the proper development of a mature vascular system (44).

Brain development and function

PLC-γ1 is highly expressed in the brain and is reported to be critical in many neurological processes (45). For example, PLC-γ1 is a known substrate of the Trk family of tyrosine kinases, which are activated by neurotrophins such as NGF (46). *In vivo* studies with mice carrying mutant forms of TrkB with impaired PLC-γ1 binding, fail to activate calcium/calmodulin-dependent kinase IV and cyclic adenosine monophosphate (cAMP) response element-binding protein thus abolishing transcriptional regulation necessary for memory consolidation (47). Similar mutations that impair binding of adaptor proteins and PLC-γ1 to TrkB were shown to abrogate formation of the cerebral cortex in developing mice (48). PLC-γ1 is also activated by members of the fibroblast growth factor receptor family during development (49). Blockage of PLC-γ1 recruitment by this receptor abolished neurite outgrowth (50). Moreover, the overexpression of PLC-γ1 in the rat ventral tegmental area of the midbrain led to changes in reward behavior and locomotor activity (51, 52) suggesting that PLC-γ1 is involved in physiological and behavioral functions including pain perception, mood, and motor control.

Immunity

The growth and proliferation of T cells requires the activation of PLC-γ1 downstream of the T-cell antigen receptor (TCR) (53). The TCR is a large complex of several signaling proteins that includes two TCR chains, typically α and β chains, that are associated with cluster of differentiation 3 (CD3). The TCR is completed by a couple of accessory molecules known as the ζ-chains. Importantly, CD3 and the ζ-chains possess

conserved sequences known as immunoreceptor tyrosine-based activation motifs (ITAM) (54). These tyrosine residues are phosphorylated by Src tyrosine kinases, e.g. lymphocyte-specific protein tyrosine kinase (Lck) and serve as docking sites for other kinases that activate adaptor proteins. One such example is linker for activation of T cell (LAT) that harbors docking sites for PLC-γ1 (55). In this context, phosphorylation of PLC-γ1 leads to the activation of three transcriptional pathways, NF-κB, Ras-ERK, and nuclear factor of activated T-cells (NFAT), that are necessary for the maturation and proper function of T cells (56). These signaling pathways have been investigated with transgenic mice harboring LAT mutations that eliminate PLC-γ1 binding. Mutation of LAT led to partial blockage of early T cell development with a polyclonal lymphoproliferative disorder and signs of autoimmune disease (57). Subsequent studies suggested that this phenotype is due to severe defects in positive and negative thymocyte selection (58).

B cells possess a parallel mechanism in which PLC-γ2 is activated downstream of the B-cell antigen receptor (BCR) (59). The BCR is associated with cluster of differentiation (CD79) which has ITAMs that recruit and activate soluble kinases, e.g. Bruton's tyrosine kinase (BTK), that phosphorylate PLC-γ2 (31). The generation of second messengers by PLC-γ2 mediate the activation of transcriptional reprogramming necessary for B cell maturation. This notion is supported by studies with PLC-γ2-null mice. These mice have several deficiencies in B cell development concurrent with a decrease in mature B cells in the bone marrow and spleen (60). Moreover, these cells had poor proliferative response upon BCR and F_c receptor stimulation. Together, these results illustrate that both PLC-γ1 and PLC-γ2 are necessary for the proper function of the immune system and mounting of an immune response.

Cell migration

The PLC-γ isozymes regulate various types of cell migration. For example, knock-down or knock-out of PLC-γ1 in mouse fibroblasts resulted in failed formation of cellular protrusions, spreading, and elongation in response to integrin engagement (61). Moreover, this same study identified β1 integrin, adaptor proteins, and Src kinases as key players in the activation of PLC-γ1 and the concomitant accumulation of intracellular calcium. Another study implicated PLC-γ2 in integrin-mediated adhesion and migration of B cells (62). Specifically, stimulation of murine and human B cells with stromal cell-derived factor 1 or chemokine ligand 13 caused integrin-mediated B cell migration downstream of BTK and PLC-γ2. In the same vein, *in vivo* studies revealed that immature B cells lacking BTK had impaired homing in lymphoid organs (62). These results indicate that both PLC-γ1 and PLC-γ2 mediate integrin-mediated migration downstream of tyrosine kinases.

PLC-γ1 is also required in growth factor-dependent cell migration. For example, Asokan et al. (63) showed that migration of mesenchymal cells required the selective inactivation of myosin IIA by PKCα and that activation of PKCα was achieved by an intracellular gradient of DAG produced and maintained by PLC-γ1.

PLC-γ isozymes in human diseases

The PLC-γ isozymes have recently emerged as causative of several human diseases, including cancers and immune disorders. The following section briefly describes how PLC-γ isozymes drive these malignancies (Fig. 1.7).

Cancers

PLC-γ isozymes are directly activated by numerous growth factors receptors that promote the growth and proliferation of cells. It is therefore expected that PLC-γ isozyme

activity contributes to the aberrant growth of cells characteristic of cancers. For example, overexpression of PLC-γ1 has been identified in breast (64, 65), prostate (65), and colon (66, 67) cancers. Direct evidence that PLC-γ isozymes promote cancer was found in glioblastoma where pharmacological inhibition of PLC-γ1 led to a decrease in glioma cell motility and invasion into brain aggregates in a fetal rat model (68). Studies have also implicated PLC-γ1 in angiosarcoma. Specifically, a single substitution (R707Q) within the cSH2 domain provoked resistance to apoptosis concurrent with an increase in migration and invasion of endothelial cells in *in vitro* assays (69). Together, these studies suggest that inhibition of PLC-γ1 may serve as an anti-invasive therapy in both glioblastoma and angiosarcoma.

With the advent of genome-wide sequencing, studies have identified acquired mutations in both PLC-γ1 and PLC-γ2 in a variety of immunoproliferative malignancies. Notably, single substitutions have been identified in human subjects with cutaneous T cell lymphoma (CTCL) (70), chronic lymphocytic leukemia (CLL) (71), and adult T-cell leukemia/lymphoma (ATL) (72).

Approximately 20% of patients with cutaneous T cell lymphoma (CTCL) possess missense mutations of PLC-γ1 including mutations within the TIM barrel (S345F) and the sPH domain (S520F) (70). Notably, both mutations are within the interface between the catalytic core and the regulatory domains of PLC-γ1 and are predicted to disrupt autoinhibitory contacts and elevate phospholipase activity to enhance TCR signaling. This prediction is further supported by the S345F mutation which was described in patients diagnosed with peripheral T cell lymphomas (PTCLs), a group of heterogeneous lymphomas characterized by chronic TCR signaling (73).

Variants of PLC-γ2 were found in approximately 30% of patients with relapsed CLL after treatment with ibrutinib, a covalent inhibitor of BTK (71). Mutation of PLC-γ2, a major

substrate for BTK, is likely the result of selective pressure by the inhibitor and may function as escape mutations to reactive the signaling pathways that control B cell survival and proliferation. This idea is demonstrated by the expression of mutant forms of PLC-γ2 in B cells, including R665W and L845F (74). These cells are unable to reestablish calcium homeostasis after BCR engagement compared to cells expressing wild-type enzyme and that quickly return to basal levels of intracellular calcium. Together, these results suggest that these mutations do not release autoinhibition; instead, the mutations maintain phospholipase activity subsequent to phosphorylation by BTK.

PLC-γ1 is also mutated in approximately 40% of patients with adult T cell leukemia/lymphoma (ATL) with a multitude of single nucleotide variants decorating the entire primary sequence of the protein (72). Mapping these substitutions onto the three-dimensional structure of PLC-γ1 reveals that most of the substitutions localize to the interface between the catalytic core and the regulatory domains. The overexpression of these substitutions in HEK293 cells led to the accumulation of intracellular inositol species indicative of high phospholipase activity (12). In fact, some of the substitutions had approximately 1,500-fold greater activity compared to wild-type PLC-γ1. The analogous substitutions also increased phospholipase activity in PLC-γ2. In contrast, mutations outside of the interface between the catalytic core and the regulatory domain are thought to have more nuanced and context-specific effects such as increased association with membranes and/or tyrosine kinases. This idea has not been tested directly.

Together, the examples discussed above demonstrate that most cancer-associated mutations disrupt PLC isozyme autoinhibition and elevate catalytic activity. The aberrant activation of PLC-γ isozymes culminates with the upregulation of the transcriptional programs that signal immune cells to proliferate and thus lead to disease.

Immune disorders

The relationship between germline mutations in PLC-γ2 and immune disorders was established via large-scale mutagenesis screens with mice. A study identified a gain-of-function substitution (D993G) in PLC-γ2 that resulted in severe autoinflammation characterized by morphological changes associated with arthritis including inflammatory infiltrates in the paws and growth retardation (75). At the molecular level, murine B cells had an increase in extracellular calcium entry and expansion of inflammatory cells. Another study identified PLC-γ2 (Y495C) which resulted in an abnormal level of murine B and T cells, and an increase in antibodies (76). Subsequent studies showed that PLC-γ2-null mice were protected from inflammation and bone erosion in a model of arthritis via the downregulation of inflammatory cell spreading and degranulation (77).

More evidence that PLC-γ2 mediates immune function was found in a cohort of 27 human patients with manifestations of immune deficiency characterized by a decrease in immunoglobulins as well as an increase in autoinflammation (78). Genome sequencing studies identified germline deletions of portions of the cSH2 and SH3 domains that led to increased phospholipase activity. Paradoxically, these mutations led to a decrease in intracellular calcium and in natural killer cell degranulation suggesting that hyperactive PLC-γ2 supports inhibitory feedback loops through the depletion of PIP_2 pools (79). Another study identified two patients with a single substitution (S707Y) within the cSH2 domain. These individuals had chronic autoinflammation characterized by an increase in phosphorylated ERK (80). Subsequent structural studies suggested that this mutation also disrupts autoinhibitory contacts between the catalytic core and the regulatory domains (26).

Neurological disorders

As mentioned previously, PLC-γ1 mediates physiological processes necessary for proper brain development and function. Consequently, PLC-γ1 has been implicated in several neurological pathologies including epilepsy as well as Huntington's and Alzheimer's disease (81)

Huntington's disease is a neurodegenerative disease associated with mutant forms of the huntingtin protein (82). Mouse models of this disease have low levels of phosphorylated PLC-γ1 (83) in addition to decreased expression of TrkB and the agonist, brain-derived neurotrophic factor (84), which are necessary for long-term potentiation in the hippocampus suggesting that downregulation of this pathway may lead to neurodegeneration characteristic of the disease. Moreover, mutant forms of TrkB that lack PLC-γ1-binding sites impair hippocampal long-term potentiation in mice similar to those induced by mutant huntingtin protein (85) supporting a correlation between disease progression and PLC-γ1.

Another example that highlights the importance of PLC-γ1 in neurological disorders is found in epilepsy. This disease is characterized by uncontrollable jerking movements (seizures) of the limbs that stem from a disruption in the normal excitation and inhibition patterns of neuronal cells (86). Excessive excitation of the TrkB has been implicated in prolonged seizures suggesting that this receptor is a plausible target for the treatment of epilepsy (87). Recent studies have shown that genetic (88) or pharmacological (89) inhibition of TrkB reduced PLC-γ1 activation and chemoconsulvant-induced seizures suggesting that inhibition of this signaling axis may benefit in patients with epilepsy.

Alzheimer's disease (AD) is a neurodegenerative disease characterized by the accumulation of amyloid plaques (90). Genetic susceptibility studies associated variants of apolipoprotein E (ApoE) with increased risk in developing AD (90). Recent susceptibility

studies identified polymorphisms in triggering receptor expression on myeloid cell-2 (TREM2), a cell-surface receptor expressed in non-neuronal cells including microglia, that is activated by ApoE and amyloid plaques (90). Activation of TREM2 recruits the tyrosine kinase Syk, which subsequently phosphorylates PLC-γ2 and the concomitant mobilization of intracellular calcium required for the liberation of inflammatory cytokines (90). Notably, a naturally-occurring and moderately active variant of PLC-γ2 (PLC-γ2 P522R) has been associated with neuroprotective phenotype in AD (91). Expression of PLC-γ2 P522R co-localizes with TREM2 and with amyloid plaques in microglial cells (91). How this single substitution within the loop that connects the sPH and the nSH2 domain is protective against AD remains to be described. Regardless, these results suggest that a small molecule that activates PLC-γ2 activity may be beneficial to treat this disease.

Concluding remarks

The PLC-γ isozymes are important signaling proteins downstream of a multitude of soluble and receptor tyrosine kinases that control diverse physiological processes. The activity of these enzymes has been directly linked to many human diseases including cancers and immune disorders. Therefore, it is essential to understand the mechanistic underpinnings of PLC-γ isozyme activation. The primary focus of this dissertation was to describe the regulation of PLC-γ isozymes using a combination of biochemistry and biophysical techniques. Chapter two describes a methodology to assess PLC activity at membranes. Chapter three describes the crystal structure of essentially full-length PLC-γ1 in detail and posits a model on how phosphorylation and cancer-associated mutations disrupt autoinhibition. Chapter four represents the bulk of my graduate work examining the dynamics of PLC-γ1 activation by kinases and membranes.

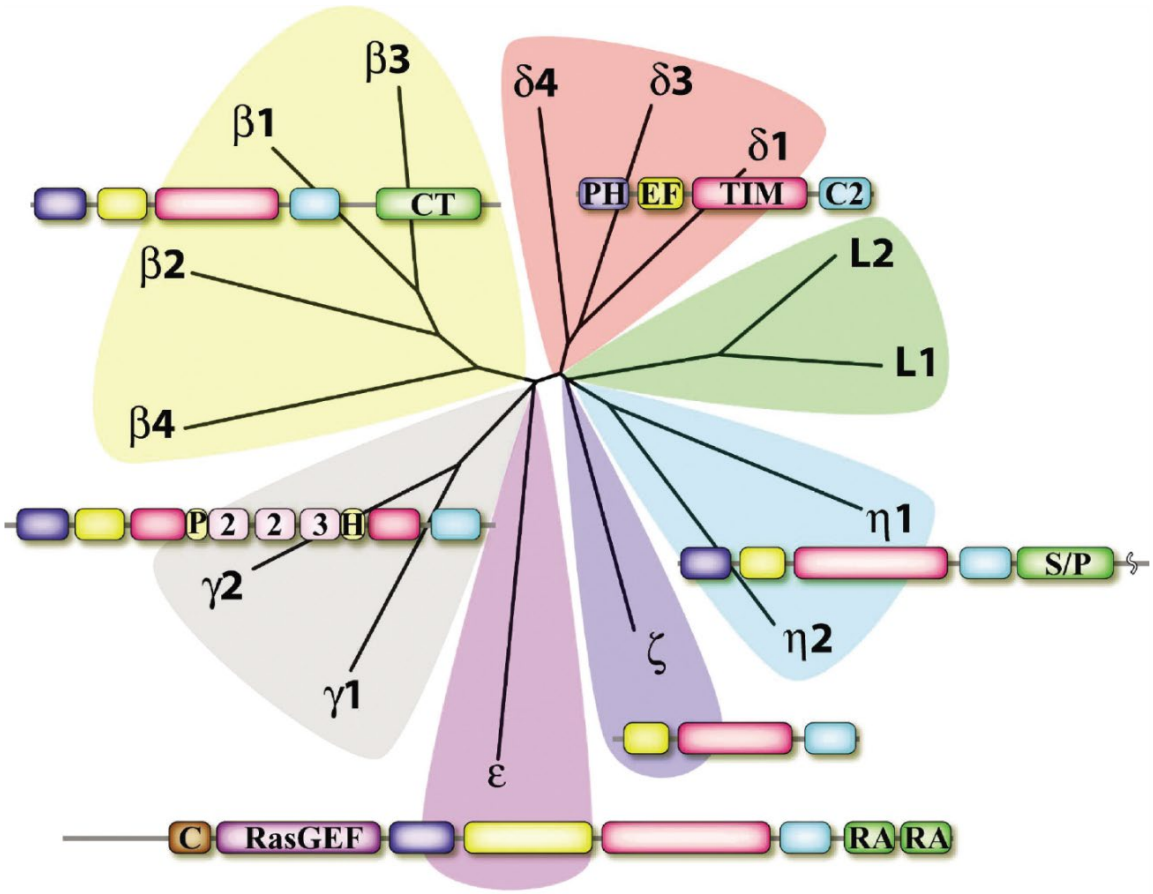

Harden TK, Sondek J. 2006.
Annu. Rev. Pharmacol. Toxicol. 46:355–79

Figure 1.1 – The thirteen mammalian phospholipase C (PLC) isozymes. The human genome encodes thirteen phospholipase C (PLC) isozymes that are grouped into six groups (-β, -γ, -δ, -ε, -ζ, -η) based on sequence similarity. The ancestral PLC-δ isozymes illustrate the conserved catalytic core shared among all PLCs, which consist of an N-terminal PH domain (purple), four pairs of EF hands (yellow), a catalytic triosephosphate isomerase (TIM) barrel (red), and a C-terminal C2 domain (blue). The rest of the PLC isozymes contain additional domains. For example, the PLC-β isozymes possess a C-terminal tail (CT), while PLC-ε has guanine nucleotide exchange factor (RasGEF) activity as well as two Ras-associating (RA) domains. The PLC-γ isozymes are unique as they possess an array of additional regulatory domains including a split pleckstrin homology domain, two Src-homology 2 (SH2) domain, and an SH3 domain.

Figure reprinted from Harden, T. K., and Sondek, J. (2006) Regulation of phospholipase C isozymes by Ras superfamily GTPases. *Annu. Rev. Pharmacol. Toxicol.* **46**, 355-79 (10.1146/annurev.pharmtox.46.120604.141223) © 2006, Annual Reviews; used with permission

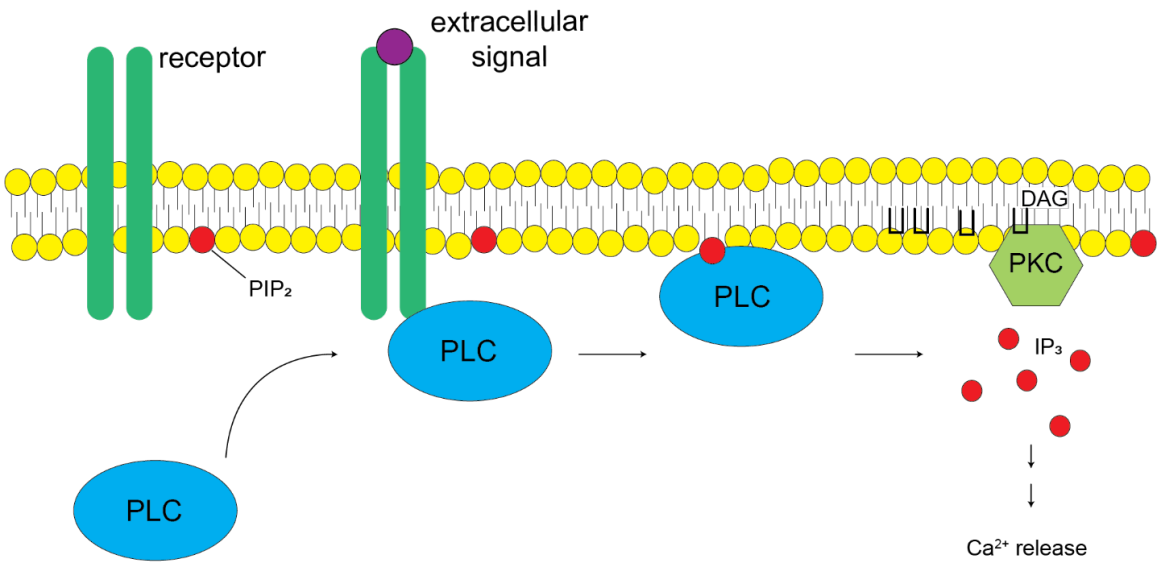

Figure 1.2 – General and versatile activation of the PLC isozymes. The majority of the mammalian PLC isozymes are basally autoinhibited. In the presence of an extracellular signal, cell-surface receptors recruit PLC isozymes from the cytosol to signaling hubs. Release of autoinhibition allows binding to membrane-embedded substrate phosphatidylinositol 4,5-bisphopshate (PIP_2). Hydrolysis of the phosphodiester bond between the inositol head group and the glycerol backbone generates the second messengers 1,2-diacylglycerol (DAG) and inositol 1,4,5-trisphoshate (IP_3). DAG remains at the membrane and activates protein kinase C (PKC) isozymes whereas IP_3 diffuses throughout the cytosol to elicit the release of intracellular calcium (Ca^{2+}) stores. This signaling pathway is required for the control of diverse biological processes.

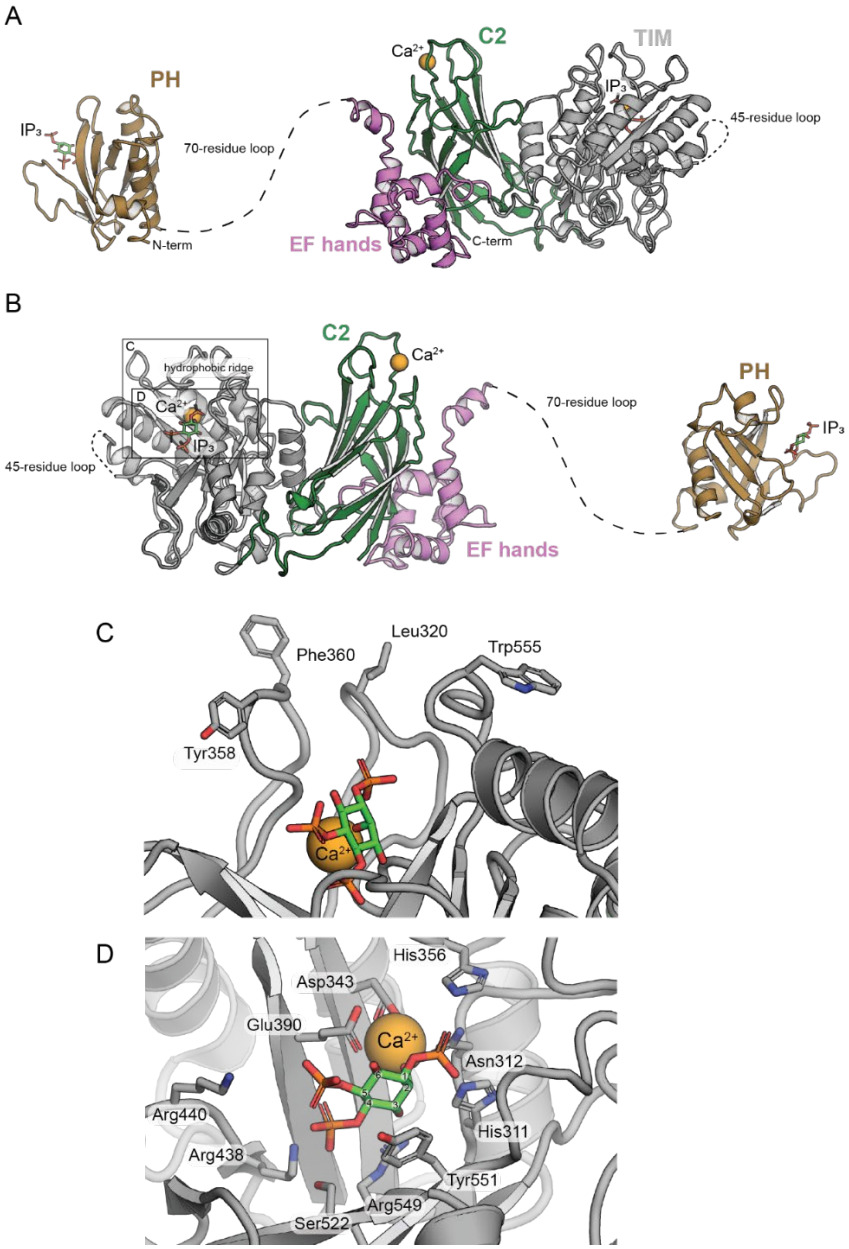

Figure 1.3 – Structure of PLC-δ1 highlights conserved domain architecture. A, Crystal structure the PLC-δ1. The N-terminal PH domain (sand, PDB ID: 1MAI) is connected to the rest of the protein via a 70-residue loop. The rest of the catalytic core (PDB ID: 1DJX) consists of an two pairs of EF hands (magenta), a catalytic triosephosphate isomerase (TIM) barrel (gray), and a C-terminal C2 domain (green). The autoinhibitory loop of 45 residues is absent from the crystal structure and depicted with a dashed line. The PH domain and the TIM barrel are bound to inositol 1,4,5-trisphohate (IP_3) shown in sticks. **B**, Same arrangement as in **A** rotated 180° to illustrate the active site cavity and hydrophobic ridge. Active site is denoted by a calcium (Ca^{2+}) ion (orange sphere) and IP_3 shown as sticks. **C**, Hydrophobic residues that line the cavity of the active site are shown as sticks. Calcium (Ca^{2+}) ion is depicted as an orange sphere and bound IP_3 shown as sticks. **D**, Residues necessary for coordination of the calcium (Ca^{2+}) ion (orange sphere), binding of IP_3, and catalysis of the hydrolysis reaction as labeled and shown as sticks. Bound IP_3 is shown as sticks.

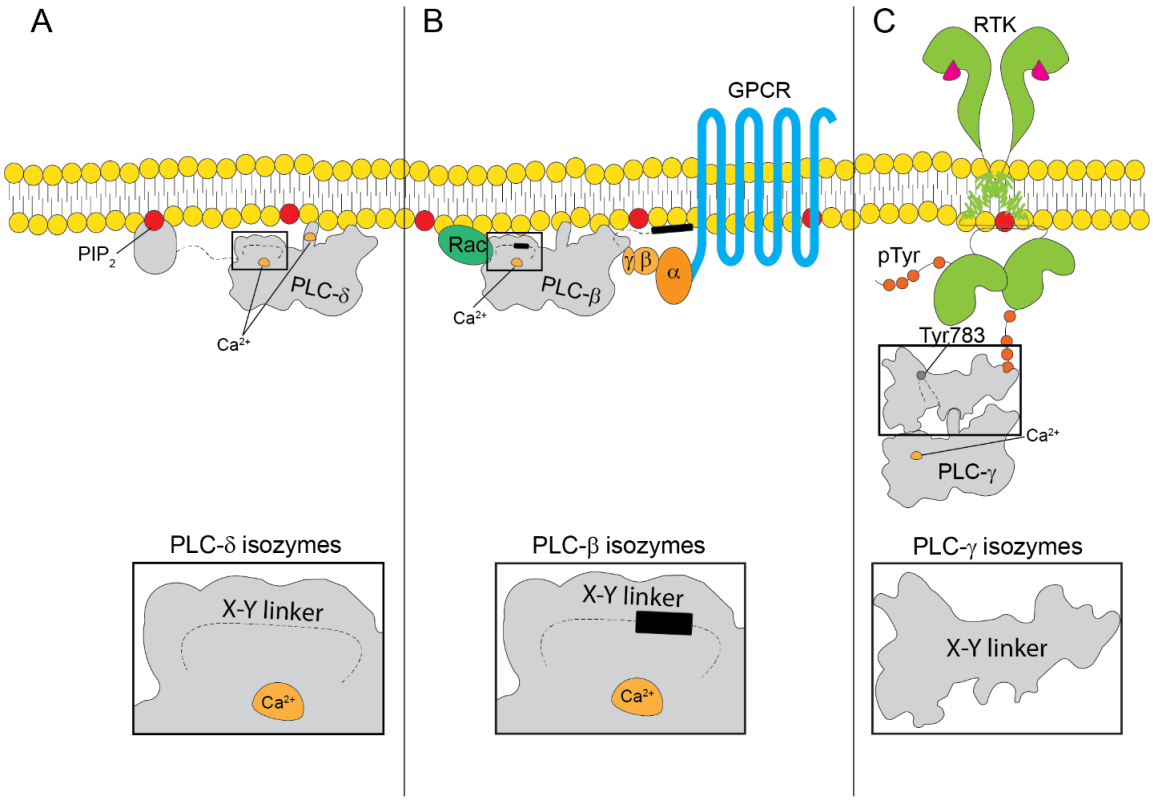

Figure 1.4 – Isozyme-specific modes of regulation. A, The PLC-δ isozymes are recruited to membranes via interactions between the N-terminal PH domain and membrane-embedded phosphatidylinositol 4,5-bisphosphate (PIP_2). Membrane association is stabilized by interactions between the C-terminal C2 domain and calcium (Ca^{2+}) ions that help coordinate membrane phospholipids. The X-Y linker of the PLC-δ isozymes is disordered, negatively charged, and prevents membrane association via electrostatic repulsion (inset). **B**, The PLC-β isozymes are activated downstream of G-protein coupled receptors (GPCR). The small GTPase Rac1 binds the N-terminal PH domain while Gα contacts portions of the EF hands as well as an extension of the C-terminal C2 domain. The X-Y linker of the PLC-β isozymes are mostly disordered and negatively charged except for a C-terminal α helix that sterically occludes access to the active site (inset). **C**, The PLC-γ isozymes are unique due to their phosphorylation-dependent activation downstream of tyrosine kinases and a highly elaborate X-Y linker that contains additional regulatory domains (inset). In the presence of an extracellular signal, receptor tyrosine kinases (RTKs) dimerize and autophosphorylate tyrosine residues C-terminal to the kinase domain. These phosphorylated tyrosines (pTyr) act as docking site for PLC-γ isozymes through interactions with the N-terminal SH2 domain within the regulatory domains. Subsequently, PLC-γ1 is phosphorylated on tyrosine residues, e.g. Tyr783 in PLC-γ1. Calcium (Ca^{2+}) ions cofactors are depicted as orange semicircles in all three panels.

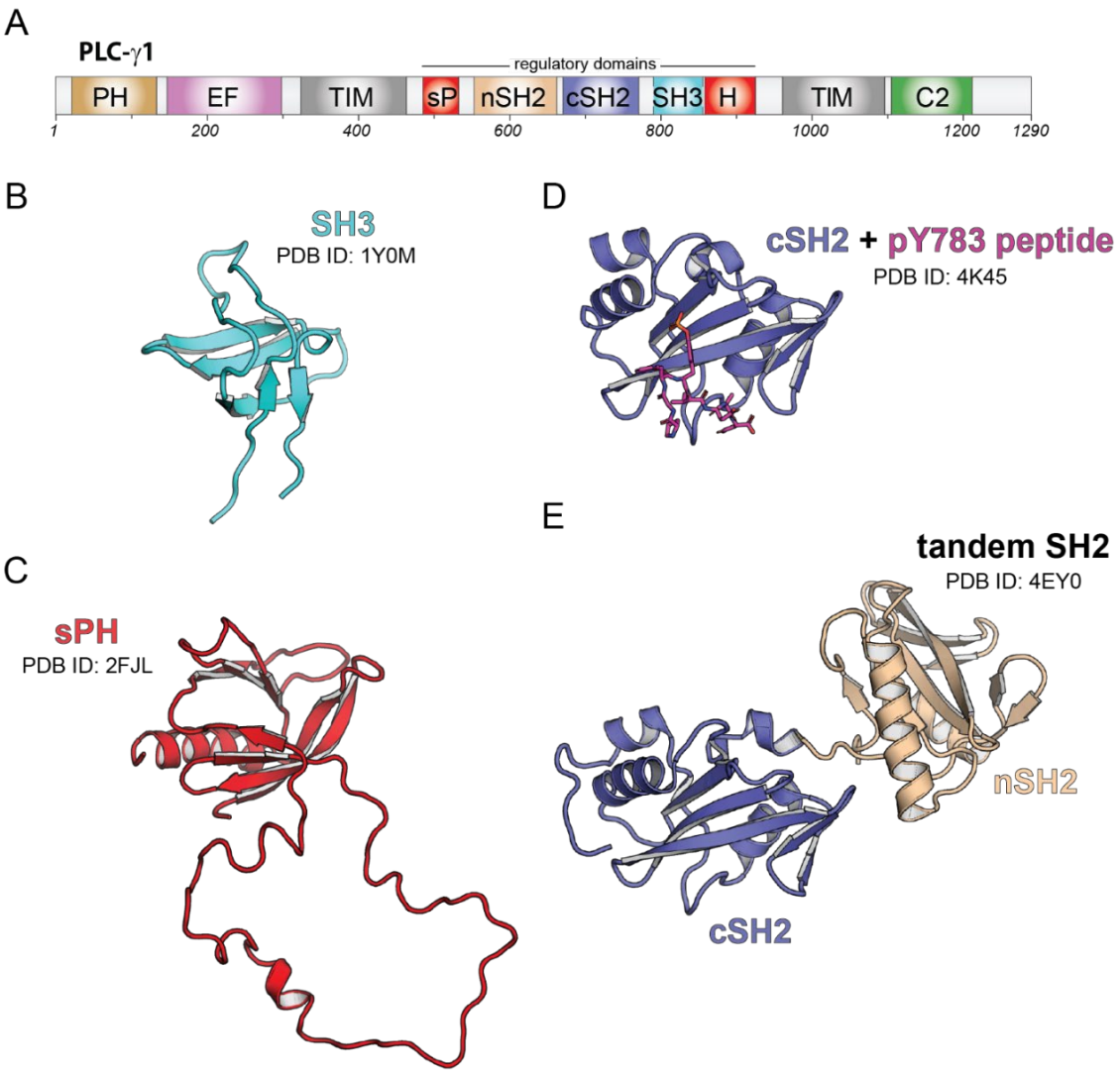

Figure 1.5 – Additional regulatory domains in the PLC-γ isozymes. A, Domain architecture of full-length PLC-γ1 drawn to scale. The regulatory array is comprised of a split pleckstrin homology (sPH) domain (red), an N-terminal *Src*-homology 2 (nSH2) domain (wheat), a C-terminal *Src*-homology 2 (cSH2) domain (slate), and an SH3 domain (cyan). These domains have been previously described in isolation and are shown in ribbon diagram. **B**, Structure of the PLC-γ1 SH3 domain (cyan, PDB ID: 1Y0M). **C**, Structure of the sPH domain (red) of PLC-γ2 (PDB ID: 2FJL). **D**, Structure of the PLC-γ1 cSH2 domain (slate) bound to a peptide (sticks) encompassing phosphorylated Tyr783 (pY783) of PLC-γ1 (PDB ID: 4K45). **E.** Structure of the PLC-γ1 nSH2 (wheat) and the cSH2 (slate) in tandem (PDB ID: 4EY0).

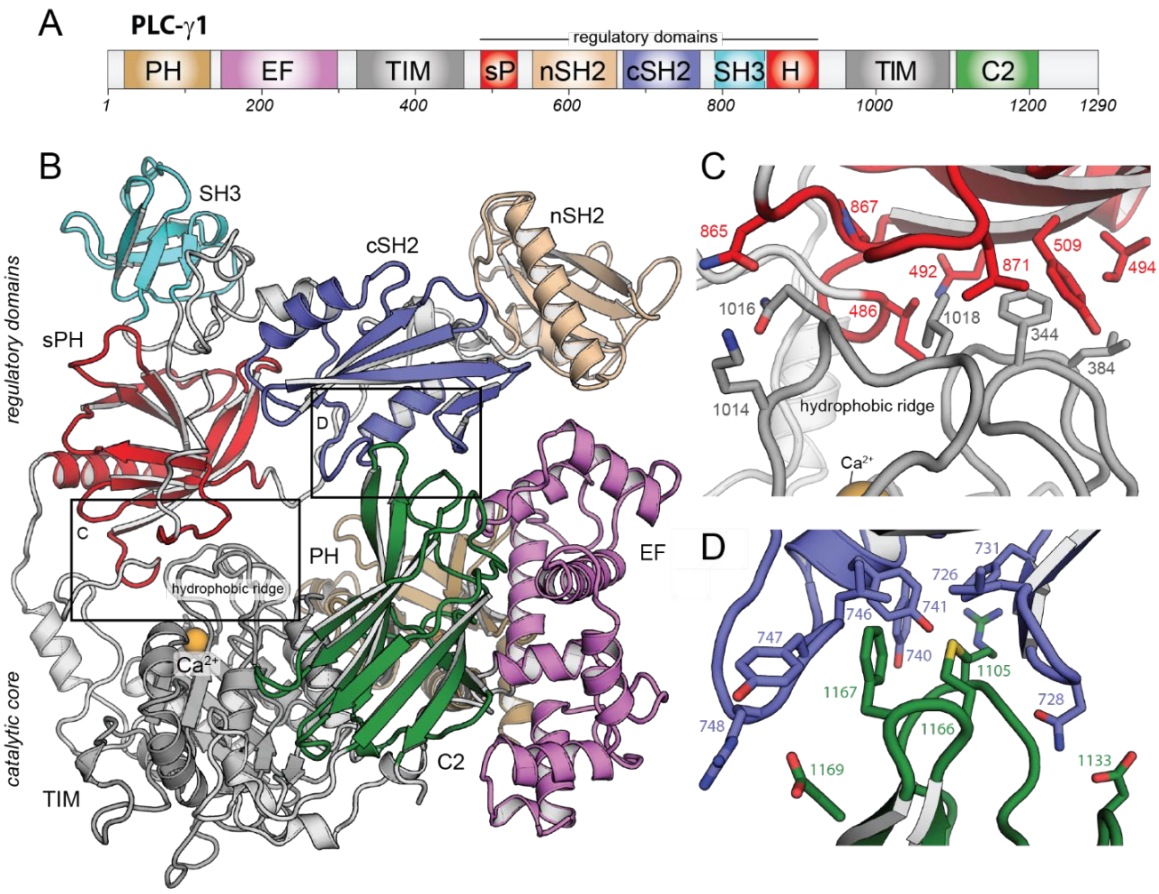

Figure 1.6 – Crystal structure of PLC-γ1. **A**, Domain architecture of full-length PLC-γ1 drawn to scale. B. Crystal structure of autoinhibited PLC-γ1 (PDB ID: 6PBC) with loops modeled. Domains colored as in **A**. The calcium ion cofactor (orange sphere) marks the active site. **C**, Structural details at the interface between the sPH domain (red) and the catalytic TIM barrel (grey). **D**, Structural details at the interface between the cSH2 domain (slate) and the C2 domain (green).

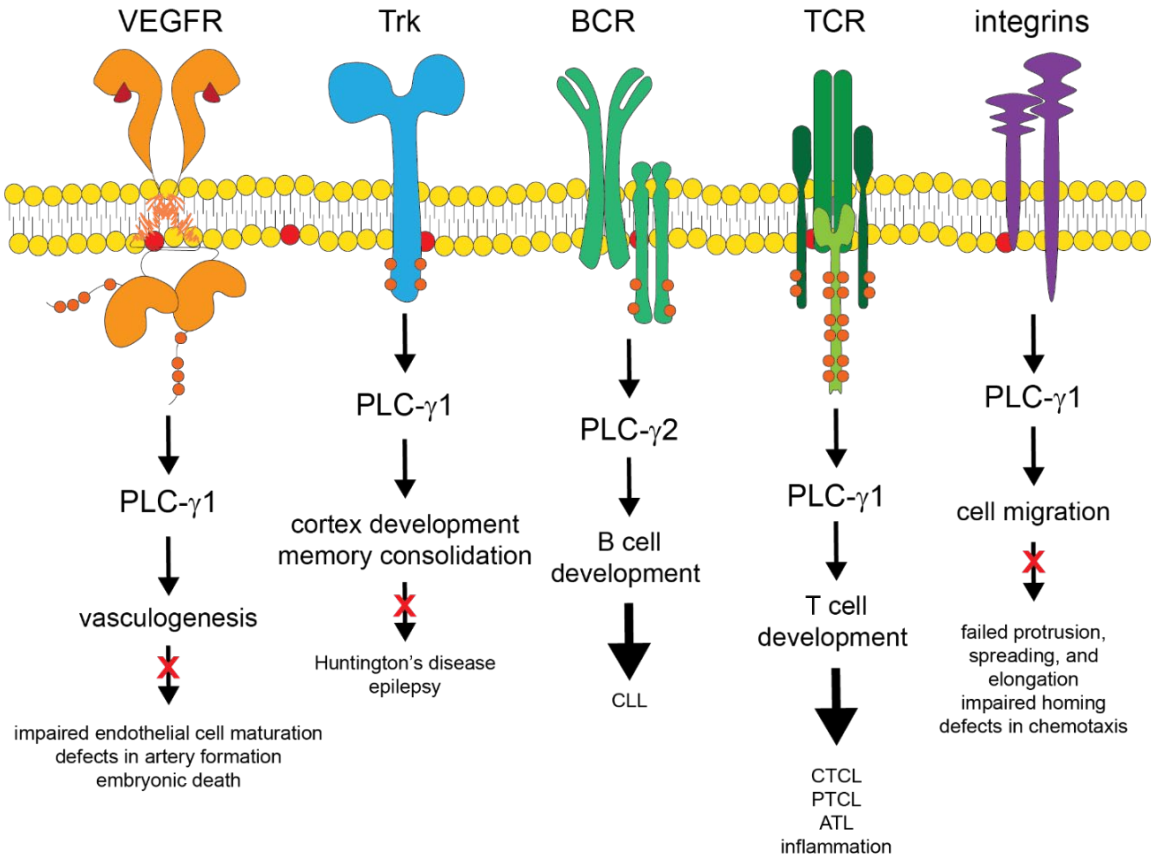

Figure 1.7 – PLC-γ isozymes as gatekeepers of health and disease. The PLC-γ isozymes are activated downstream of a multitude of cell-surface receptors. Depending in the cell context, PLC-γ isozymes are activated by vascular endothelial growth factor receptor (VEGFR), Trk family of tyrosine kinases, immune receptors such as the B-cell antigen receptor (BCR) and the T-cell antigen receptor (TCR), and integrins. The intracellular portions of these receptors are phosphorylated (orange circles) that act as docking sites for PLC-γ isozymes. Upon phosphorylation-dependent activation, the PLC-γ isozymes control a variety of physiological processes including endothelial cell differentiation, brain cortex development, proliferation of immune cell, and cell migration. Either silencing or constitutive activation of PLC-γ isozyme activity leads to human diseases including cancers and immune dysregulation.

REFERENCES

1. Newton, A. C., Bootman, M. D., and Scott, J. D. (2016) Second Messengers. *Cold Spring Harb. Perspect. Biol.* **8**(8), a005926 (10.1101/cshperspect.a005926)

2. Rhee, S. G. (2001) Regulation of phosphoinositide-specific phospholipase C. *Annu. Rev. Biochem.* **70**, 281-312 (10.1146/annurev.biochem.70.1.281)

3. Kadamur, G., and Ross, E. M. (2013) Mammalian Phospholipase C. *Annu. Rev. Physiol.* **75**, 127-154 (10.1146/annurev-physiol-030212-183750)

4. Gresset, A., Sondek, J., and Harden, T. K. (2012) The Phospholipase C Isozymes and Their Regulation. *Subcell. Biochem.* **58**, 61-94 (10.1007/978-94-007-3012-0_3)

5. Essen, L., Perisic, O., Cheung, R., Katan, M., and Williams, R. L. (1996). Crystal structure of a mammalian phosphoinositide-specific phospholipase Cδ. *Nature* **380**, 595-602

6. Imaoka, T., Lynham, J. A., and Haslam, R. J. (1983) Purification and characterization of the 47,000-dalton protein phosphorylated during degranulation of human platelets. *J. Biol. Chem.* **258**(18), 11404-11414

7. Yoon, H. S., Hajduk, P. J., Petros, A. M., Olejniczak, E. T., Meadows, R. P., and Fesik, S. W. (1994) Solution structure of a pleckstrin-homology domain. *Nature* **369**, 672–675 (10.1038/369672a0)

8. Garcia, P., Gupta, R., Shah, S., Morris, A. J., Rudge, S. A., Scarlata, S., Petrova, V., McLaughlin, S., and Rebecchi, M. J. (1995) The Pleckstrin Homology Domain of Phospholipase C-δ1 binds with High Affinity to Phosphatidylinositol 4,5-Bisphosphate in Bilayer Membranes. *Biochemistry* **34**, 16228-16234 (10.1021/bi00049a039)

9. Lemmon, M. A., Ferguson, K. M., O'Brien, R., Sigler, P. B., and Schlessinger, J. (1995) Specific and high affinity binding of inositol phosphates to an isolated pleckstrin homology domain. *Proc. Natl. Aca. Sci.* **92**, 10472-10476 (10.1073/pnas.92.23.10472)

10. Rebecchi, M. J., Peterson, A., and McLaughlin, S. (1992) Phosphoinositide-Specific Phospholipase C-δ1 Binds with High Affinity to Phospholipid Vesicles Containing Phosphatidylinositol 4,5-Bisphosphate. *Biochemistry* **31**, 12742-12747

11. Snyder, J. T., Singer, A. U., Wing, M. R., Harden, T. K., and Sondek, J. (2003) The Pleckstrin Homology Domain of Phospholipase C-β2 as an Effector Site for Rac. *J. Biol. Chem.* **278**(23), 21099-21104 (10.1074/jbc.M301418200)

12. Hajicek, N., Keith, N. C., Siraliev-Perez, E., Temple, B. R. S., Huang, W., Zhang, Q., Harden, T. K., and Sondek, J. (2019) Structural basis for the activation of PLC-γ isozymes by phosphorylation and cancer-associated mutations. eLife **8**, e51700 (10.7554/eLife.51700)

13. Chazin, W. J. (2011) Relating Form and Function of EF-hand Calcium Binding Proteins. *Acc. Chem. Res.* **44**(3), 171-179. (10.1021/ar100110d)

14. Kumar, V. D., Lee, L., and Edwards, B. F. P. (1990) Refined crystal structure of calcium-liganded carp parvalbumin 4.25 at 1.5-Å resolution. *Biochemsitry* **26**(6), 1404-1412

15. Hicks, S. N., Jezyk, M. R., Gershburg, S., Seifert, J. P., Harden, T. K., and Sondek, J. (2008) General and versatile autoinhibition of PLC isozymes. *Mol. Cell.* **31**(3), 383–394 (10.1016/j.molcel.2008.06.018)

16. Jezyk, M. R., Snyder, J. T., Gershberg, S., Worthylake, D. K., Harden, T. K., and Sondek, J. (2006) Crystal structure of Rac1 bound to its effector phospholipase C-β2. *Nat. Struct. Mol. Biol.* **13**, 1135–1140 (10.1038/nsmb1175)

17. Charpentier, T. H., Waldo, G. L., Barrett, M. O., Huang, W., Zhang, Q., Harden, T. K., and Sondek, J. (2014) Membrane-induced Allosteric Control of Phospholipase C-β Isozymes. *J. Biol. Chem.* **289**, 29545-29557 (10.1074/jbc.M114.586784)

18. Corbalan-Garcia, S., and Gomez-Fernandez, J. C. (2013) Signaling through C2 domains: More than one lipid target. *Biochim. Biophys. Acta.* **1838**(6), 1536-1547 (10.1016/j.bbamem.2014.01.008)

19. Grobler, J. A., Essen, L., Williams, R. L., and Hurley, J. H. (1996) C2 domain conformational changes in phospholipase C-δ1. *Nat. Struct. Biol.* **3**, 788–795 (10.1038/nsb0996-788)

20. Essen, L. O., Perisic, O., Lynch, D. E., Katan, M., and Williams, R. L. (1997) A ternary metal binding site in the C2 domain of phosphoinositide-specific phospholipase C-δ1. *Biochemistry* **36**, 2753-2762 (10.1021/bi962466t)

21. Wierenga, R. K. (2001) The TIM-barrel fold: a versatile framework for efficient enzymes. FEBS Letters 492(3). 193-198 (10.1016/S0014-5793(01)02236-0)

22. Ellis, M. V., James, S. R., Perisic, O., Downes, C. P., Williams, R. L., and Katan, M. (1998) Mutational analysis of residues within the active site and hydrophobic ridge of PLC-δ1. *J. Biol. Chem.* **273**(19), 11650-11659 (10.1074/jbc.273.19.11650)

23. Waldo, G. L., Ricks, T. K., Hicks, S. N., Cheever, M. L., Kawano, T., Tsuboi, K., Wang, X., Montell, C., Kozasa, T., Sondek, J., and Harden, T. K. (2010) Kinetic Scaffolding Mediated by a Phospholipase C-β and Gq Signaling Complex. *Science* **330**, 974-980 (10.1126/science.1193438)

24. Gresset, A., Hicks, S. N., Harden, T. K., and Sondek, J. (2010) Mechanism of Phosphorylation-Induced Activation of Phospholipase C-γ Isozymes. *J. Biol. Chem.* **285**, 35836-35847 (10.1074/jbc.M110.166512)

25. Hajicek, N., Charpentier, T. H., Rush, J. R., Harden, T. K., and Sondek, J. (2013) Autoinhibition and Phosphorylation-induced Activation of Phospholipase C-γ isozymes. *Biochemistry* **52**, 4810-4819 (10.1021/bi400433b)

26. Bunney, T. D., Esposito, D., Mas-Droux, C., Lamber, E., Baxendale, R. W., Martins, M., Cole, A., Svergun, D., Driscoll, P. C., and Katan, M. (2012) Structural and Functional Integration of the PLCγ Interaction Domains Critical for Regulatory Mechanisms and Signaling Deregulation. *Structure* **20**, 2062-2075 (10.1016/j.str.2012.09.005)

27. Peters, K. G., Marie, J., Wilson, E., Ives, H. E., Escobedo, J., Del Sario, M., Mirda, D., and Williams, L. T. (1992) Point mutation of an FGF receptor abolishes phosphatidylinositol turnover and Ca2+ flux but not mitogenesis. *Nature* **358**, 678-681. (10.1038/358678a0)

28. Mohammadi, M., Honegger, A. M., Rotin, D., Fischer, R., Bellot, F., Li, W., Dionne, C. A., Jaye, M., Rubinstein, M., and Schlessinger, J. (1991) A tyrosine-phosphorylated carboxy-terminal peptide of the fibroblast growth factor receptor (Flg) is a binding site for the SH2 domain of phospholipase C-γ1. *Molec. Cell. Biol.* **11**, 5068-5078 (10.1128/MCB.11.10.5068)

29. Kim, J. W., Sim, S. S., Kim, U. H., Nishibe, S., Wahl, M. I., Carpenter, G., and Rhee, S. G. (1990) Tyrosine residues in bovine phospholipase C-gamma phosphorylated by the epidermal growth factor receptor in vitro. *J. Biol. Chem.* **265**, 3940-3943

30. Serrano, C. J., Graham, L., DeBell, K., Rawat, R., Very, M. C., Bonvini, E., Rellahan, B. L., and Reischl, I. G. (2005) A new tyrosine phosphorylation site in PLCγ1: the role of tyrosine 775 in immune receptor signaling. *J. Immunol*. **174**(10), 6233-6237 (10.4049/jimmunol.174.10.6233)

31. Watanabe, D., Hashimoto, S., Ishiai, M., Matsushita, M., Baba, Y., Kishimoto, T., Kurosaki, T., and Tsukada, S. (2001) Four tyrosine residues in phospholipase C-γ 2, identified as Btk-dependent phosphorylation sites, are required for B cell antigen receptor-coupled calcium signaling. *J. Biol. Chem.* **276**(42), 38595-38601 (10.1074/jbc.M103675200)

32. Kim, H. K., Kim, J. W., Zilberstein, A., Margolis, B., Kim, J. G., Schlessinger, J., and Rhee, S. G. (1991) PDGF Stimulation of Inositol Phospholipid Hydrolysis Requires PLC-γ1 Phosphorylation on Tyrosine Residues 783 and 1254. *Cell* **65**(3), 435-441 (10.1016/0092-8674(91)90461-7)

33. Piechulek, T., Rehlen, T., Walliser, C., Vatter, P., Moepps, B., and Gierschik, P. (2005) Isozyme-specific Stimulation of Phospholipase C-γ2 by Rac GTPases. *J. Biol. Chem.* **280**, 38923-38931 (10.1074/jbc.M509396200)

34. Walliser C., Ratlich, M., Harris, R., Everett, K. L., Josephs, M. B., Vatter, P., Esposito, D., Driscoll, P. C., Katan, M., Gierschik, P., and Bunney, T. D. (2008) Rac Regulates Its Effector Phospholipase Cγ2 through Interaction with a Split Pleckstrin Homology Domain. *J. Biol. Chem.* **283**, 30351-30362 (10.1074/jbc.M803316200)

35. Bae, J. H., Lew, E. D., Yuzawa, S., Tome, F., Lax, I., and Schlessinger, J. (2009) The Selectivity of Receptor Tyrosine Kinase Signaling Is Controlled by a Secondary SH2 Domain Binding Site. *Cell* **138**, 514-524 (10.1016/j.cell.2009.05.028)

36. Huang, Z., Marsiglia, W. M., Roy, U. B., Rahimi, N., Ilghari, D., Wang, H., Chen, H., Gai, W., Blais, S., Neubert, T. A., Mansukhani, A., Traaseth, N. J., Li, X., and Mohammadi, M. (2016) Two FGF Receptor Kinase Molecules Act in Concert to Recruit and Transphosphorylate Phospholipase Cγ. *Mol. Cell.* **61**, 98-110 (10.1016/j.molcel.2015.11.010)

37. Kaneko, T., Li, L., and Li, S. S. (2008) The SH3 Domain: A Family of Versatile Peptide- and Protein-Recognition Module. *Front. Biosci.* **13**, 4938-4952 (10.2741/3053)

38. Sherman, E., Barr, V. A., Merrill, R. K., Regan, C. K., Sommers, C. L., and Samelson, L. E. (2016) Hierarchical Nanostructure and Synergy of Multimolecular Signaling Complexes. *Nat Commun.* **7**, 12161 (10.1038/ncomms12161)

39. Yablonski, D., Kadlecek, T., and Weiss, A. (2001) Identification of a Phospholipase C-γ1 (PLC-γ1) SH3 Domain-Binding Site in SLP-76 Required for T-Cell Receptor-Mediated Activation of PLC-γ1 and NFAT. *Mol. Cell Biol.* **21**(13), 4208-4218 (10.1128/MCB.21.13.4208-4218.2001)

40. Deng, L., Velikovsky, C. A., Swaminathan, C. P., Cho, S., and Mariuzza, R. A. (2005) Structural Basis for Recognition of the T Cell Adaptor Protein SLP-76 by the SH3 Domain of Phospholipase Cγ1. *J. Mol. Bio.* **352**, 1-10 (10.1016/j.jmb.2005.06.072)

41. Carmeliet, P. (2000) Mechanisms of angiogenesis and arteriogenesis. *Nat. Med*. **6**:389-395 (10.1038/74651)

42. Ji, Q. S., Winnier, G.E., Niswender, K.D., Horstman, D., Wisdom, R., Magnuson, M.A., and Carpenter, G. (1997) Essential role of the tyrosine kinase substrate phospholipase C-γ1 in mammalian growth and development. *Proc. Natl. Acad. Sci.* **94**:2999-3003 (10.1073/pnas.94.7.2999)

43. Lawson, N. D., Mugford, J. W., Diamond, B. A., and Weinstein, B. M. (2003) Phospholipase C γ-1 Is Required Downstream of Vascular Endothelial Growth Factor During Arterial Development. *Genes Dev.* **17**(11), 1346-1351 (10.1101/gad.1072203)

44. Guo, D., Jia, Q., Song, H. Y., Warren, R. S., and Donner, D. B. (1995) Vascular Endothelial Cell Growth Factor Promotes Tyrosine Phosphorylation of Mediators of Signal Transduction Contain SH2 Domains. Association with Endothelial Cell Proliferation. *J. Biol. Chem.* **270**(12), 6729-6733 (10.1074/jbc.270.12.6729)

45. Yang, Y. R., Choi, J. H., Chang, J., Kwon, H. M., Jang, H., Ryu, S. H., and Suh, P. (2012) Diverse cellular and physiological roles of phospholipase C-γ1. Adv. Enzyme Regul. 52, 138-151 (10.1016/j.advenzreg.2011.09.017)

46. Huang, E.J., and Reichardt, L.F. (2003) Trk receptors: roles in neuronal signal transduction. *Annu. Rev. Biochem.* **72**, 609-642 (10.1146/annurev.biochem.72.121801.161629)

47. Minichiello, L., Calella, A. M., Medina, D. L., Bonhoeffer, T., Klein, R., and Korte, M. (2002) Mechanism of TrkB-mediated hippocampal long-term potentiation. *Neuron* **36**:121-137 (10.1016/s0896-6273(02)00942-x)

48. Minichiello, L., Medina, D. L., Sciarretta, C., Calella, A. M., von Bohlen und Halbach, O., and Unsicker K. (2004) TrkB regulates neocortex formation through the Shc/PLCγ-mediated control of neuronal migration. *EMBO J.* **23**:3803-3814 (10.1038/sj.emboj.7600399)

49. Thisse, B., and Thisse, C. (2005) Functions and regulations of fibroblast growth factor signaling during embryonic development. *Dev. Bio.* **287**, 390-402 (10.1016/j.ydbio.2005.09.011)

50. Yang, Y. R., Follo, M. Y., Cocco, L., and Suh, P. (2013) The physiological roles of primary phospholipase C. *Adv. Biol. Regul.* **53**, 232-241 (10.1016/j.jbior.2013.08.003)

51. Bolanos, C. A., Neve, R. L., and Nestler, E. J. (2005) Phospholipase C γ in distinct regions of the ventral tegmental area differentially regulates morphine-induced locomotor activity. *Synapse* **56**, 166–169 (10.1002/syn.20136)

52. Bolanos, C. A., Perrotti, L. I., Edwards, S., Eisch, A. J., Barrot, M., Olson, V. G., Russell, D. S., Neve, R. L., and Nestler, E. J. (2003) Phospholipase Cγ in distinct regions of the ventral tegmental area differentially modulates mood-related behaviors. *J. Neurosci*. **23**, 7569–7576 (10.1523/JNEUROSCI.23-20-07569.2003)

53. Carpenter, G., and Ji, Q. (1999) Phospholipase C-γ as a Signal-Transducing Element. *Exp. Cell Res.* **253**(1), 15-24 (10.1006/excr.1999.4671)

54. Love, P. E., and Hayes, S. M. (2010) ITAM-mediated Signaling by the T-Cell Antigen Receptor. *Cold Spring Harb. Perspect. Biol.* **2**(6), a002485 (10.1101/cshperspect.a002485)

55. Chuck, M. I., Zhu, M., Shen, S., and Zhang, W. (2010) The Role of the LAT-PLC-gamma1 Interaction in T Regulatory Cell Function. *J. Immunol.* **184**(5), 2476-2486 (10.4049/jimmunol.0902876)

56. Rao, A., Luo, C., and Hogan, P. G. (1997) Transcription Factors of the NFAT Family: Regulation and Function. *Annu Rev. Immunol.* **15**, 707-747 (10.1146/annurev.immunol.15.1.707)

57. Sommers, C. L., Park, C., Lee, J., Feng, C., Fuller, C. L., Grinberg, A., Hildebrand, J. A., Lacana, E., Menon, R. K., Shores, E. W., Samelson, L. E., and Love, P. E. (2002) A LAT mutation that inhibits T cell development yet induces lymphoproliferation. *Science* **296**, 2040–2043 (10.1126/science.1069066)

58. Sommers, C. L., Lee, J., Steiner, K. L., Gurson, J. M., DePersis, C. L., El-Khoury, D., Fuller, C. L., Shores, E. W., Love, P. E., and Samelson, L. E. (2005) Mutation of the phospholipase C-γ 1-binding site of LAT affects both positive and negative thymocyte selection. *J. Exp. Med.* **201**, 1125-1134 (10.1084/jem.20041869)

59. Hashimoto, A., Takeda, K., Inaba, M., Sekimata, M., Kaisho, T., Ikehara, S., Homma, Y., Akira, S., and Kurosaki, T. (2000) Essential Role of Phospholipase C-γ2 in B Cell Development and Function. *J. Imuunol.* **165**, 1738-1742 (10.4049/jimmunol.165.4.1738)

60. Wang, D., Feng, J.,Wen, R., Marine, J. C., Sangster, M. Y., Parganas, E., Hoffmeyer, A., Jackson, C. W., Cleveland, J. L., Murray, P. J., and Ihle, J. N. (2000) Phospholipase Cγ2 is essential in the functions of B cell and several Fc receptors. *Immunity* **13**, 25–35 (10.1016/s1074-7613(00)00005-4)

61. Jones, N. P., Peak, J., Brader, S., Eccles, S. A., and Katan, M. (2005) PLCγ1 is essential for early events in integrin signaling required for cell motility. *J. Cell Sci.* **118**, 2695-2706 (10.1242/jcs.02374)

62. de Gorter, D. J. J., Beuling, E., Kersseboom, R., Middendrop, S., van Gils, J. M., Hendriks, R. W., Pals, S. T., and Spaargaren, M. (2007) Bruton's Tyrosine Kinase and Phospholipase C γ2 Mediate Chemokine-Controlled B Cell Migration and Homing. *Immunity* **26**, 93-104 (10.1016/j.immuni.2006.11.012)

63. Asokan, S. B., Johnson, H. E., Rahman, A., King, S. J., Rotty, J. D., Lebedeva, I. P., Haugh, J. M., and Bear, J. E. (2014) Mesenchymal Chemotaxos Requires Selective Inactivation of Myosin II at the Leading Edge via a Noncanonical PLCγ/PKCα Pathway. *Dev. Cell* **31**,1-14 (10.1016/j.devcel.2014.10.024)

64. Arteaga, C. L., Johnson, M. D., Todderud, G., Coffey, R. J., Carpenter, G., and Page, D. L. (1991) Elevated content of the tyrosine kinase substrate phospholipase C-γ1 in primary human breast carcinomas. *Proc. Natl. Acad. Sci.* **88**, 10435-10439 (10.1073/pnas.88.23.10435)

65. Shepard, C. R., Kassis, J., Whaley, D. L., Kim, H. G., and Wells, A. (2007) PLCγ contributes to metastasis of in situ-occurring mammary and prostate tumors. *Oncogene* **26**, 3020-3026 (10.1038/sj.onc.1210115)

66. Park, J., Lee, Y. H., Kim, S. S., Park, K. J., Noh, D., Ryu, S. H., and Suh, P. (1994) Overexpression of Phospholipase C-γ1 in Familial Adenomatous Polyposis. *Cancer Res*. **54**, 2240-2244.

67. Nomoto, K., Tomita, N., Miyake, M., Xhu, D., LoGerfo, P. R., and Weinstein, I. B. (1995) Expression of Phospholipases γ1, β1, δ1 in Primary Human Colon Carcinomas and Colon Carcinoma Cell Lines. *Mol. Carcinogen.* **12**, 146-152 (10.1002/mc.2940120306)

68. Khoshyomn, S., Penar, P. L., Rossi, J., Wells, A., Abramson, D. L., and Bhushan, A. (1999) Inhibition of Phospholipase C-γ1 Activation Blocks Glioma Cell Motility and Invasion of Fetal Rat Brain Aggregates. *Neurosurgery* **44**(30), 568-577 (10.1097/00006123-199903000-00073)

69. Kunze, K., Spieker, T., Gamerdinger, U., Nau, K., Berger, J., Dreyer, T., Sindermann, J. R., Hoffmeier, A., Gattenlohner, S., and Brauninger, A. (2014) A Recurrent Activating PLCG1 Mutation in Cardiac Angiosarcomas Increases Apoptosis Resistance and Invasiveness of Endothelial Cells. *Cancer Res.* **74**(21) 6173-6183 (10.1158/0008-5472.CAN-14-1162)

70. Vaque, J. P., Gomez-Lopez, G., Monsalvez, V., Varela, I., Martinez, N., Perez, C., Dominguez, O., Grana O., Rodriguez-Peralto, J. L., Rodriguez-Pinilla, S. M., Gonzalez-Vela, C., Rubio-Camarillo, M., Martin-Sanchez, E., Pisano, D. G.,

Papadavid, E., Papadaki, T., Requena, L., Garcia-Marco, J. A., Mendez, M., Provencio, M., Hospital Mercedes, Suarez-Massa, D., Postigo, C., San Segundo, D., Lopez-Hoyos, M., Ortiz-Romero, P. L., Piris, M., A., and Sanchez-Beato, M. (2014) PLCG1 mutations in cutaneous T-cell lymphomas. *Blood* **123**, 2034-2043 (10.1182/blood-2013-05-504308)

71. Landau, D. A., Sun, C., Rosebrock, D., Herman, S. E. M., Fein, J., Sivina, M., Underbayev, C., Liu, D., Hoellenriegel, J., Ravichandran, S., Farooqui, M. Z. H., Xhang, W., Cibuluskis, C., Zviran, A., Neuberg, D. S., Livitz, D., Bozic, I., Leshchiner, I., Getz, G., Burger, J. A., Wiestner, A., and Wu, C. J. (2017) The evolutionary landscape of chronic lymphocytic leukemia treated with ibrutinib targeted therapy. *Nat. Commun.* **8**(1), 2185 (10.1038/s41467-017-02329-y)

72. Kataoka, K., Nagata, Y., Kitanaka, A., Shiraishi, Y., Shimamura, T., Yasunaga, J., Totoki, Y., Chiba, K., Sato-Otsubo, A., Nagae, G., Ishii, R., Muto, S., Kotani, S., Watatani, Y., Takeda, J., Sanada, M., Tanaka, H., Suzuki, H., Sato, Y., Shiozawa, Y., Yoshizato, T., Yoshida, K., Makishima, H., Iwanaga, M., Ma, G., Nosaka, K., Hishizawa, M., Itonaga, H., Imaizumi, Y., Munakata, W., Ogasaware, H., Sato, Y., Sasai, K., Muramoto, K., Penova, M., Kawaguchi, T., Nakamura, H., Hama, N., Shide, K., Kubuki, Y., Hidaka, T., Kameda, T., Nakamaki, T., Ishiyama, K., Miyawaki, S., Yoon, S., Tobinai, K., Miyazaki, Y., Takaori-Kondo, A., Matsuda, F., Takeuchi, K., Nureki, O., Aburatani, H., Watanabe, T., Shibata, T., Matsuoka, M., Miyano, S., Shimoda, K., and Ogawa, S. (2015) Integrated molecular analysis of adult T cell leukemia/lymphoma. *Nat. Genet.* 47(11):1304-1315. (10.1038/ng.3415)

73. Manso, R., Rodriguez-Pinilla, S. M., Gonzalez-Rincon, J., Gomez, S., Monsalvo, S., Llamas. P., Rojo, F., Perez-Callejo, D., Cereceda, L., Limeres, M. A., Maeso, C., Ferrando, L., Perez-Seoane, C., Rodriguez, G., Arrinda, J. M., Garcia-Bragado, F., Franco, R., Rodriguez-Peralto, J. L., Gonzalez-Carrero, J., Martin-Davila, F., Piris, M. A., and Sanchez-Beato, M. (2015) Recurrent presence of the PLCG1 S345F mutation in nodal peripheral T-cell lymphomas. *Haematologica* **100**, e25-e27 (10.3324/haematol.2014.113696)

74. Woyach, J. A., Furman, R. R., Liu, T. M., Ozer, H. G., Zapatka, M., Ruppert, A. S., Xue, L., Li, D. H., Steggerda, S. M., Versele, M., Dave, S. S., Zhang, J., Yilmaz, A. S., Jaglowski, S. M., Blum, K. A., Lozanski, A., Lozanski, G., James, D. F., Barrientos, J. C., Lichter, P., Stilgenbauer, S., Buggy, J. J., Chang, B. Y., Johnson, A. J., and Byrd, J. C. (2014) Resistance mechanisms for the Bruton's tyrosine kinase inhibitor ibrutinib. *N. Engl. J. Med.* **370**(24), 2286–2294 (10.1056/NEJMoa1400029)

75. Yu, P., Constien, R., Dear, N., Katan, M., Hanke, P., Bunney, T. D., Kunder, S., Quintanilla-Martinez, L., Huffstadt, U., Schröder, A., Jones, N. P., Peters, T., Fuchs, H., de Angelis, M. H., Nehls, M., Grosse, J., Wabnitz, P., Meyer, T. P. H., Yasuda, K., Schiemann, M., Schneider-Fresenius, C., Jagla, W., Russ, A., Popp, A., Josephs, M., Marquardt, A., Laufs, J., Schmittwolf, C., Wagner, H., Pfeffer, K., and Mudde, G. C. (2005) Autoimmunity and Inflammation Due to a Gain-of-Function Mutation in Phospholipase Cγ2 that Specifically Increases External Ca^{2+} Entry. *Immunity* **22**(4), 451-465 (10.1016/j.immuni.2005.01.018)

76. Abe, K., Fuchs, H., Boersma, A., Hans, W., Yu, P., Kalaydjiev, S., Klaften, M., Adler, T., Calzada-Wack, J., Mossbrugger, I., Rathkolb, B., Rozman, J., Prehn, C., Maraslioglu, M., Kametani, Y., Shimada, S., Adamski, J., Busch, D.H., Esposito, I., Klingenspor, M., Wolf, E., Wurst, W., Gailus-Durner, V., Katan, M., Marschall, S., Soewarto, D., Wagner, S. and de Angelis, M.H. (2011) A novel N-ethyl-N-nitrosourea–induced mutation in phospholipase Cγ2 causes inflammatory arthritis, metabolic defects, and male infertility in vitro in a murine model. *Arthritis & Rheumatism*, **63**, 1301-1311 (10.1002/art.30280)

77. Cremasco, V., Graham, D. B., Novack, D. V., Swat, W., and Faccio, R. (2008) Vav/Phospholipase Cγ2-mediated control of a neutrophil-dependent murine model of rheumatoid arthritis. *Arthritis Rheum.* **58**(9), 2712–2722 (10.1002/art.23757)

78. Ombrello, M. J., Remmers, E. F., Sun, G., Freeman, A. F., Datta, S., Torabi-Parizi, P., Subramanian, N., Bunney, T. D., Baxendale, R. W., Martins, M. S., Romberg, N., Komarow, H., Aksentijevich, I., Kim, H. S., Ho, J., Cruse, G., Jung, M., Gilfillan, A. M., Metcalfe, D. D., Nelson, C., O'Brien, M., Wisch, L., Stone, K., Douek, D. C., Ghandi, C., Wanderer, A. A., Lee, H., Nelson, S. F., Shianna, K. V., Cirulli, E. T., Goldtstein, D. B., Long, E. O., Moir, S., Meffre, E., Holland, S. M., Kastner, D. L., Katan, M., Hoffman, H. M., and Milner, J. D. (2012) Cold urticaria, immunodeficiency, and autoimmunity related to PLCG2 deletions. *N. Engl. J. Med.* **366**(4), 330–338 (10.1056/NEJMoa1102140)

79. Koss, H., Bunney, T. D., Behjati, S., and Katan, M. (2014) Dysfunction of phospholipase Cγ in immune disorders and cancer. *Trends Biochem. Sci.* **39**, 603-611 (10.1016/j.tibs.2014.09.004)

80. Zhou, Q., Lee, G., Brady, J., Datta, S., Katan, M., Sheikh, A., Martins, M. S., Bunney, T. D., Santich, B. H., Moir, S., Kuhns, D. B., Long-Priel, D. A., Ombrello, A., Stone, D., Ombrello, M. J., Khan, J., Milner, J. D., Kastner, D. L., and Aksentijevich, I. (2012) A Hypermorphic Missense Mutation in PLCG2, Encoding Phospholipase Cγ2, Causes a Dominantly Inherited Autoinflammatory Disease with Immunodeficiency. *Am. J. Hum. Genet.* **91**(4), 713-720 (10.1016/j.ajhg.2012.08.006)

81. Jang, H., Yang, Y. R., Kim, J. K., Choi, J. H., Seo, Y., Lee, Y. H., Lee, J. E., Ryu, S. H., and Suh, P. (2013) Phospholipase C-γ1 involved in brain disorders. *Adv. Biol. Regul.* **53**(1), 51-62 (10.1016/j.jbior.2012.09.008)

82. Roos, R. A. (2010) Huntington's disease: a clinical review. *Orphanet. J. Rare Dis.* **5**, 40 (10.1186/1750-1172-5-40)

83. Giralt, A., Rodrigo, T., Martin, E. D., Gonzalez, J. R., Mila, M., Cena, V., Dierssen, M., Canals, J. M., and Alberch, J. (2009) Brain-derived neurotrophic factor modulates the severity of cognitive alterations induced by mutant huntingtin: involvement of phospholipase C γ activity and glutamate receptor expression. *Neuroscience* **158**(4), 1234–1250 (10.1016/j.neuroscience.2008.11.024)

84. Gines, S., Bosch, M., Marco, S., Gavalda, N., Diaz-Hernandez, M., Lucas, J. J., Canals, J. M., and Alberch, J. (2006) Reduced expression of the TrkB receptor in

Huntington's disease mouse models and in human brain. *Eur. J. Neurosci.* **23**(3), 649-658 (10.1111/j.1460-9568.2006.04590.x)

85. Gruart, A., Sciarretta, C., Valenzuela-Harrington, M., Delgado-García, J. M., and Minichiello, L. (2007) Mutation at the TrkB PLCγ-docking site affects hippocampal LTP and associative learning in conscious mice. *Learn Mem.* **14**(1):54-62 (10.1101/lm.428307)

86. Scharfman, H. E. (2007) The neurobiology of epilepsy. *Curr. Neurol. Neurosci. Rep.* **7**(4),348–354 (10.1007/s11910-007-0053-z)

87. Danzer, S. C., He, X., and McNamara, J. O. (2004) Ontogeny of seizure-induced increases in BDNF immunoreactivity and TrkB receptor activation in rat hippocampus. *Hippocampus* **14**:345–355 (10.1002/hipo.10190)

88. He, X. P., Pan, E., Sciarretta, C., Minichiello, L., and McNamara, J. O. (2010) Disruption of TrkB-Mediated Phospholipase Cγ Signaling Inhibits Limbic Epileptogenesis. *J. Neurosci.* **30** (18), 6188-6196 (10.1523/JNEUROSCI.5821-09.2010)

89. Gu, B., Huang, Y. Z., He, X., Joshi, R. B., Jang, W., and McNamara, J. O. (2015) A Peptide Uncoupling BDNF Receptor TrkB from Phospholipase Cγ1 Prevents Epilepsy Induced by Status Epilepticus. *Neuron* **88**(3), 484-491 (10.1016/j.neuron.2015.09.032)

90. Wolfe, C. M., Fitz, N. F., Nam, K. N., Lefterov, I., and Koldamova, R. (2018) The Role of APOE and TREM2 in Alzheimer's Disease-Current Understanding and Perspectives. *Int J Mol Sci.* **20**(1), 81 (10.3390/ijms20010081)

91. Magno, L., Lessard, C. B., Martins, M., Lang, V., Cruz, P., Asi, Y., Katan, M., Bilsland, J., Lashley, T., Chakrabarty, P., Golde, T. E., and Whiting, P. J. (2019) Alzheimer's disease phospholipase C-γ-2 (PLCG2) protective variant is a functional hypermorph. *Alz. Res. Therapy* **11,** 16 (10.1186/s13195-019-0469-0)

CHAPTER II: FLUOROGENIC XY-69 TO MEASURE PLC ACTIVTIY[1]

Background

The thirteen mammalian phospholipase C (PLC) isozymes are divided into six subgroups (-β, -γ, -δ, -ε, -ζ, -η) based on sequence similarity and share a conserved catalytic core (1). Due to autoinhibition, the basal activities of PLCs are minimal in cells (2, 3). When activated, PLCs hydrolyze the minor membrane phospholipid phosphatidylinositol 4,5-bisphosphate (PIP_2) at the inner leaflet of the plasma membrane to generate the second messengers 1,2-diacylglycerol (DAG) and inositol 1,4,5-trisphosphate (IP_3). These second messengers activate protein kinase C (PKC) isozymes and promote the release of intracellular Ca^{2+} stores, respectively (4). The consumption of PIP_2 also contributes to changes in the functions of membrane proteins such as ion channels (5). Consequently, PLCs are important signaling proteins that regulate diverse cellular processes including proliferation, migration, and nerve conductance. Conversely, aberrant regulation of PLCs contributes to various diseases such as cancer (6-8), Alzheimer's disease (9, 10), and rheumatoid arthritis (11, 12). PLCs, particularly the PLC-γ isozymes, have emerged as promising therapeutic targets.

Despite extensive studies on PLCs, it remains challenging to continuously and directly monitor PLC activity at membranes with high sensitivity and throughput. Traditionally, the phospholipase activities of PLCs have been quantified using radiolabeled substrates (13-16). However, these formats have substantial limitations.

[1] This chapter was submitted for publication as a book chapter in Methods in Molecular Biology. The original citation is as follows: Carr, A. J., Siraliev-Perez, E., Huang, W., Sondek, J. and Zhang, Q. "Fluorogenic XY-69 in lipid vesicles for measuring activity of phospholipase C isozymes". *Methods Mol. Biol.* (In press).

Primarily, they do not allow for continuous monitoring of PLCs. In addition, the use of radioactive materials requires special training, handling, storage, equipment, and facilities that are less common than in previous decades. Indeed, radioactive PIP_2 has recently been discontinued by all chemical vendors and it is expensive to obtain such reagents through custom synthesis. Several chromogenic or fluorogenic PIP_2 analogs have been developed to continuously monitor PLC activity (17-21). However, most of these compounds are either inefficient substrates of PLCs or have other issues such as requiring a secondary enzymatic reaction not related to PLCs. Importantly, none of these compounds reliably report PLC activity at the membranes.

We created XY-69 as a membrane-associated PIP_2 analog that works as a selective fluorogenic reporter of PLC activity (22). XY-69 contains fluorescein as a fluorophore and 4-(dimethylaminoazo)benzene-4-carboxylic (DABCYL) acid as a dark quencher that absorbs emission energy from fluorescein and dissipates it as heat. PLC isozymes hydrolyze XY-69 to separate DABCYL from fluorescein leading to a large increase in fluorescence intensity that is readily monitored in real-time. The assay works both in detergent micelles and in lipid vesicles that more closely resemble biological membranes and avoids the quench and work-up steps otherwise needed in radioactivity-based assays. Furthermore, XY-69 functions in a microplate format which enables high-throughput discovery of molecules that modulate PLC activity. When presented in lipid vesicles, XY-69 captures the membrane-dependent activation of PLC activity by $G\alpha_q$ (22), the subunit of G-protein G_q that is known to activate PLC-β isozymes (14, 23, 24), or by conformational changes due to mutations (25). Consequently, XY-69 is a compelling replacement for radioactive PIP_2 to monitor PLC activity with the added advantages of continuous reaction monitoring and high-throughput. Assays based on XY-69 are readily applicable to both purified PLC isozymes and lysates from cell lines or animal tissues.

To further optimize the assays based on XY-69 to measure PLC activity, we have investigated the impact of varying lipid composition, pH, free Ca^{2+} concentration, and vesicle size on assay performance. Here, we describe optimized assay conditions and a detailed protocol to measure the activity of purified, cancer-associated mutant PLC-γ1 (D1165H) (8) with XY-69 embedded in lipid vesicles. The described protocol also applies to other PLC isozymes and may be modified to include kinases, effectors, peptides, and small molecules in the assay.

Materials

Equipment and supplies

1. Basic pH meter
2. 0.45 μm polyethersulfone (PES) syringe filters
3. 12 x 75 mm borosilicate culture tubes
4. Dry nitrogen (N_2) line equipped with plastic hose and glass Pasteur pipet
5. Vacuum pump
6. Black 384-shallow well microplate
7. Ultrasonic dismembrator
8. 5/64" Probe microtip for sonicator
9. Multimode plate reader
10. Ring stand
11. Dynamic light scattering (DLS) instrument
12. 40 μL plastic cuvettes with stoppers
13. Water bath
14. Dewar flask
15. Septum

16. Pipette
17. Pipette tips
18. Syringe
19. Vortex mixer

Lipids and other chemicals

1. 10 mg/mL (13.2 mM) L-α-phosphatidylethanolamine (PE; liver, bovine) stock solution in chloroform ($CHCl_3$), stored at -20°C under N_2
2. 1 mg/mL (912 μM) L-α-phosphatidylinositol-4,5-bisphosphate (PIP_2; brain, porcine; ammonium salt) stock solution in $CHCl_3$:methanol (MeOH):H_2O (20:9:1; v/v/v), stored at -20°C under N_2
3. 210 μM XY-69 stock solution in H_2O, stored at -80°C under N_2, wrapped in aluminum foil
4. HPLC grade MeOH
5. Acetone
6. Sodium hydroxide (NaOH)
7. 4-(2-hydroxyethyl)piperazine-1-ethanesulfonic acid (HEPES)
8. Potassium chloride (KCl)
9. Ethylene glycol-bis(2-aminoethylether)-N,N,N',N'-tetraacetic acid (EGTA)
10. Calcium chloride ($CaCl_2$)
11. 1,4-Dithiothreitol (DTT)

Proteins

1. PLC-γ1 (residues 21-1215) referred to as PLC-γ1 (WT)
2. PLC-γ1 (residues 21-1215) D1165H referred to as PLC-γ1 (D1165H)
3. Fatty acid-free bovine serum albumin (FAF BSA)

Methods

Overview

The final assay is carried out in a 384-well plate at a volume of 12 μL. The assay mixture contains HEPES (33.9 mM, pH 7.4), KCl (70 mM), EGTA (3 mM), $CaCl_2$ (2.35 mM), DTT (2 mM), FAF BSA (0.17 mg/mL), PE (192 μM), PIP_2 (48 μM), XY-69 (0.5 μM), and the desired concentration of PLC isozyme (see Note 1). Under these conditions, the free Ca^{2+} concentration is approximately 390 nM (see Notes 2, 3). The assay takes approximately 3 hours from reagent set-up to completion of data acquisition.

Preparation of buffers

1. Prepare stock solution A (see Note 4) containing 120 mM HEPES (pH 7.4) (see Note 5), 420 mM KCl, 18 mM EGTA, and 14.1 mM $CaCl_2$.
2. Make 1 mL of lipid vesicle assay buffer (LVAB) fresh for the assay by adding 12 μL of 1 M DTT (stored at -20°C) to 988 μL of the stock solution A.
3. Make 1.2 mL of PLC dilution buffer (PLCDB) by mixing 200 μL of LVAB, 120 μL of 10 mg/mL FAF BSA, and 880 μL of H_2O (see Note 6).
4. Make lipid sonication buffer containing 20 mM HEPES (pH 7.4).

Generation of lipid films and lipid vesicles

1. Briefly vortex and spin-down a thawed aliquot of XY-69 stock solution (210 μM in H_2O), then transfer 1.5 μL to the bottom of a borosilicate culture tube.
2. Dry with a gentle stream of N_2 for 5 min.
3. Allow PIP_2 and PE stock solutions to equilibrate to room temperature, then vortex briefly.
4. Transfer 34.1 μL of PIP_2 stock solution (912 μM) to the bottom of the tube containing XY-69. Tap the tube gently to re-dissolve the XY-69 flake.
5. Add 9.4 μL of PE stock solution (13.2 mM) into the PIP_2/XY-69 solution, followed by 20 μL of HPLC grade MeOH (see Note 7). Dry this mixture down to an opaque film on the bottom of the tube using a gentle stream of N_2 (see Note 8).
6. Leave the lipid film (see Note 9) under a gentle stream of N_2 for at least another 60 min to remove the bulk of organic solvent, then remove remaining traces of solvent by applying high vacuum (0.5 mtorr) for at least 60 min (see Note 10).
7. Add 450 μL of lipid sonication buffer to the dry lipid film, and then clamp the tube securely to a ring stand (see Note 11).
8. Submerge the probe tip of a sonicator halfway down into the solution. The probe tip should be positioned vertically and centered in the tube (see Note 12).
9. Place the tube in a Dewar flask containing iced-water (ice bath) and cool the solution for 45 seconds.
10. Pulse the sonicator at 20% output for three cycles of 5 seconds ON, 15 seconds OFF (see Note 13).
11. Remove the tube from the ice bath and cover the opening with a septum. Confirm that the solution is free of particulate matter and that no lipid film remains on the

bottom of the tube. Allow the solution to equilibrate to room temperature for at least 15 min.

12. Subject the lipid vesicles to freeze-thaw (see Note 14) by immersing the tube in a Dewar flask containing acetone-dry ice (dry ice bath, -78°C) for 40 seconds with gentle shaking, followed by immersing in a water bath (35°C) for 70 seconds with gentle shaking. Repeat this process for a total of 6 cycles.
13. Add 90 μL of LVAB directly to the solution at room temperature, and then vortex on a medium intensity setting for 20 sec.
14. Protect the resulting lipid vesicle solution (LVS) from light and store at room temperature (~20°C) until needed for the assay. This solution is calculated to give 1.2 times the desired concentration of lipids in the final assay, since 10 μL of LVS will be mixed with 2 μL of PLC solution to make a 12 μL reaction mixture.

Measurement of PLC activity

1. Dilute PLC proteins using ice-cold PLCDB to 6 times the final concentration in the assay, since PLC solution composes 2 μL out of the final 12 μL in the reaction (see Note 15).
2. Keep PLC solutions on ice until needed for the assay.
3. Warm up the plate reader and allow to equilibrate to assay temperature (see Note 16).
4. Set the excitation wavelength at 485 nm and emission detection wavelength at 520 nm by using a FITC 485 excitation filter and emission 520 filter (see Note 17).
5. To perform the assay in quadruplicate, distribute 2 μL aliquots of PLC solution of a given concentration into four sequential wells of a 384-well microplate (see Note 18). Repeat for each desired concentration of enzyme. Blank PLCDB can be used as a PLC-free or “BSA-only” control.

6. Add 10 μL of LVS into each well containing PLC solution to initiate the assay and immediately insert the assay plate into the plate reader for measurement (see Note 19).
7. Record fluorescence at required time points at 60 second intervals for 20 to 60 min (see Note 20).
8. Use the remaining LVS for dynamic light scattering (DLS) analysis.
9. Add 8 μL of blank PLCDB to a cuvette, followed by 40 μL of LVS and mix gently with a pipette. The resulting mixture contains the same buffer and lipid component concentrations as the microplate PLC assay. Cap the cuvette and insert the sample into the DLS instrument for measurement at a temperature matching the relevant PLC assay conditions (see Note 21).

Notes

1. The parameters presented here are optimal for the range of 1 to 100 nM PLC-γ1 (WT), and 0.1 to 50 nM PLC-γ1 (D1165H).
2. The concentration of free calcium ion is calculated using the Maxchelator program, which accounts for temperature, pH, and ionic strength of the assay mixture, as well as the concentrations of EGTA and total calcium ($CaCl_2$).
3. All PLC isozymes are calcium-dependent, and a calcium ion binds to the active site within the TIM barrel. Therefore, the concentration of free Ca^{2+} is an essential component for signal generation in the XY-69 assay. Fig. 2.1A shows that with 0.3 nM PLC-γ1 (D1165H), 100 nM free Ca^{2+} (this is near basal cytosolic levels)(26) produces modest rate of hydrolysis. However, rates of hydrolysis plateau at concentrations of free Ca^{2+} greater than 400 nM. These results are consistent with a binding affinity (K_d) of ~250 nM for $CaCl_2$ in PLC-γ1 (WT). At 100 μM free Ca^{2+} the assay reagents precipitated, which terminated PLC activity.

4. All stock solutions are made with Milli-Q grade water, adjusted to the desired pH using 8 M NaOH, filtered through a 0.45 μm filter, and stored at 4 °C.
5. The pH of the XY-69 assay buffer controls the protonation state of key amino acid residues and influences the concentration of free Ca^{2+} ions, thereby regulating PLC activity. PLC-γ isozymes are typically purified using HEPES buffer at a pH of 7.4. We have examined PLC-γ1 activity in 34 mM HEPES across a pH range of 6.5 to 8.5 at 20°C and 30°C with the results shown in Fig. 2.1B. These data suggest an optimal assay buffer pH of 7.4 ± 0.2, and that deviating from this range causes precipitous loss of PLC-γ1 activity.
6. The final composition of PLCDB includes 20 mM HEPES (pH 7.4), 70 mM KCl, 3 mM EGTA, 2.35 mM $CaCl_2$, 2 mM DTT, and 1 mg/mL FAF BSA. We recommend making PLCDB fresh for the assay and cool the solution on ice prior to making PLC dilutions.
7. The addition of MeOH leads to a more even, homogenous film as the volume is reduced under the N_2 stream. Warmth from the hands also helps to prevent early precipitation of lipids due to evaporative cooling.
8. The goal is to maintain XY-69, PE, and PIP_2 on the bottom of the tube where the resulting film will be most efficiently reached by energy from the sonication probe tip. We recommend drying the film gently to avoid blowing lipid solutions up the sides of the tube and rotate the tube slowly while drying in order to form an even layer.
9. We have investigated the effects of composition of the lipid film on the assay. The assay tolerates a wide range of vesicles with different lipid compositions. We obtained the best data quality using lipid vesicles with a final PE/PIP_2 content of 220/20 or 192/48 μM.

10. We recommend use of high vacuum when drying lipid films, but if one is not available then leave the lipid films under streaming N_2 for at least two hours.
11. The outcome of lipid vesicle formation by probe sonication depends on several factors, including solution volume, temperature, vessel size and shape, lipid concentration, transducer percent output, pulse time, probe tip immersion depth, and probe tip diameter. Due to the sensitivity of this assay to the properties of lipid vesicles, deviation from the recommended parameters may affect assay performance and require re-optimization.
12. If probe tip placement is too high, then foaming of the solution may occur. If probe placement is too low, inadequate circulation of contents may cause a problem. Review manufacturer's instructions for additional tips on optimizing this step.
13. If the scale of LVS is changed, this step may require re-optimization of tube size, sonication power output, sonication time, and/or probe tip depth.
14. The freeze-thaw step increases the size of lipid vesicle.
15. When the solutions containing PLC isozymes are mixed, we recommend gentle pipette mixing or inversion only.
16. This assay has been successfully performed in our laboratory at temperatures ranging from 20°C to 37°C. Running the assay at room temperature offers simplicity, and PLC activity generally increases with temperature under the listed conditions without detriment to data quality.
17. Other default settings may need to be optimized depending on the type of microplate and plate reader used.
18. The use of multichannel pipettes is recommended for minimizing error and reducing the amount of time it takes to assemble the assay. Otherwise, the experimenter should work quickly to avoid losing early data points on highly active samples. Keep any microplates and feeder solutions covered as much as practical

to exclude dust, minimize evaporation, and protect fluorescent molecules from light.

19. The addition of 10 μL LVS into 2 μL PLC solution should provide adequate mixing of assay components. A single gentle pipette mix of each well may be useful for homogenizing more complex samples. Additionally, gentle tapping on the side of the microplate may help even out all menisci prior to placing in the reader.
20. The representative enzymatic reaction progression curves with different concentrations of PLC-γ1 (D1165H) in two lipid vesicle conditions are shown in Fig. 2.2.
21. Membrane curvature and vesicle size have been shown to influence vesicle binding (27), domain conformation (28), and catalytic activity (29, 30) of phospholipase enzymes. Consequently, we investigated the effects of vesicle size on the XY-69 based assay. Lipid vesicles generated from probe sonication alone have Z-average size (Z_{av}) in the range of 150-160 nm (Fig. 2.3A). We noticed that repeated freezing and thawing (freeze-thaw) of sonicated lipids produces larger vesicles ranging from 180 to 250 nm (Fig. 2.3B). The autoinhibited, wild type PLC-γ1 has significantly higher activity in smaller-sized lipid vesicles (Fig. 2.3C) than in larger-sized ones (Fig. 2.3D). The relative activity of constitutively active mutant PLC-γ1 (D1165H) to that of wild type enzyme is approximately 2-fold in vesicles prepared from probe sonication alone. This ratio increased to 9-fold when lipid vesicles were prepared by first probe sonication and then freeze-thaw. Therefore, membrane-dependent regulation of PLC activity due to external stimulations or mutations are better monitored with XY-69 embedded in larger lipid vesicles.

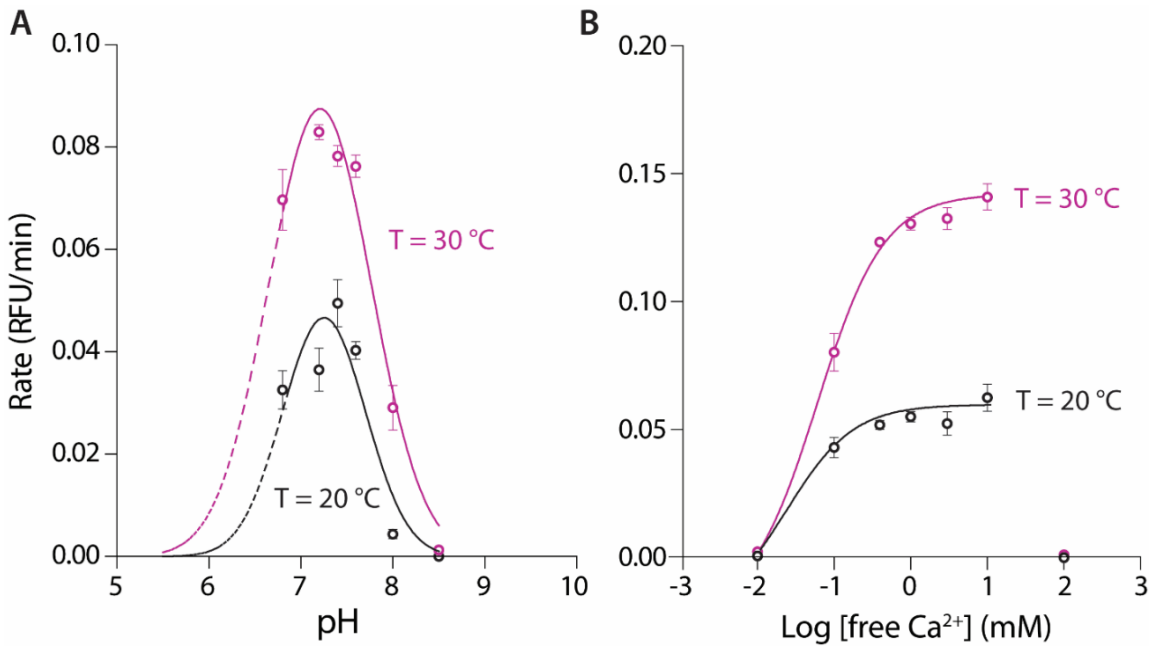

Figure 2.1 – Effects of pH and free Ca^{2+} concentration on XY-69 hydrolysis. A. pH effect. Lipid vesicles consisting of PE (192 μM), PIP_2 (48 μM) and XY-69 (0.5 μM) in assay buffers with varying pH were added to PLC-γ1 (D1165H) (1 nM) at 20°C or 30°C. The initial velocity of XY-69 hydrolysis was measured and plotted against pH. The free Ca^{2+} concentration was 390 nM. **B**. Effect of free Ca^{2+} concentration. The initial velocity of XY-69 (0.5 μM) hydrolysis by PLC-γ1 (D1165H) (1 nM) was measured with varying concentration of free Ca^{2+} in the assay buffer (pH 7.4) at 20°C or 30°C.

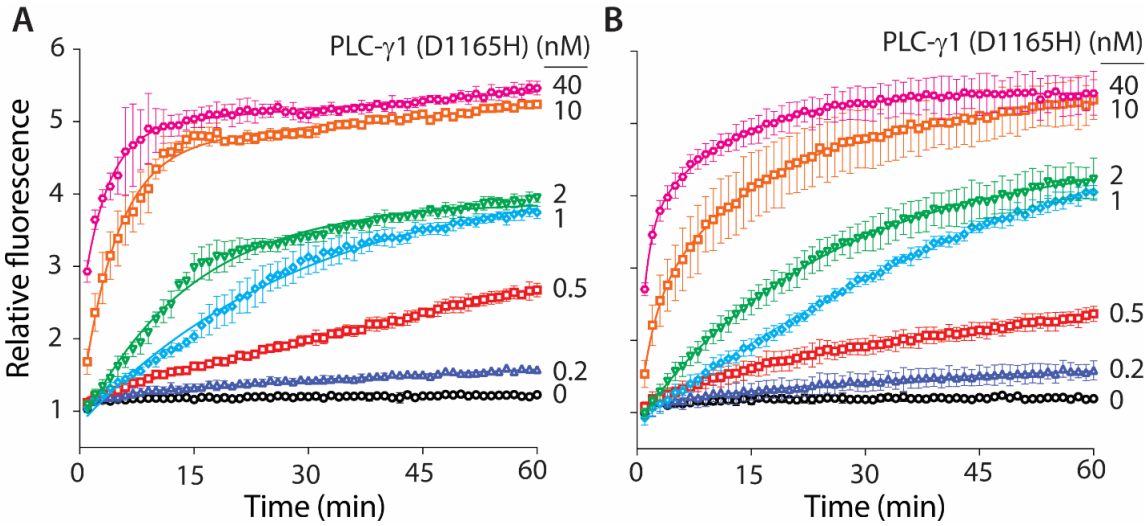

Figure 2.2 – Phospholipase activity of PLC-γ1 (D1165H) in lipid vesicles. A. XY-69 (0.5 μM) was embedded into lipid vesicles containing PE (200 μM) and PIP_2 (20 μM) and added to PLC-γ1 (D1165H) with indicated concentration to initiate the hydrolysis. The reaction progression at 20°C was monitored continuously for 60 min by fluorescence ($\lambda_{ex}/\lambda_{em}$ = 344/520 nm). The final assay buffer has a pH of 7.4 and free Ca^{2+} concentration at 390 nm. **B**. The concentration of PE and PIP_2 in lipid vesicles was 192 and 48 μM, respectively. The experiment was run similarly as described in **A**.

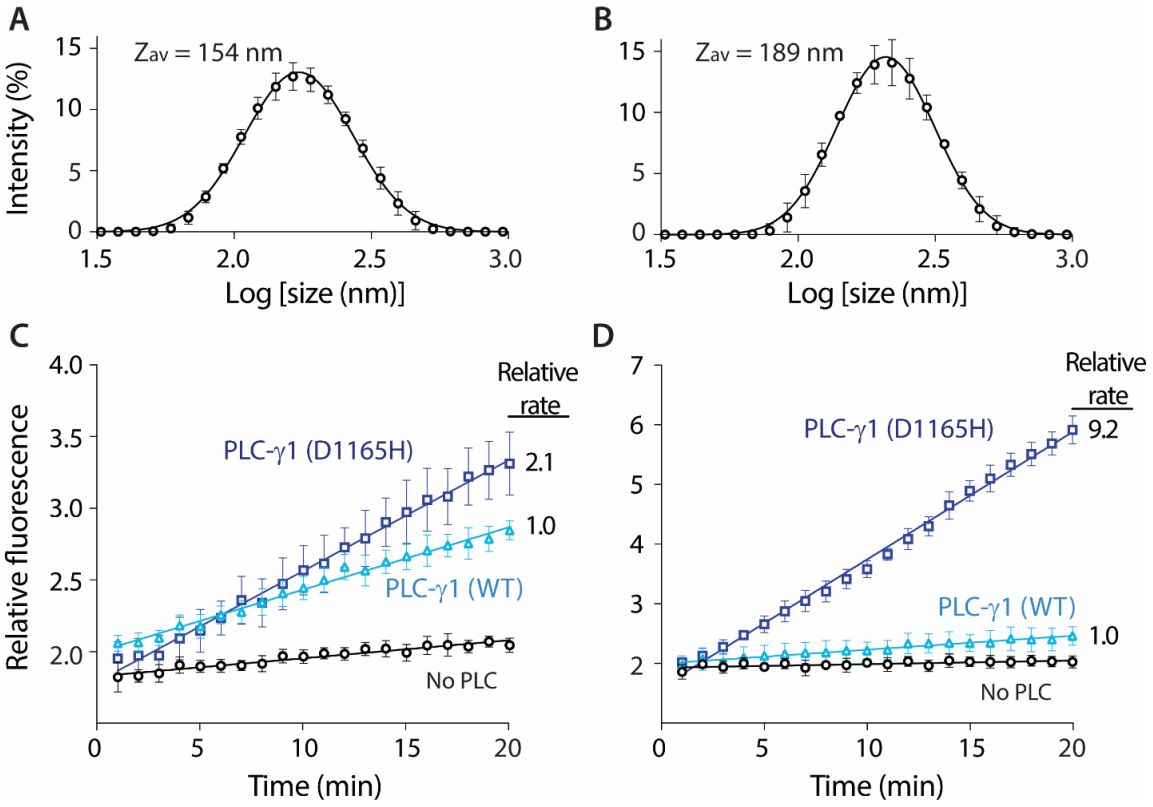

Figure 2.3 – Size of lipid vesicle affects the relative rate of XY-69 hydrolysis. A, **B**. The z-average (z_{av}) particle size of lipid vesicles were measured by dynamic light scattering (DLS). Lipid vesicles were formed either by probe sonication only (**A**) or by first probe sonication and then freeze-thaw (**B**). **C**, **D**. XY-69 (0.5 μM) hydrolysis by PLC-γ1 (WT) or PLC-γ1 (D1165H) at 20°C was monitored by fluorescence (λex/λem = 344/520 nm). Lipid vesicles were formed either by probe sonication only (**C**) or by first probe sonication and then freeze-thaw (**D**). All lipid vesicles contain PE (192 μM) and PIP_2 (48 μM). The final pH of the assay buffer was 7.4 and the free Ca^{2+} concentration was 390 nM.

REFERENCES

1. Harden TK, Sondek J (2006) Regulation of phospholipase C isozymes by Ras superfamily GTPases. Annu Rev Pharmacol Toxicol 46:355-379. doi:10.1146/annurev.pharmtox.46.120604.141223

2. Hicks SN, Jezyk MR, Gershburg S et al (2008) General and versatile autoinhibition of PLC isozymes. Mol Cell 31:383-394. doi:10.1016/j.molcel.2008.06.018

3. Hajicek N, Charpentier TH, Rush JR et al (2013) Autoinhibition and phosphorylation-induced activation of phospholipase C-γ isozymes. Biochemistry 52:4810-4819. doi:10.1021/bi400433b

4. Rhee SG (2001) Regulation of phosphoinositide-specific phospholipase C. Annu Rev Biochem 70:281-312. doi:10.1146/annurev.biochem.70.1.281

5. Balla T (2013) Phosphoinositides: tiny lipids with giant impact on cell regulation. Physiol Rev 93:1019-1137. doi:10.1152/physrev.00028.2012

6. Koss H, Bunney TD, Behjati S et al (2014) Dysfunction of phospholipase C-γ in immune disorders and cancer. Trends Biochem Sci 39:603-611. doi:10.1016/j.tibs.2014.09.004

7. Martins M, McCarthy A, Baxendale R et al (2014) Tumor suppressor role of phospholipase C-ε in Ras-triggered cancers. Proc Natl Acad Sci U S A 111:4239-4244. doi:10.1073/pnas.1311500111

8. Kataoka K, Nagata Y, Kitanaka A et al (2015) Integrated molecular analysis of adult T cell leukemia/lymphoma. Nat Genet 47:1304-1315. doi:10.1038/ng.3415

9. Sims R, van der Lee SJ, Naj AC et al (2017) Rare coding variants in PLCG2, ABI3, and TREM2 implicate microglial-mediated innate immunity in Alzheimer's disease. Nat Genet 49:1373-1384. doi:10.1038/ng.3916

10. Magno L, Lessard CB, Martins M et al (2019) Alzheimer's disease phospholipase C-γ2 (PLCG2) protective variant is a functional hypermorph. Alzheimers Res Ther 11:16. doi:10.1186/s13195-019-0469-0

11. Cremasco V, Graham DB, Novack DV et al (2008) Vav/Phospholipase C-γ2-mediated control of a neutrophil-dependent murine model of rheumatoid arthritis. Arthritis Rheum 58:2712-2722. doi:10.1002/art.23757

12. Afroz S, Giddaluru J, Vishwakarma S et al (2017) A Comprehensive Gene Expression Meta-analysis Identifies Novel Immune Signatures in Rheumatoid Arthritis Patients. Front Immunol 8:74. doi:10.3389/fimmu.2017.00074

13. Waldo GL, Ricks TK, Hicks SN et al (2010) Kinetic scaffolding mediated by a phospholipase C-β and Gq signaling complex. Science 330:974-980. doi:10.1126/science.1193438

14. Smrcka AV, Hepler JR, Brown KO et al (1991) Regulation of polyphosphoinositide-specific phospholipase C activity by purified Gq. Science 251:804-807. doi:10.1126/science.1846707

15. Seifert JP, Snyder JT, Sondek J et al (2006) Direct activation of purified phospholipase C-ε by RhoA studied in reconstituted phospholipid vesicles. Methods Enzymol 406:260-271. doi:10.1016/S0076-6879(06)06019-8

16. Litosch I (2000) Regulation of phospholipase C-β1 activity by phosphatidic acid. Biochemistry 39:7736-7743. doi:10.1021/bi000022y

17. Liu Y, Mihai C, Kubiak R et al (2007) Phosphorothiolate analogues of phosphatidylinositols as assay substrates for phospholipase C. Chembiochem 8:1430-1439. doi:10.1002/cbic.200700061

18. Rukavishnikov AV, Zaikova TO, Birrell GB et al (1999) Synthesis of a new fluorogenic substrate for the continuous assay of mammalian phosphoinositide-specific phospholipase C. Bioorg Med Chem Lett 9:1133-1136. doi:10.1016/s0960-894x(99)00166-3

19. Zaikova TO, Rukavishnikov AV, Birrell GB et al (2001) Synthesis of fluorogenic substrates for continuous assay of phosphatidylinositol-specific phospholipase C. Bioconjug Chem 12:307-313. doi:10.1021/bc0001138

20. Rose TM, Prestwich GD (2006) Synthesis and evaluation of fluorogenic substrates for phospholipase D and phospholipase C. Org Lett 8:2575-2578. doi:10.1021/ol060773d

21. Huang W, Hicks SN, Sondek J et al (2011) A fluorogenic, small molecule reporter for mammalian phospholipase C isozymes. ACS Chem Biol 6:223-228. doi:10.1021/cb100308n

22. Huang WG, Wang XY, Endo-Streeter S et al (2018) A membrane-associated, fluorogenic reporter for mammalian phospholipase C isozymes. J Biol Chem 293:1728-1735. doi:10.1074/jbc.RA117.000926

23. Waldo GL, Boyer JL, Morris AJ et al (1991) Purification of an AlF4- and G-protein bg-subunit-regulated phospholipase C-activating protein. J Biol Chem 266:14217-14225

24. Harden TK, Morris AJ, Waldo GL et al (1991) Avian G-protein-regulated phospholipase C. Biochem Soc Trans 19:342-346. doi:10.1042/bst0190342

25. Hajicek N, Keith NC, Siraliev-Perez E et al (2019) Structural basis for the activation of PLC-γ isozymes by phosphorylation and cancer-associated mutations. eLife 2019;8:e51700 doi: 10.7554/eLife.51700

26. Clapham DE (2007) Calcium signaling. Cell 131:1047-1058. doi:10.1016/j.cell.2007.11.028

27. Wehbi H, Feng J, Kolbeck J et al (2003) Investigating the interfacial binding of bacterial phosphatidylinositol-specific phospholipase C. Biochemistry 42:9374-9382. doi:10.1021/bi034195+

28. Uekama N, Aoki T, Maruoka T et al (2009) Influence of membrane curvature on the structure of the membrane-associated pleckstrin homology domain of phospholipase C-δ1. Biochim Biophys Acta 1788:2575-2583. doi:10.1016/j.bbamem.2009.10.009

29. Ahyayauch H, Villar AV, Alonso A et al (2005) Modulation of PI-specific phospholipase C by membrane curvature and molecular order. Biochemistry 44:11592-11600. doi:10.1021/bi050715k

30. Burack WR, Biltonen RL (1994) Lipid bilayer heterogeneities and modulation of phospholipase A2 activity. Chem Phys Lipids 73:209-222. doi:10.1016/0009-3084(94)90182-1

CHAPTER III: STRUCTURAL BASIS FOR ACTIVATION OF PLC-γ ISOZYMES[2]

Background

The 13 phospholipase C (PLC) isozymes expressed in humans preferentially hydrolyze the membrane phospholipid phosphatidylinositol 4,5-bisphosphate (PIP_2) to generate the second messengers diacylglycerol and inositol 1,4,5-trisphosphate (IP_3) (1, 2). Diacylglycerol is retained within membranes where it recruits and activates numerous proteins including conventional isoforms of protein kinase C. In contrast, IP_3 diffuses throughout the cytosol where it binds to IP_3 receptors embedded in endoplasmic reticulum leading to mobilization of sequestered calcium. PLC-mediated depletion of PIP_2 also modulates the activities of several ion channels and proteins with phosphoinositide-binding domains. Thus, the PLCs coordinate fluctuations in PIP_2 levels and the bifurcating signaling pathways emanating from PIP_2 hydrolysis to regulate numerous cellular processes, including fertilization and embryogenesis, cell proliferation and differentiation, as well as various types of cell migration (3-6).

The two PLC-γ isozymes, PLC-γ1 and PLC-γ2, are unique among the PLCs in that they are directly activated by tyrosine phosphorylation. PLC-γ1 and PLC-γ2 are phosphorylated on equivalent sites, Tyr783 and Tyr759, respectively, and this phosphorylation is typically required to stimulate phospholipase activity. Several classes of tyrosine kinases phosphorylate and activate the PLC-γ isozymes. These include many receptor tyrosine kinases (RTKs) including Trk receptors (7, 8) and many growth factor receptors such as EGFR (9-13).

[2] This chapter previously appeared as an article in the journal eLife. The original citation is as follows: Hajicek, N., Keith, N. C., Siraliev-Perez, E., Temple, B. R. S., Huang, W., Zhang, Q., Harden, T. K. and Sondek, J. (2019) "Structural basis for the activation of PLC-γ isozymes by phosphorylation and cancer-associated mutations". *eLife* 8, e51700.

A second large group is soluble tyrosine kinases coupled to immune receptors and includes members of the Src, Syk, and Tec families (14-16). In this way, the PLC-γ isozymes are poised to transduce signals initiated by a wide variety of extracellular stimuli.

The regulated, phosphorylation-dependent activation of PLC-γ1 and -γ2 controls numerous aspects of biology including proper development of the vascular, neuronal, and immune systems during embryonic development, adaptive immune responses, neuronal transmission, bone homeostasis, chemotaxis, and platelet aggregation (17). The PLC-γ isozymes have also recently emerged as drivers of several human diseases (18). Notably, genome-wide sequencing studies have demonstrated that PLC-γ1 and PLC-γ2 are frequently and recurrently mutated in several leukemias and lymphomas. In fact, PLC-γ1 is the most frequently (~40%) mutated gene in adult T cell leukemia/lymphoma, where mutant forms of the isozyme are presumed to drive oncogenesis through enhanced phospholipase activity coupled to elevated NFAT- and NF-κB-dependent transcription (19-20). Moreover, activating mutations in PLC-γ2 arise with high frequency (~30%) in patients with B cell leukemias treated with ibrutinib (21), a covalent inhibitor of Bruton's tyrosine kinase (BTK). PLC-γ2 is a major BTK substrate and mutations in PLC-γ2 likely function as escape mutations, reactivating pathways controlling cell survival and proliferation that are usually rendered quiescent by ibrutinib treatment. Mutated, and presumably active, forms of the PLC-γ isozymes are also found in patients with angiosarcomas (22), and several disorders associated with dysregulated immune responses (23, 24), inflammatory bowel disease (25), and familial steroid-sensitive nephrotic syndrome (26, 27). A naturally occurring variant of PLC-γ2 that is moderately active is strongly associated with protection from late-onset Alzheimer's disease (28, 29) and highlights the notion that aberrant PLC activity can be either deleterious or beneficial

depending on the context. However, for the vast majority of mutant forms of PLC-γ1 and PLC-γ2, an increase in lipase activity has not been demonstrated directly.

While the PLC-γ isozymes control essential aspects of both normal and disease-associated cellular processes, the molecular mechanisms controlling these enzymes remain elusive. Broadly, phosphorylation-dependent activation of PLC-γ1 and PLC-γ2 is controlled by an array of regulatory domains unique to these isozymes. In particular, the regulatory array harbors the obligatory sites of tyrosine phosphorylation (9, 10, 30), and also includes an SH2 domain (nSH2) required for tyrosine kinase binding (31). The array also mediates basal autoinhibition of phospholipase activity, since removal or mutation of a second SH2 domain (cSH2) within the array results in robust and constitutive activation of PLC-γ isozymes *in vitro* and in cells (30, 32). The regulatory array is completed by a split PH (sPH) domain and an SH3 domain, which modulate PLC activity by scaffolding numerous signaling and adaptor proteins (33, 34).

Although these general aspects of the regulation of PLC-γ1 and PLC-γ2 are well-documented, several fundamental questions remain unresolved. For example, the other half of the autoinhibitory interface formed by the cSH2 domain has not been identified, and how this domain enforces autoinhibition of phospholipase activity is unknown. Possibilities include physical occlusion of the lipase active site, steric hindrance that prevents the enzyme from engaging membranes, or a combination of both as is observed for the PLC-β isozymes (35). Although the cSH2 domain is presumed to be the primary arbiter of autoinhibition, several reports have also implicated the sPH domain in maintaining an autoinhibited state (30, 36). How this domain might contribute to autoinhibition is unknown.

Similarly unclear is how autoinhibition is relieved by tyrosine phosphorylation. Phosphorylated Tyr783 in PLC-γ1 binds with nanomolar affinity to the cSH2 domain, and

this engagement presumably couples a large, but ill-defined conformational rearrangement within the array to activation (30, 32, 37). However, even these few mechanistic details are under debate since an alternative model posits engagement of RTKs by the cSH2 domain as an initial step required for activation (38).

The paucity of mechanistic understanding of the activation of the PLC-γ isozymes is largely attributable to a lack of structural information. While structures of isolated portions of the regulatory array of PLC-γ1 are available, these structures provide an incomplete and sometimes erroneous context for defining how the array integrates the functions of basal autoinhibition and phosphorylation-dependent activation. There are no structures of full-length PLC-γ isozymes.

Here we describe the 2.5 Å-resolution crystal structure of essentially full-length PLC-γ1. The structure highlights a regulatory array exquisitely positioned to prevent membrane engagement of the catalytic core while simultaneously arranged to scaffold tyrosine kinases and additional regulatory proteins into a signaling nexus. Kinases have unfettered access to the nSH2 domain of the regulatory array and will dock here initially. In contrast, the phosphotyrosine binding pocket within the cSH2 domain is buried through interactions with the catalytic core. Docked kinases are well positioned to phosphorylate Tyr783 located within a nearby solvent-exposed loop and phosphorylated Tyr783 (pTyr783) is expected to bind the cSH2 domain to disrupt its interaction with the catalytic core. This disruption is predicted to favor a substantial rearrangement of PLC-γ1 required for productive membrane engagement and hydrolysis of PIP_2. The structure also explains how cancer-associated substitutions disrupt autoinhibition to elevate basal PLC-γ1 activity and contribute to supra-activation of the isozyme in the context of receptor overexpression. The combined effects of substitution and tyrosine phosphorylation

suggest that cellular context, e.g., overexpression of EGFR found in many cancers, will be especially important for understanding diseases modulated by the PLC-γ isozymes.

Materials and Methods

DNA constructs

Mammalian expression constructs- Gibson Assembly cloning (39) was used to introduce single amino acid substitutions into full-length rat PLC-γ1 (UniProt accession number P10686; 96% identical to human PLC-γ1) and human PLC-γ2 (P16885) in a modified pcDNA3.1 expression vector that incorporates an HA epitope tag at the N-terminus of the expressed protein. The entire open reading frame of all constructs was confirmed by automated dideoxy sequencing.

Bacterial expression constructs- The construct encoding a constitutively active form of the soluble kinase domain of FGFR2 (FGFR2K E565A) was described previously (30).

Baculovirus transfer vectors- PLC-γ1(21-1215) was amplified from full-length rat PLC-γ1 by PCR and then subcloned into a modified pFastBacHT1 vector that incorporates a His_6 tag followed by a tobacco etch virus (TEV) protease recognition sequence at the N-terminus of the expressed protein. Transfer vectors encoding PLC-γ1(21-1215) harboring the P867R or D1165H substitutions were generated similarly, using the full-length mutant forms of PLC-γ1 as PCR templates. The Δ25 deletion, which replaces residues 766-790 of PLC-γ1 with a Ser-Gly-Ser linker, was introduced into the transfer vector encoding PLC-γ1(21-1215) by standard primer-mediated mutagenesis. PLC-γ1(21-1215) and PLC-γ1(21-1215) Δ25 were amplified by PCR and subcloned into the modified pcDNA3.1 expression vector described above using a ligation-independent cloning strategy (40).

Protein expression and purification

PLC-γ1(21-1215) Δ25- Recombinant baculovirus encoding His_6-PLC-γ1(21-1215) Δ25 was prepared using the Bac-to-Bac Baculovirus Expression System according to the manufacturer's protocol (Invitrogen). Four liters of HighFive (*T. ni*) cells at a density of ~2.0 x 10^6 cells/mL were infected with amplified baculovirus stock (10 - 15 mL/L) and harvested ~60 h post-infection by centrifugation at 6,000 rpm in a Beckman JA-10 rotor at 4°C. All subsequent centrifugation and chromatography steps were performed at 4°C.

The cell pellet was resuspended in 200 mL of ice-cold buffer N1 (20 mM HEPES (pH 7.5), 300 mM NaCl, 10 mM imidazole, 10% v/v glycerol, 0.1 mM EDTA, and 0.1 mM EGTA) supplemented with 10 mM 2-mercaptoethanol and protease inhibitor cocktail prior to lysis using an EmulsiFlex-C5 homogenizer. Crude lysate was centrifuged at 50,000 rpm for 1 h in a Beckman Ti70 rotor. The supernatant was filtered through a 0.45 μm PES low protein-binding filter and loaded onto a 5 mL HisTrap HP IMAC column equilibrated in buffer N1 supplemented with 5 mM 2-mercaptoethanol. The column was washed with 15 column volumes (CV) of buffer N1, followed by 15 CV of 2.5% buffer N2 (buffer N1 + 1 M imidazole and 5 mM 2-mercaptoethanol). Bound proteins were eluted with 40% buffer N2. Fractions containing PLC-γ1 were pooled and dialyzed overnight in the presence of 2% w/w TEV protease to remove the His_6 tag in buffer containing 20 mM HEPES (pH 7.5), 300 mM NaCl, 10% v/v glycerol, 1 mM DTT, 1 mM EDTA, and 0.1 mM EGTA. The sample was subsequently diluted 2-fold with buffer N1 and applied to a 5 mL HisTrap HP column. Flow-through fractions containing cleaved PLC-γ1 were pooled, diluted 3-fold with buffer Q1 (20 mM HEPES (pH 7.5) and 2 mM DTT), and loaded onto an 8 mL SourceQ anion exchange column equilibrated in 10% buffer Q2 (buffer Q1 + 1 M NaCl). Bound proteins were eluted in a linear gradient of 10% - 60% buffer Q2 over 50 CV. Fractions containing PLC-γ1 were pooled, concentrated using a VivaSpin 50K MWCO centrifugal concentrator,

and applied to a 16 mm x 700 mm HiLoad Superdex 200 size exclusion column equilibrated in buffer containing 20 mM HEPES (pH 7.5), 150 mM NaCl, and 2 mM DTT. Pure PLC-γ1 was concentrated as described above to a final concentration of 40 - 50 mg/mL, aliquoted, snap-frozen in liquid nitrogen, and stored at -80°C until use. Wild-type PLC-γ1(21-1215), PLC-γ1(21-1215) P867R, and PLC-γ1(21-1215) D1165H used for biochemical assays were purified using the method described above except that the buffer for size exclusion chromatography was supplemented with 5% v/v glycerol.

FGFR2K E565A - The soluble kinase domain of FGFR2 (residues 458-778) harboring a His_6 tag at its N-terminus was expressed in the Rosetta2 pLysS strain of *E. coli* (Novagen). Cells were grown at 37°C in TB medium containing 0.1 mg/mL ampicillin and 0.034 mg/mL chloramphenicol to an OD_{600} of ~3.0. Protein expression was induced for 2 h at 30°C with 0.1 mM IPTG (final concentration). Cells were collected by centrifugation, resuspended in lysis buffer (20 mM HEPES (pH 7.5), 300 mM NaCl, 10 mM 2-mercaptoethanol, 10 mM imidazole, 10 mM $MgCl_2$, 10 μM ATP, 10% v/v glycerol, and protease inhibitor cocktail), and lysed using an EmulsiFlex-C5 homogenizer. CHAPS was then added to a final concentration of 0.5% w/v and the lysate incubated at 4°C for 30 min. Soluble lysate was prepared by ultracentrifugation and the kinase domain isolated by IMAC on a HisTrap HP column. The protein was further purified by size exclusion chromatography on a Sephacryl 200 size exclusion column equilibrated in 20 mM HEPES (pH 7.5), 200 mM NaCl, 2 mM DTT, and 5% v/v glycerol. Protein was aliquoted, snap-frozen in liquid nitrogen, and stored at -80°C until use.

Size-exclusion chromatography coupled to multi-angle light scattering

Multi-angle light scattering measurements were performed using a Wyatt DAWN HELEOS II light scattering instrumentation (with Wyatt Optilab T-rEX refractometer and Wyatt dynamic light scattering module) coupled to a Superdex 200 10 mm x 300 mm GL

size exclusion column. Following equilibration with buffer containing 20 mM HEPES (pH 7.4), 150 mM NaCl, and 0.02% w/v NaN_3, 50 μL of PLC-γ1(21-1215) proteins at 2 mg/mL were loaded onto the column. Data analysis was performed with ASTRA software version 6 (Wyatt Technologies).

Crystallization of PLC-γ1(21-1215) Δ25

Native PLC-γ1(21-1215) Δ25- Crystals of PLC-γ1(21-1215) Δ25 were grown initially by sitting drop vapor diffusion. PLC-γ1(21-1215) Δ25 was diluted to 20 mg/mL in buffer containing 20 mM HEPES (pH 7.5), 150 mM NaCl, 5 mM DTT, and 0.25% w/v CHAPSO. Two hundred nanoliters of this protein solution was mixed with 100 nanoliters of reservoir solution (200 mM di-sodium tartrate and 20% w/v PEG 3,350) and equilibrated against a 30 μL reservoir. Crystals grew as a cluster of thin plates and appeared after 9 days at 20°C. Diffraction quality crystals of PLC-γ1(21-1215) Δ25 were grown at 20°C by microseeding hanging drops. Protein solution was prepared by diluting PLC-γ1(21-1215) Δ25 to 40 mg/mL in buffer containing 20 mM HEPES (pH 7.5), 150 mM NaCl, 5 mM DTT, and 0.25% w/v CHAPSO. Solutions of seed crystals were obtained by vortexing crystals of PLC-γ1(21-1215) Δ25 with a glass bead in buffer containing 200 mM di-sodium tartrate, 25% w/v PEG 3,350, 150 mM NaCl, 5 mM DTT, and 0.25% w/v CHAPSO. Seed crystals were diluted 100-fold in the same buffer prior to use. Drops were prepared by mixing, in order, 1 μL of reservoir solution (12.5% w/v PEG 3,350, 50 mM di-sodium tartrate, and 5% v/v glycerol), 2 μL of protein solution, and 0.5 μL of seed solution. Drops were equilibrated against a 500 μL reservoir. Crystals ~100 μm on the longest edge appeared after 1-2 days and were flash-frozen in liquid nitrogen on nylon loops.

Gadolinium-derivatized PLC-γ1(21-1215) Δ25- PLC-γ1(21-1215) Δ25 (335 μM) was treated with a 50-fold molar excess of EGTA for 1 h at 4°C. The protein was then

exchanged into crystallization buffer (20 mM HEPES (pH 7.5), 150 mM NaCl, 5 mM DTT, 5 μM EGTA, 1 mM $GdCl_3$, and 0.25% w/v CHAPSO) using a 7K MWCO Zeba spin desalting column (Thermo Scientific). The final protein concentration in this solution was 36 mg/mL. A solution of seed crystals was prepared as described above except that the buffer contained 50 mM di-sodium tartrate, 20% w/v PEG 3,350, 5% v/v glycerol, 150 mM NaCl, 5 mM DTT, 0.25% w/v CHAPSO, 5 μM EGTA, and 1 mM $GdCl_3$. Drops were prepared by mixing, in order, 1 μL of reservoir solution (12.5% w/v PEG 3,350, 25 mM di-sodium tartrate, and 10% v/v glycerol), 2 μL of protein solution, and 0.5 μL of seed solution. Drops were equilibrated against a 500 μL reservoir. Crystals grew at 20°C and were transferred from the mother liquor and soaked in buffer containing 25 mM HEPES (pH 7.5), 150 mM NaCl, 5 mM DTT, 0.25% w/v CHAPSO, 12.5% w/v PEG 3,350, 10% v/v glycerol, and 5 mM $GdCl_3$ for 3 min at room temperature. Crystals were mounted on nylon loops and flash-frozen in liquid nitrogen.

X-ray diffraction data collection and structure determination

X-ray diffraction data were collected on crystals of native PLC-γ1(21-1215) Δ25 at the Southeast Regional Collaborative Access Team (SER-CAT) beamline 22-BM at the Advanced Photon Source at Argonne National Laboratory. One scan totaling 200° of data was collected at 100 K on a MAR 200 CCD detector. Each frame was exposed for 10 sec and consisted of a 1° oscillation.

Gadolinium-derivatized crystals of PLC-γ1(21-1215) Δ25 were used to collect a single-wavelength anomalous diffraction (SAD) dataset at the gadolinium absorption peak (λ = 7,244.3 eV). Data were acquired at SER-CAT beamline 22-ID on a Rayonix MX300-HS CCD detector. Each frame consisted of a 1° oscillation and was exposed for 1 sec. A

total of 240° of data were collected at 100 K in 30° wedges using an inverse beam strategy. Both sets of diffraction data were indexed, integrated, and scaled using HKL2000 (41).

Phases for the gadolinium-bound form of PLC-γ1(21-1215) Δ25 were solved by SAD using the AutoSol routine in the Phenix software suite (42). A partial model of this structure was built using AutoBuild (43) and used as a molecular replacement search model to solve phases for the structure of native PLC-γ1(21-1215) Δ25. The remainder of the model was then built in an iterative process that consisted of manual model building in Coot (44) followed by restrained refinement in Phenix. The structure was validated using MolProbity (45) and molecular representations produced with PyMOL. Complete data collection and refinement statistics are shown in Supplementary File 1.

Quantification of phospholipase activity in cells

To quantify basal phospholipase activity, HEK293 cells were plated at a density of ~75,000 cells/well in 12-well cluster plates and transiently transfected with 100 ng of vector encoding wild-type or mutant forms of PLC-γ1. Twenty-four hours post-transfection, cells were metabolically labeled overnight in serum-free, inositol-free medium containing 1 μCi of [^{3}H]*myo*-inositol and 10 mM LiCl. Accumulation of [^{3}H]inositol phosphates was quantified as described previously (46). In all experiments, counts that accumulated in cells transfected with empty vector (~500 - 1,000 cpm) were subtracted as background.

EGFR-dependent activation of PLC-γ1 and PLC-γ2 was quantified in HEK293 cells transiently co-transfected with 200 ng of vector expressing various forms of the PLC-γ isozymes and 100 ng of vector expressing wild-type EGFR. Cells were metabolically labeled as described above, except LiCl was omitted from the radiolabeling medium. Cells received a 30 min challenge with the indicated concentrations of recombinant human EGF (Invitrogen) diluted in Hank's Balanced Salt Solution containing 20 mM HEPES (pH 7.5), 10 mM LiCl, and 200 μg/mL fatty acid-free bovine serum albumin (BSA).

Expression of each form of PLC-γ1 and PLC-γ2 was confirmed by immunoblotting of cell lysates using a monoclonal antibody against the HA epitope (BioLegend, clone 16B12). Lysates were also probed with a monoclonal antibody against β-actin (SigmaAldrich, clone AC-15) as a loading control. All immunoblots represent a single exposure from one experiment, and the HA epitope and α-actin were detected on the same blot. Immunoblots were loaded with all mutant versions of PLC-γ1 or PLC-γ2 in numerical order; bands were subsequently cropped and then reordered in Photoshop to reflect the order in which data are presented in bar graphs and dose-response curves. The identity of the HEK293 cell line was not authenticated, and testing for mycoplasma contamination was not performed.

In vitro quantification of phospholipase activity

WH-15 fluorogenic assay - Assays utilizing WH-15 as enzyme substrate were performed as described previously (47) with the following modifications. WH-15 (3 μM, final concentration) was solubilized in a final assay buffer containing 50 mM HEPES (pH 7.4), 70 mM KCl, 3 mM EGTA, 2.9 mM $CaCl_2$, 50 μg/mL fatty acid-free BSA, 2 mM DTT, and 0.25% w/v sodium cholate. Baseline fluorescence was stabilized for 10 min, and fluorescence intensity then was quantified for an additional 15 min following addition of various forms of purified PLC-γ1(21-1215) (1 nM, final concentration). Fluorescence intensity was converted to pmol of 6-aminoquinoline using a standard curve, and initial rates of WH-15 hydrolysis were calculated from the slope of linear data points.

XY-69 fluorogenic assay - All assays with XY-69 (48) were performed at 30°C in 384-well plates in a PHERAstar multi-mode plate reader. Data were recorded for 30 min at intervals of 1 min using excitation and emission wavelengths of 485 nm and 520 nm, respectively. Fluorescence intensity was normalized to a blank reaction lacking phospholipase, and initial rates of XY-69 hydrolysis were calculated from the slope of the

linear portion of the curve. The amount of wild-type and mutant forms of PLC-γ1(21-1215) used in all experiments was adjusted to maintain assay linearity with respect to time and protein concentration. To prepare mixed micelles, XY-69 (5 μM, final concentration) was dried under a stream of nitrogen and solubilized by sonication in a final assay buffer containing 30 mM HEPES (pH 7.4), 70 mM KCl, 3 mM EGTA, 2.35 mM $CaCl_2$, 2 mM DTT, and 0.5% w/v sodium cholate. PLC-γ1(21-1215) proteins (0.5 - 1 nM, final concentration) were diluted in 20 mM HEPES (pH 7.4), 50 mM NaCl, 1 mg/mL fatty acid-free BSA, and 2 mM DTT. Reactions were initiated by adding 10 μL of detergent micelles to 2 μL of PLC-γ1.

Phospholipid vesicles were prepared by combining XY-69, porcine brain phosphatidylinositol 4,5-bisphosphate (PIP_2), and bovine liver phosphatidylethanolamine (PE) and drying the mixture under a stream of nitrogen. Lipids were resuspended by sonication in 20 mM HEPES (pH 7.4). PLC-γ1(21-1215) proteins (0.5 - 1 nM, final concentration) were diluted as described above for mixed micelle assays. Assays were initiated by adding 10 μL of phospholipid vesicles to 2 μL of PLC-γ1 and performed in a final assay buffer consisting of 20 mM HEPES (pH 7.4), 70 mM KCl, 3 mM EGTA, 2.35 mM $CaCl_2$, and 2 mM DTT. Final concentrations of XY-69, PIP_2, and PE were 5 μM, 20 μM, and 220 μM, respectively.

In vitro kinase assay- Equimolar concentrations (35 μM) of PLC-γ1(21-1215) and FGFR2K E565A were incubated on ice in buffer containing 20 mM HEPES (pH 7.4), 50 mM NaCl, 10 mM $MgCl_2$, 0.2 mM Na_3VO_4, 50 ng/mL fatty acid-free BSA, 2 mM DTT, and 0.5 mM ATP. After 1 h, a portion of the reaction mixture was diluted with 20 mM HEPES (pH 7.4), 50 mM NaCl, 1 mg/mL fatty acid-free BSA, and 2 mM DTT. Phospholipase activity was quantified using XY-69 incorporated into mixed micelles or phospholipid vesicles as described above. The concentrations of PLC-γ1(21-1215) and FGFR2K

E565A were both 1 nM in the final reaction mixture. Phosphorylation of PLC-γ1(21-1215) was analyzed by native PAGE on PhastGel homogeneous medium containing 7.5% polyacrylamide followed by staining with Coomassie Brilliant blue.

[^{3}H]PIP$_2$ hydrolysis assay- Quantification of lipase activity using phospholipid vesicles consisting of 200 μM PE, 20 μM PIP$_2$, and ~5,000 cpm/assay [^{3}H]PIP$_2$ was performed as described previously (46).

Homology modeling

PLC-γ2(14-1190) - A model of PLC-γ1(21-1215) containing residues 766-790 was generated with Modeller v9.16 (49) using the structure of PLC-γ1(21-1215) Δ25 as the template. This model of PLC-γ1 was then used as the template to build a model of PLC-γ2(14-1190).

Molecular dynamics simulations

Structural model of PLC-γ1(21-1215) Δ25- The X-ray crystal structure of autoinhibited PLC-γ1 included a number of missing regions presumably due to local disorder. Missing regions that were expected to contain secondary structural elements included: i) helix E of EF hand 2 (residues 190-206) and ii) helix E of EF hand 3 (residues 226-246). In order to build the missing helices, HHpred (50) was used to search for suitable templates. The fragment from the structure of cuttlefish PLC21 (PDB code: 3QR0) (51) containing helix F of EF hand 2 through helix F of EF hand 3 provided the best superimposition on the PLC-γ1 structure and was used as a template for building helix E of EF hand 3. Residues 226 - 233 were deleted from the X-ray structure prior to building a model of this EF hand. The apo structure of troponin C (PDB code: 1TNP) (52) containing helix F of EF hand 1 through helix F of EF hand 2 provided the best superimposition on the structure of PLC-γ1 and was used as the template for building helix

E of EF hand 2. The remaining loops missing from the structure of PLC-γ1 were built as random coils with no regular secondary structural elements. A structural model of PLC-γ1 containing all residues from Glu21 - Lys1215, except for the shortened activation loop, was generated with Modeller v9.16 using the autoinhibited PLC-γ1 structure as the template. The wild-type PLC-γ1 model was subsequently mutated in PyMOL to generate the PLC-γ1(D1165H) model used for molecular dynamics simulations.

Accelerated molecular dynamics simulations- Accelerated molecular dynamics (aMD) simulations utilize an enhanced sampling method that applies a bias or boost potential to the true potential that effectively raises the minima in the potential energy surface, leading to an enhanced escape rate and sampling of longer timescale events with shorter MD simulations. Using the Amber v14 software package (53), conventional MD (cMD) simulations of PLC-γ1 and PLC-γ1(D1165H) in explicit solvent were used for equilibration, followed by a 5 nsec cMD simulation for calculating the boost potential, followed by completion of 145 nsec of boosted aMD simulations. The explicit solvent systems for PLC-γ1 and PLC-γ1(D1165H) were generated using LEaP and contained 1,173 amino acid residues (PLC-γ1: 18,877 atoms, PLC-γ1(D1165H): 18,882), Na^+ ions for charge neutralization (PLC-γ1: 25 ions, PLC-γ1(D1165H): 24 ions), and TIP3P water molecules in an octahedral box (PLC-γ1: 39,688 TIP3P, PLC-γ1(D1165H): 39,700), for total system sizes of ~138,000 atoms. The ff14SB force field (54) was used for parameterization and simulations run using pmemd.cuda. First, the systems underwent minimization for 10,000 steps with a convergence criterion of 0.05 kcal/mol-Å. This was followed by 200 psec dynamics (NVT ensemble) for heating, with the thermostat target temperature increasing linearly from 0K to 300K over the course of the 200 psec using a Berendsen thermostat with a relaxation time of 0.5 psec. Protein atoms were restrained with a harmonic potential of weight 1.0 kcal/mol-$Å^2$. For relaxation and density

equilibration, 300 psec dynamics (NPT ensemble) were completed using the Langevin thermostat with a collision frequency of 2.0 $psec^{-1}$ and isotropic pressure scaling with a relaxation time of 1.0 psec. At this stage, protein atoms were restrained with weight 0.1 kcal/mol-$Å^2$. During the next 500 psec of dynamics (NPT ensemble), there were no restraints placed on protein atoms. The last step of cMD was a 5 nsec simulation with snapshots saved every 5 psec. All simulations were under periodic boundary conditions, with a 1 fsec time-step with hydrogen atoms constrained by SHAKE.

Boost potential parameters were determined from the average dihedral energy (Ed) and total potential energy (Ep) over the last 5 nsec of cMD according to the protocol described by Pierce, *et al*. (55):

$$EthreshD = Ed + (4 \text{ kcal mol}^{-1} \text{ residue}^{-1} * \# \text{ solute residues})$$

$$alphaD = (0.2)*(4 \text{ kcal mol}^{-1} \text{ residue}^{-1} * \# \text{ solute residues})$$

$$EthreshP = Ep + (0.16 \text{ kcal mol}^{-1} \text{ atom}^{-1} * \# \text{ atoms})$$

$$alphaP = (0.16 \text{ kcal mol}^{-1} \text{ atom}^{-1} * \# \text{ atoms})$$

Using this formulation, the boost potential parameters were EthreshD=19821, alphaD=938.4, EthreshP=-395856, and alphaP=22075. for PLC-γ1 aMD, and EthreshD=19842, alphaD=938.4, EthreshP=-395818, and alphaP=22081 for PLC-γ1(D1165H) aMD.

Two independent simulations with the same starting conformation but different velocity distributions were completed for both PLC-γ1 and PLC-γ1(D1165H). Results from the analysis were consistent between each pair of replicate trajectories, and results from one representative trajectory for each protein are presented in Fig. 2.4. Coordinate trajectories were processed using cpptraj for determining the average structure over the 75 - 150 nsec period of the simulation, where the conformation appeared to settle into a

meta-stable state, as well as the correlated motions for Cα atoms during the first 75 nsec leading to the meta-stable state.

Results

Structure of full-length PLC-γ1

In addition to the aforementioned array of regulatory domains, the PLC-γ isozymes also possess a set of core domains common to most other isoforms of PLC: an N-terminal PH domain, two pairs of EF hands, a catalytic TIM barrel, and a C2 domain. The regulatory array bisects the TIM barrel, subdividing this domain into the X- and Y-boxes (Fig. 3.1a, 3.2). To facilitate crystallization, several regions predicted to be disordered were removed from the construct used for structure determination. In particular, 20 and 75 residues were deleted from the N- and C-terminus, respectively. In addition, an internal loop of 25 residues connecting the cSH2 and SH3 domains was removed and replaced with a flexible linker; we refer to this internal deletion as Δ25 (Fig. 3.2, also see Materials and Methods). The crystallized construct therefore contains residues 21-765 and 791-1215 of PLC-γ1.

The cSH2/SH3 domain loop contains Tyr783, which is required for phosphorylation-dependent activation of PLC-γ1. However, we have demonstrated previously that this loop is not directly required for autoinhibition (30), and consistent with this notion, the crystallized form of PLC-γ1 was autoinhibited in cells (Fig. 3.3a). While nuanced differences in regulation between the wild-type and crystallized version of PLC-γ1 cannot be excluded, the latter faithfully recapitulated the mutational activation of the wild-type enzyme (Fig. 3.3a). In addition, deletion of the cSH2/SH3 domain loop had no measurable effect on the hydrodynamic radius or specific activity of the purified protein (Fig. 3.3b), further demonstrating that removal of the loop did not significantly alter the biochemical properties of the enzyme.

The 2.5 Å crystal structure of essentially full-length rat PLC-γ1 readily explains the autoinhibition of the PLC-γ isozymes. In particular, the regulatory array sits “atop” the conserved catalytic core and blocks the core from productively engaging membranes (Fig. 3.1b). In addition, the overall structure is highly electronegative (Fig. 3.4), and this property will also inhibit lipase activity by disfavoring interactions with negatively charged membranes. In particular, the overall negative charge of the PH domain indicates that it is unlikely to bind phosphatidylinositol 3,4,5-trisphosphate as previously reported (56). For PLCs to hydrolyze membrane-embedded PIP_2, the hydrophobic ridge of the catalytic TIM barrel must insert into lipid bilayers (57). However, in the case of PLC-γ1, the hydrophobic ridge interacts with portions of the sPH domain in the regulatory array; this arrangement is expected to effectively block membrane engagement. The active site sits beneath the hydrophobic ridge and is readily located by the bound Ca^{2+} cofactor (Fig. 3.3c). As implied by the visibility of the Ca^{2+} cofactor, the active site is fully solvent exposed and could presumably hydrolyze soluble substrates not embedded in lipid bilayers.

Two major interfaces lock the regulatory array on top of the catalytic core. The first is the aforementioned sPH domain interacting with the hydrophobic ridge of the TIM barrel (Fig. 3.1c). Here, residues from the sPH domain interdigitate with residues of the hydrophobic ridge in a “zipper-like” arrangement. A second interface is formed between loops of the cSH2 domain and the C2 domain of the catalytic core (Fig. 3.1d). In this case, the BG and EF loops of the cSH2 domain clasp prominent turns of the C2 domain—almost as if the loops are pinching the C2 domain. The pinched region of the C2 domain is an additional membrane anchor point in the PLC-δ isozymes, where Ca^{2+} mediates between the C2 domain and negatively-charged membranes (58, 59). Based on sequence conservation and overall charge distribution, this region of the C2 domain of PLC-γ1 also seems likely to interact with Ca^{2+} and membranes, although this idea has not been tested.

The analogous portion of the C2 domain of PLC-γ2 is anticipated to engage Ca^{2+} in a similar manner. Of note, this loop was implicated in the Ca^{2+}-dependent translocation of PLC-γ2 to the plasma membrane necessary for amplification of the Ca^{2+} signaling cascade in B cells (60). The two interfaces between the regulatory array and catalytic core do not overlap, but the sPH and cSH2 domains within the regulatory array brace each other through the C-terminal portion of the SH3 domain that lies between them (Fig. 3.1e): picture an arch with the tail end of the SH3 domain acting as the keystone.

The structure of full-length and autoinhibited PLC-γ1 immediately evokes a straightforward mechanism for its activation upon tyrosine phosphorylation. The same BG and EF loops of the cSH2 domain that pinch the C2 domain are also used to engage pTyr783 and surrounding regions (32) (Fig. 3.1f, 3.5). Therefore, when Tyr783 is phosphorylated, we propose that it will compete with the C2 domain for binding to the cSH2 domain. This competition would presumably disengage the cSH2 domain from the C2 domain to initiate a rearrangement of the regulatory array relative to the catalytic core. Moreover, perturbations at the interface of the cSH2 and C2 domains may propagate to the interface between the sPH domain and TIM barrel through keystone residues of the SH3 domain tail to amplify the original structural rearrangements. Indeed, the structure suggests that a wholesale rearrangement of the regulatory array relative to the catalytic core is required for productive membrane engagement by PLC-γ1 (Fig. 3.1g). This idea is consistent with previous studies using small-angle X-ray scattering (SAXS) that showed phosphorylation of PLC-γ1 is coupled to a conformational change that has yet to be defined (61).

The SAXS studies were also used by Bunney and colleagues to analyze the arrangement of domains within PLC-γ1. They posited a fundamentally distinct arrangement of domains relative to the crystal structure presented here. In particular, the

sPH and cSH2 domains were modeled as occupying the central volume of the SAXS envelope with the nSH2 and SH3 domains assuming flanking positions. In this model, the sPH domain does not contact the PLC core. This arrangement of domains would necessarily require a different mode of autoinhibition with the main autoinhibitory interface formed between the cSH2 domain the TIM barrel.

The overall structure of PLC-γ1 also supports the multivalent scaffolding properties of the PLC-γ isozymes required for proper signaling (62-64). In particular, both the nSH2 and SH3 domains are organized within the overall structure for unfettered access to cognate ligands (Fig. 3.5, 3.6). For example, the phosphotyrosine binding pocket of the nSH2 domain is fully solvent exposed and the major site for engagement of phosphorylated RTKs (31, 65, 66). Likewise, the canonical polyproline binding site of the SH3 domain is positioned to readily engage various proteins. Relevant examples include the scaffolding protein SLP-76 (67), the E3 ubiquitin ligase Cbl (68), and the guanine nucleotide exchange factor Vav1 (33, 69, 70)—all of which must be engaged by PLC-γ1 for the proper clustering of T cell receptors and subsequent downstream signaling. PLC-γ2 mediates similar clustering in response to active B cell receptors (71) and presumably will be structurally similar to PLC-γ1.

In addition, the monomeric GTPase Rac2 binds the sPH domain of PLC-γ2 to elevate lipase activity (72, 73) and the equivalent surface within the sPH domain of PLC-γ1 is fully exposed to solvent (Fig. 3.5). This last observation suggests that binding of Rac2 would not disrupt the overall structure of autoinhibited PLC-γ2. Rather, Rac2 may stabilize an active conformation of PLC-γ2 once PLC-γ2 is engaged with membranes as previously suggested (74).

In counterpoint to the above examples, the canonical phosphotyrosine binding site of the cSH2 domain is buried in the structure of PLC-γ1. This site is presumably reserved

as the “trigger” for phospholipase activation upon engagement of pTyr783. Therefore, pTyr783 is suggested to function as an intramolecular ligand that can effectively compete for the buried surface of the cSH2 domain. This situation is in contrast to intermolecular competitors such as kinases that would need to overcome substantial entropic penalties in order to bind the cSH2 domain.

Tyr783 in PLC-γ1 is presumed to be the primary site of phosphorylation coupled to enzyme activation (9, 30). Eight additional tyrosines are phosphorylated (positions 186, 472, 481, 771, 775, 959, 977, and 1254), but these sites appear dispensable for RTK-dependent activation in cells (61). In contrast, activation of PLC-γ1 by soluble tyrosine kinases requires phosphorylation of both Tyr775 and Tyr783 (75) and this situation is similar for PLC-γ2 where the analogous tyrosines (positions 753, 759) are also phosphorylated during phospholipase activation (76-79). How dual sites of phosphorylation cooperate to drive phospholipase activity is an open question but presumably shares aspects of regulation described above. Additional tyrosines (positions 1197, 1217) of PLC-γ2 are also phosphorylated and implicated in regulation (79), but these sites are not conserved in PLC-γ1.

Interfacial regulation

While the structure of PLC-γ1 strongly suggests that it must undergo a substantial rearrangement in order to gain access to its membrane-resident substrate, PIP_2, this idea is speculative without substantiation. We formally tested this idea using two bespoke fluorescent substrates of mammalian PLCs (Fig. 3.7). The first case, WH-15, is a soluble analogue of PIP_2 (80). It is predicted to have unimpeded access to the active site of PLC-γ1 and mutations assumed to relieve autoinhibition by wholesale rearrangement should not affect basal specific activity for the hydrolysis of WH-15. This is in fact the case since wild-type PLC-γ1 and a set of mutated forms that are constitutively active in cells (32) (also

see below) have essentially identical capacity to hydrolyze WH-15 *in vitro* (Fig. 3.7a). In contrast, XY-69 is a fluorescent substrate of PLCs that was specifically designed to embed into lipid bilayers (48). When XY-69 in lipid vesicles was presented to the same set of PLCs, there was now a dramatic difference in hydrolytic rates (Fig. 3.7b). Wild-type PLC-γ1 had very low specific activity, while the mutated forms were up to 30-fold more active. This discrimination presumably reflects the capacity of mutations to disrupt the interface between the regulatory domains and the catalytic core to favor a form of PLC-γ1 better able to engage PIP_2 in membranes. Discrimination was greatly diminished—albeit not completely eliminated—when XY-69 was solubilized in detergent micelles (Fig. 3.7c). These results are consistent with the postulation that autoinhibition arises from the overall spatial arrangement of PLC-γ1 that prevents it from productively engaging membranes. Mutations that destabilize this arrangement are proposed to concomitantly relieve autoinhibition and allow PLC-γ1 better access to membranes and PIP_2.

Accelerated molecular dynamics (aMD) simulations support the proposed mechanism of activation. In particular, all-atom simulations of PLC-γ1 reproducibly highlighted a flexible set of regulatory domains relative to a virtually static catalytic core (Fig. 3.8a, 3.9). Moreover, this flexibility increased for simulations of a constitutively active mutant form of PLC-γ1 harboring a single substitution (D1165H) within the C2 domain at the interface with the phosphotyrosine-binding site of the cSH2 domain (Fig. 3.10). Of note, D1165H corresponds to the D1140G substitution in PLC-γ2; PLC-γ2(D1140G) has been identified in patients with relapsed chronic lymphocytic leukemia treated with ibrutinib (81). For both wild-type and mutant PLC-γ1, the correlated motions indicate that the regulatory domains tended to move as a relatively rigid block (Fig. 3.8b).

Comparisons of average structures derived from the aMD simulations highlight increased disorganization within the interface between the cSH2 and C2 domains upon

mutation (Fig. 3.8c). For example, Asp 1165 resides within the β5/β6 turn of the C2 domain where it participates in two hydrogen bonds that stabilize the turn that forms a major part of the interface with the cSH2 domain. Substitution of Asp 1165 to His (D1165H) disrupts the proximal hydrogen-bonding network and results in the partial unfolding of the β5 and β6 strands of the C2 domain during simulations. The collapse of this region is linked to an approximately 30° rotation of the cSH2 domain as it moves toward the C2 domain by approximately 10 Å. The relative movements of the C2 and cSH2 domains are propagated to the rest of the regulatory array due to its propensity to move as a block. Movements are essentially identical for a constitutively active mutant form of PLC-γ1 harboring two substitutions (Y747E+R748E) within the phosphotyrosine-binding site of the cSH2 domain and on the opposite side of the interface from Asp 1165 (Fig. 3.9-3.11). This result suggests that diverse mutations within the cSH2/C2 domain interface will favor similar movements.

PLC-γ isozymes in cancers

The PLC-γ isozymes are frequently mutated in several leukemias (19, 81) and lymphomas(20, 82-84). In particular, PLC-γ1 is the most frequently mutated protein in adult T cell leukemia/lymphoma (19). In this disease, sites of substitution in PLC-γ1 are found throughout the entire primary sequence with clusters at several hotspots (Fig. 3.12a). This rather uninformative arrangement is dramatically clarified when the entire set of substitutions is mapped onto the structure of autoinhibited PLC-γ1 (Fig. 3.12b). Now, the majority of sites localize to the interfaces formed between the PLC core and the regulatory array. This three-dimensional clustering strongly suggests that most cancer-associated substitutions in PLC-γ1 disrupt the placement of the regulatory domains atop the core to disfavor autoinhibition. Indeed, in a panel of PLC-γ1 isozymes expressed in HEK293 cells,

cancer-associated substitutions at these interfaces produced a spectrum of constitutively active phospholipases—sometimes exceeding 1,500-fold greater activity than wild-type PLC-γ1 (Fig. 3.12c). Cancer-associated mutations within the equivalent regions of PLC-γ2 produced similar enhancements, indicating conserved regulation between the two isozymes (Fig. 3.13).

Cancer-derived mutations outside the autoinhibitory interfaces generally produced the smallest increases in basal lipase activities—but these increases were nonetheless significant in comparison to the wild-type isozyme (Fig. 3.12c, inset). How might these additional mutations lead to constitutive phospholipase activity? Based on the sites of mutation within the structure of autoinhibited PLC-γ1, three mechanisms are likely. First, substitutions may increase the affinity of the active form of PLC-γ1 for membranes. This option is likely the case for R48W located in the PH domain near the presumed interface with membranes. A similar mode leading to elevated phospholipase activation was proposed for a substituted form of PLC-γ2 that causes arthritis in mice and has increased affinity for membranes relative to wild-type PLC-γ2 (85). Second, substitutions might disrupt interactions provided by the keystone residues of the SH3 domain that buttress the organization of the sPH and cSH2 domains needed to maintain autoinhibition. Representative substitutions include R687W and R753H and additional examples are found in both PLC-γ1 (Fig. 3.12) and -γ2 (Fig. 3.13, 3.14). Of note, R687W is analogous to R665W in PLC-γ2 and arises in patients with relapsed chronic lymphocytic leukemia treated with ibrutinib (21). Finally, mutations within the nSH2 domain, e.g., Q606R and D625Y, are near the binding site for phosphotyrosine (31) and may increase affinity for phosphorylated kinases.

The PLC-γ isozymes are normally activated upon phosphorylation, especially by diverse growth factor receptors. Therefore, the cancer-associated mutations in PLC-γ1

were further tested for effects on lipase activity after co-expression of PLC-γ1 and the epidermal growth factor receptor (EGFR) (Fig. 3.15). In all cases, a high concentration of EGF used to activate the receptor produced elevated lipase activity relative to wild-type PLC-γ1. This result indicates an untapped reserve of lipase activity that is, at least partially, released by these cancer-associated mutations in response to EGF. This point is further emphasized for lipase responses measured at varying concentrations of EGF for a representative subset of mutant PLC-γ1 isozymes with varying levels of constitutive activation (Fig. 3.15b, upper graph). Both P867R and D1165H occur at the autoinhibitory interfaces and produced substantially elevated lipase activity relative to wild-type PLC-γ1 at all concentrations of EGF. In contrast, R48W occurs at the predicted interface of the active isozyme with membranes and abnormally elevated lipase activity of PLC-γ1(R48W) manifests only at high concentrations of EGF. This functional difference possibly reflects a mechanistic difference: P867R and D1165H likely destabilize the inactive ensemble of PLC-γ1 while simultaneously favoring active forms of the isozyme; in contrast, R48W has no substantive effect on the inactive population under these conditions and presumably only stabilizes the active isozyme once bound to membranes (Fig. 3.15b, lower graph).

Regardless of the mechanistic details, these functional results suggest important biological ramifications. Namely, the lipase activity of mutant PLC-γ isozymes should be dependent on cellular context. For example, PLC-γ1 or -γ2 harboring mutations such as R48W that preferentially stabilize active ensembles may be essentially quiescent until the isozymes are activated by phosphorylation. These situations are relatively nuanced in comparison to more robustly activating mutations, e.g., P867R and D1165H, that disrupt core aspects of autoinhibition. However, the more subtly activating substitutions may nonetheless contribute to cancer in cells with high levels of active kinases such as upon

the overexpression of EGFR or other growth factor receptors—situations with widespread clinical relevance (86)

Discussion

The structure of full-length, autoinhibited PLC-γ1 provides a first clear view of the regulated activation of the PLC-γ isozymes. The overall picture is of a catalytic core that is conserved among all PLCs and that is prevented from spuriously hydrolyzing PIP_2 by a set of interdependent regulatory domains stationed to preclude access of the active site to membranes. Additionally, the regulatory domains are organized to integrate numerous molecular inputs that ultimately control phospholipase activity and mediate necessary scaffolding functions (Fig. 3.16). Importantly, the nSH2 domain is optimally positioned to readily bind phosphorylated kinases and align them to promote the phosphorylation of Tyr783 needed for activation of PLC-γ1. Although capable of engaging phosphorylated portions of kinases (87), the equivalent surface of the cSH2 domain is buried through interactions with the C2 domain and is unlikely to initiate engagement of kinases as previously suggested (38).

However, the two SH2 domains might work in concert upon receptor engagement to facilitate the binding of phosphorylated Tyr783 to the cSH2 domain. This idea is supported by the comparison of the full-length structure of PLC-γ1 with a structure of the two SH2 domains of PLC-γ1 bound to the phosphorylated kinase domain of FGFR1 (31). Based on this comparison, the βA/αA loop of the nSH2 domain is rearranged to accommodate pTyr766 of FGFR1 and this rearrangement leads to additional movements of the cSH2 domain (Fig. 3.17). In the full-length structure, equivalent movements upon binding FGFR1 would open the surface of the cSH2 domain that binds pTyr783, effectively priming it to engage pTyr783. Engagement of pTyr783 by the cSH2 domain is presumed to unlatch the cSH2 domain from the catalytic core and initiate what is likely to be a

relatively massive rearrangement of the regulatory domains with respect to the core before the core can engage membranes and hydrolyze PIP_2.

The model of activation described above provides the mechanistic underpinnings for understanding the mutational landscape of the PLC-γ isozymes associated with disease. In particular, most of the substitutions and small deletions in these isozymes that are linked to cancers (19, 21, 81) or autoimmune disease (23) occur at the interfaces between the core and regulatory domains based on the structure of autoinhibited PLC-γ1. These mutations disrupt these interfaces, release autoinhibition, and favor conformations that engage membranes to promote constitutive phospholipase activity. Shifted conformational equilibria may also explain the supra-activation of mutant forms of PLC-γ1 by EGFR. That is, mutant forms of PLC-γ1 that are predisposed to be “open” may also have a greater propensity to bind EGFR and a lower probability of turning off.

Constitutive activation varies greatly, ranging from approximately 10-fold to over 1,500-fold, with important cellular implications: highly active forms are expected to drive downstream signaling under all circumstances while more subtly active forms are likely to promote disease only within specific cellular contexts. An excellent example of this latter class includes mutated forms of PLC-γ2 (R665W or L845F) that arise in patients treated with ibrutinib. B cells harboring either mutant of PLC-γ2 possess normal calcium homeostasis until B cell receptors are activated, at which point intracellular calcium levels rise and remain elevated, while in the equivalent wild-type case, calcium homeostasis is rapidly reestablished (21). Both mutant forms have essentially wild-type phospholipase activity at low levels of expression but are hypersensitive to activation by Rac2 (74). These results suggest that once active, the mutant forms of PLC-γ2 are stabilized at membranes by binding to Rac2. That is, the mutations are cryptic until the isozymes are activated, at which point the mutated PLC-γ2 isozymes are slow to return to their autoinhibited state.

Similar context-dependent activation of mutant forms of the PLC-γ isozymes should also occur upon activation by kinases. PLC-γ1(R48W) provides an example: it has essentially wild-type phospholipase activity until co-expressed with high levels of active EGFR. Analogous scenarios may be wide-spread in cancers where tyrosine kinases are constitutively active upon substitution, truncation, fusion, or overexpression—all conditions shown to activate PLC-γ1 (88, 89). Alternatively, the activation of RTKs by stromal components contributes to treatment-resistant cancers (90) and roles for wild-type and mutant PLC-γ isozymes under these conditions need to be explored.

On a final note, the interfacial regulation of the PLC-γ isozymes suggests promising avenues for their isozyme-specific, allosteric modulation by small molecules to advance related chemical biology and on-going drug discovery. Namely, compounds that inhibit the movement of the regulatory domains relative to the catalytic core should also prevent membrane engagement and consequent PIP_2 hydrolysis. Such compounds might treat cancers and immune diseases driven by constitutively active forms of the PLC-γ isozymes. Conversely, allosteric modulators that stabilize active forms of the PLC-γ isozymes might bolster immunotherapies (91) or provide promising leads for the treatment of Alzheimer's disease where a naturally occurring hypermorphic variant of PLC-γ2 is linked to protection from this disease (28).

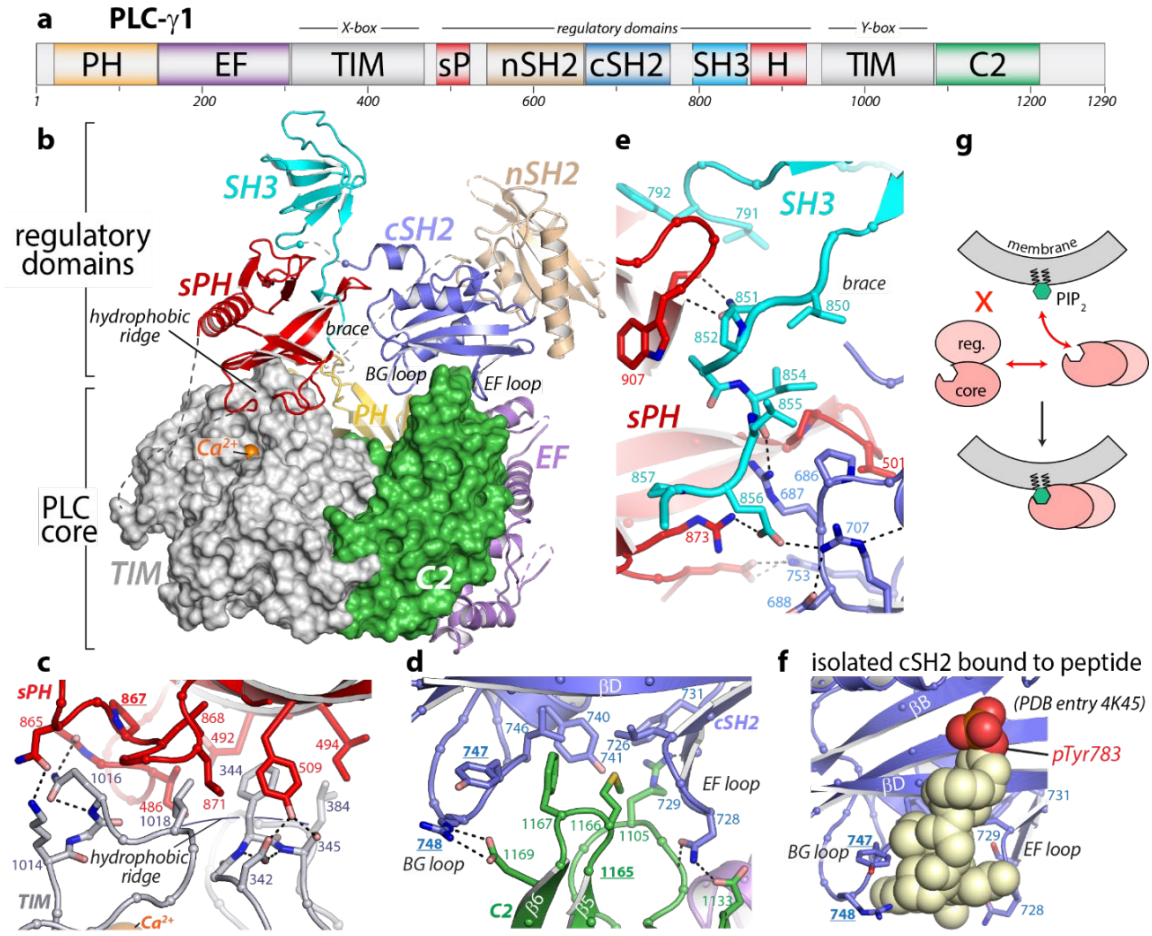

Figure 3.1 – Crystal structure of autoinhibited PLC-γ1. a, Domain architecture of PLC-γ1 drawn to scale. **b**, 2.5 Å resolution structure of PLC-γ1, domains are colored as in **a**; TIM barrel and C2 domain are depicted as surfaces to highlight interactions with regulatory domains. The calcium cofactor (orange sphere) marks the active site and dashed lines indicate regions not built due to the absence of observable electron density. Borders of the Δ25 deletion (residues 766-790) used to facilitate crystallization are indicated with spheres. The hydrophobic ridge of the TIM barrel, which interacts with lipid membranes to facilitate catalysis, is occluded by the sPH domain. This arrangement of the sPH domain is supported by contacts with the cSH2 domain and further reinforced by a "brace" formed by the C-terminal extension of the SH3 domain. **c-d**, Structural details between the regulatory and core domains of PLC-γ1. **e**, Expanded view of the SH3 domain. **f**, Structure of the isolated cSH2 domain of PLC-γ1 bound to a peptide (spheres) encompassing phosphorylated Tyr783 (red) of PLC-γ1. Orientation is approximately the same as in panels **b** and **d**. For panels **c-f**, interfacial residues are numbered, dashed lines are hydrogen bonds, and residues mutated in Figure 7 are underlined. **g**, Schematic emphasizing large conformational change that is proposed to occur before PLC-γ1 can access membrane-resident PIP_2.

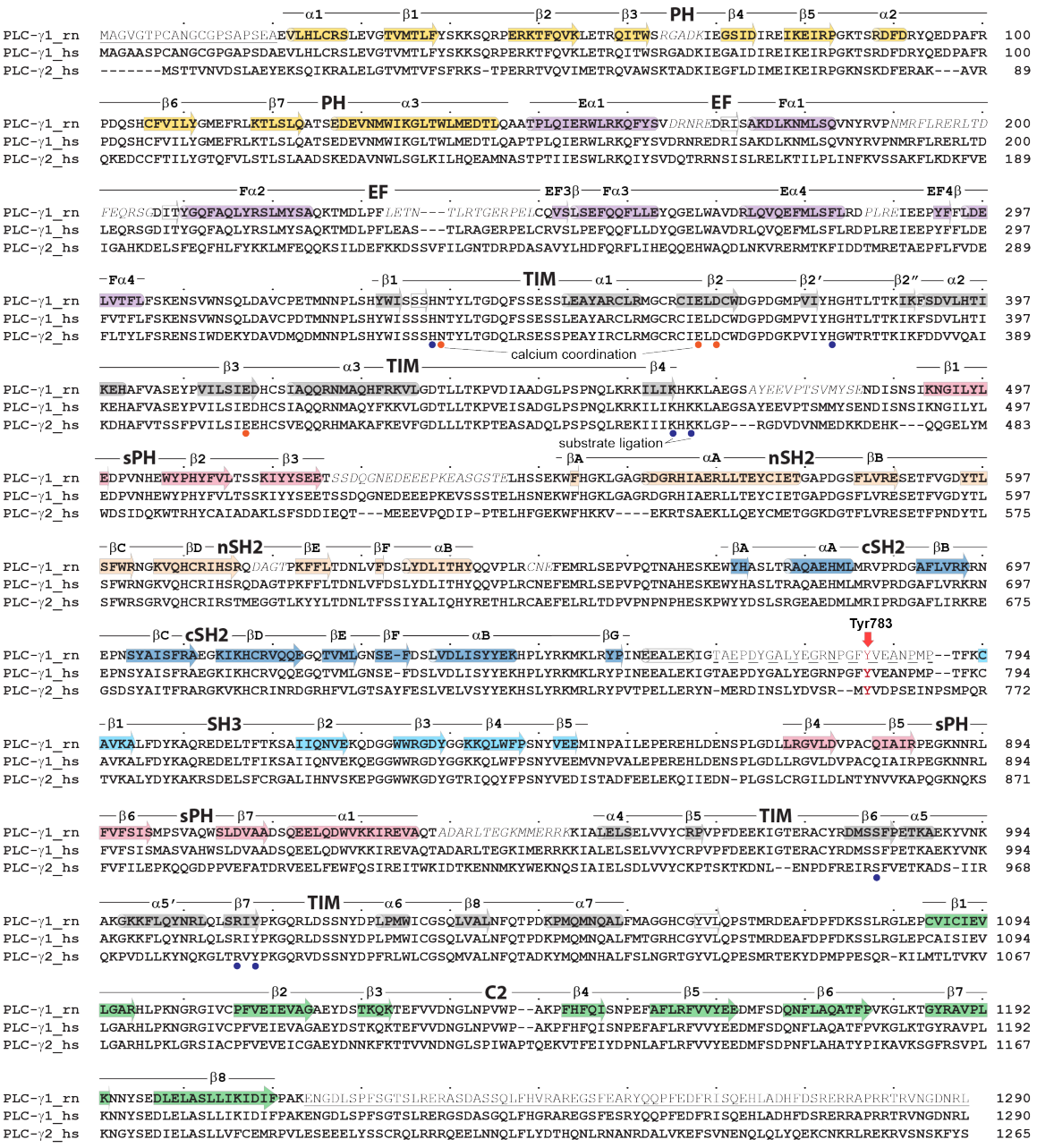

Figure 3.2 – Primary sequence alignment of PLC-γ isozymes. The sequence of rat PLC-γ1 (PLC-γ1_rn, UniProt accession number P10686), human PLC-γ1 (PLC-γ1_hs, P19174), and human PLC-γ2 (PLC-γ2_hs, P16885) were aligned using ClustalW. Dots denote every 10th residue. Underlined residues were removed from the crystallization construct and the D25 deletion is highlighted with a dashed underline. Electron density was not observed for residues in italics. Secondary structure (α-helices, cylinders; β-strands, arrows) was assigned using DSSP. Tyr783 in PLC-γ1 and Tyr759 in PLC-γ2 are highlighted in red. Substrate ligation defined based on structural homology to PLC-γ1 and -γ2.

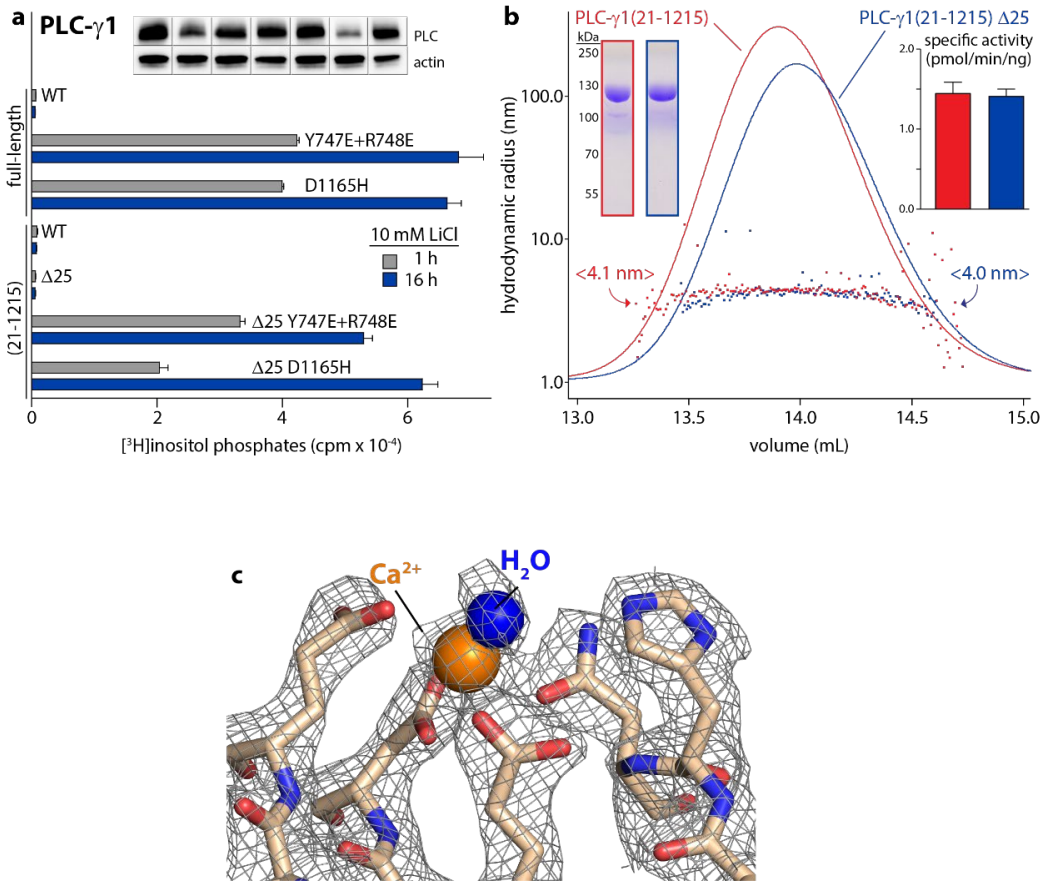

Figure 3.3 – Crystallographic-grade PLC-γ1(21-1215) Δ25 is fully autoinhibited in cells and in vitro. a, Phospholipase activity of various forms of PLC-γ1 in cells. Data are the mean ± SEM of triplicate samples from a single experiment that is representative of data obtained in two independent experiments. Immunoblots of cell lysates are presented in the same order as the bar graph. **b**, Analysis of purified PLC-γ1(21-1215) and PLC-γ1(21-1215) Δ25 by size exclusion chromatography coupled to multi-angle light scattering. One hundred micrograms of the indicated protein were applied to a Superdex 200 size exclusion column. Elution was monitored by UV absorbance (colored lines) and simultaneously analyzed by multi-angle light scattering to determine hydrodynamic radius (colored squares). The mean radius for each protein is indicated in angle brackets. Two micrograms of each protein were separated by SDS-PAGE and stained with Coomassie Brilliant blue (left inset) to assess purity. Specific activities were quantified using phospholipid vesicles containing 200 μM PE and 20 μM [^{3}H]PIP_2 (right inset). Data are presented as the mean ± SEM and were pooled from three independent experiments. **c**, Electron density map (wire mesh) of the active site of PLC-γ1(21-1215) Δ25 ($2F_o - F_c$ contoured at 1.5 σ).

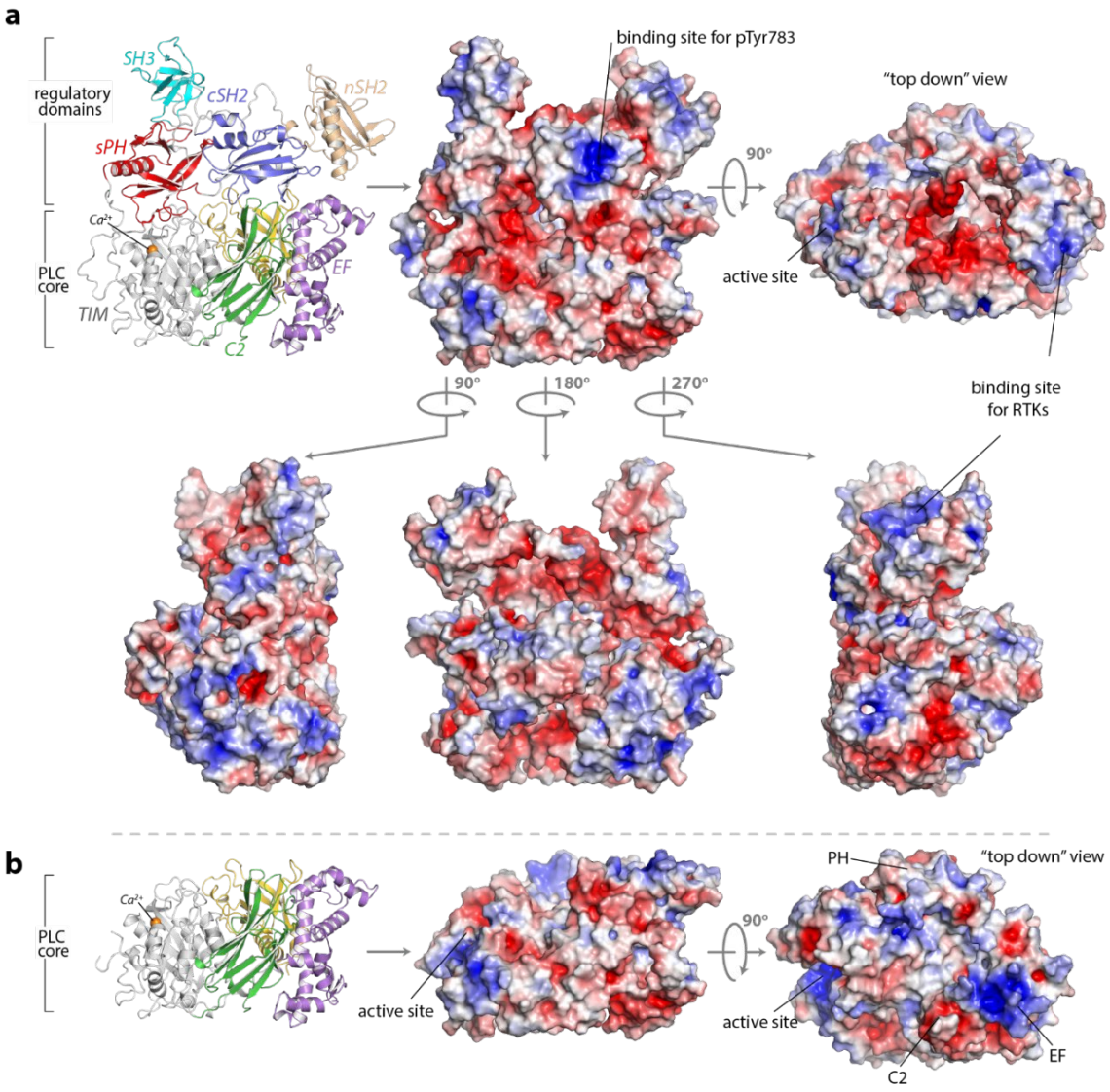

Figure 3.4 – Surface of autoinhibited PLC-γ1 is electronegative. The solvent-accessible surface area of PLC-γ1 (a) or the core of the protein (b) was calculated and colored according to electrostatic potential (red, -5 kT/e; blue, 5 kT/e). Charges were calculated using AMBER and electrostatic surfaces were calculated using APBS executed within PyMOL.

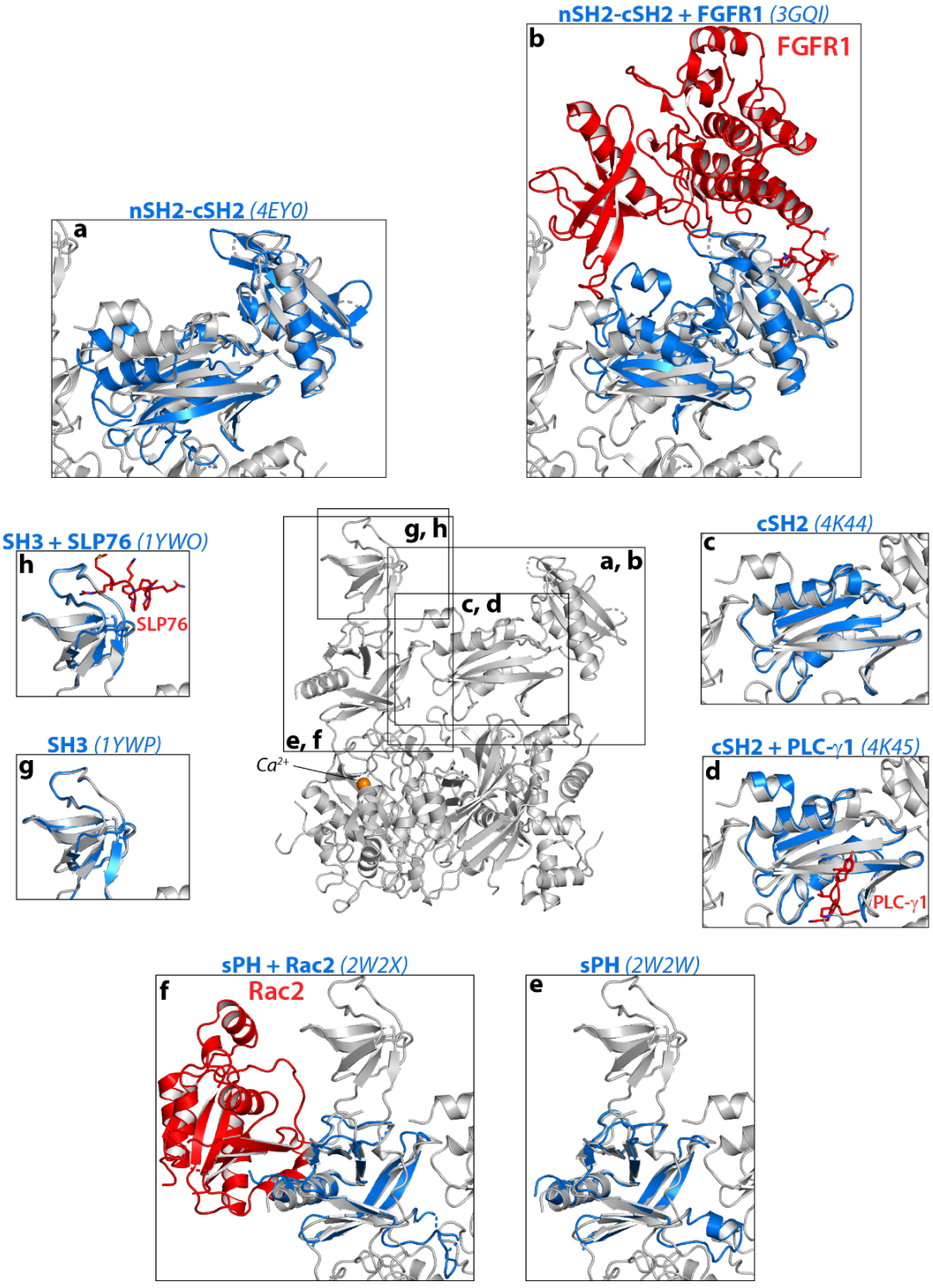

Figure 3.5 – Structural comparisons of autoinhibited PLC-γ1 and fragments. a-h, The structure of autoinhibited PLC-γ1 (gray) was aligned with the indicated structures of isolated domains from PLC-γ1 or PLC-γ2 (blue). Binding partners co-crystallized with isolated domains are red. PDB accession numbers are listed in parentheses. In **a-b**, the tandem SH2 domains were aligned using the nSH2 domain.

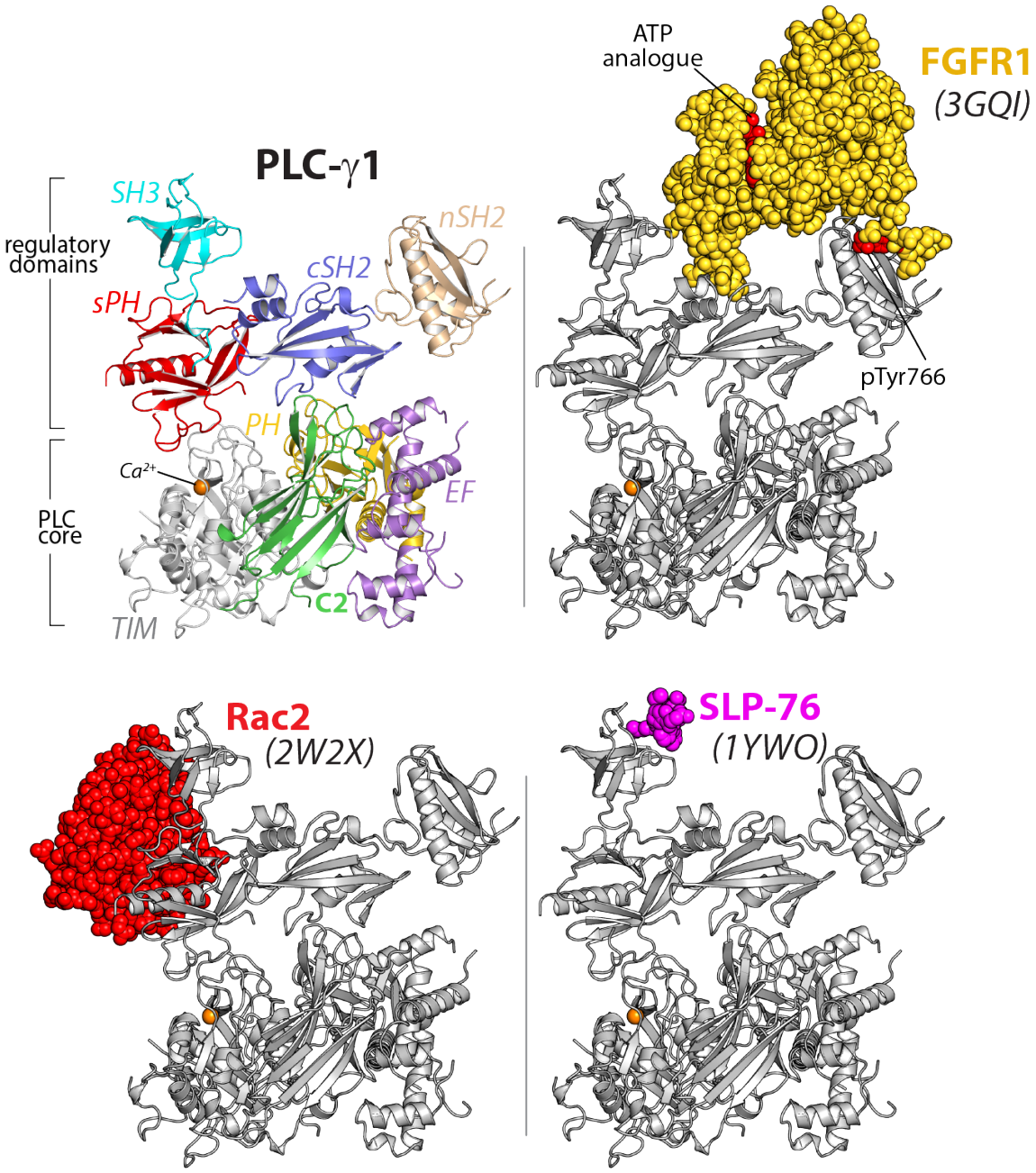

Figure 3.6 – The regulatory domains are organized to integrate multiple inputs. Structures of fragments of PLC-γ1 or -γ2 bound to biologically relevant proteins were superimposed on the structure of PLC-γ1 (gray ribbon) and partner proteins highlighted in color as space filling models. PDB accession numbers are listed in parentheses and the domain architecture of PLC-γ1 is shown at upper left in the same orientation.

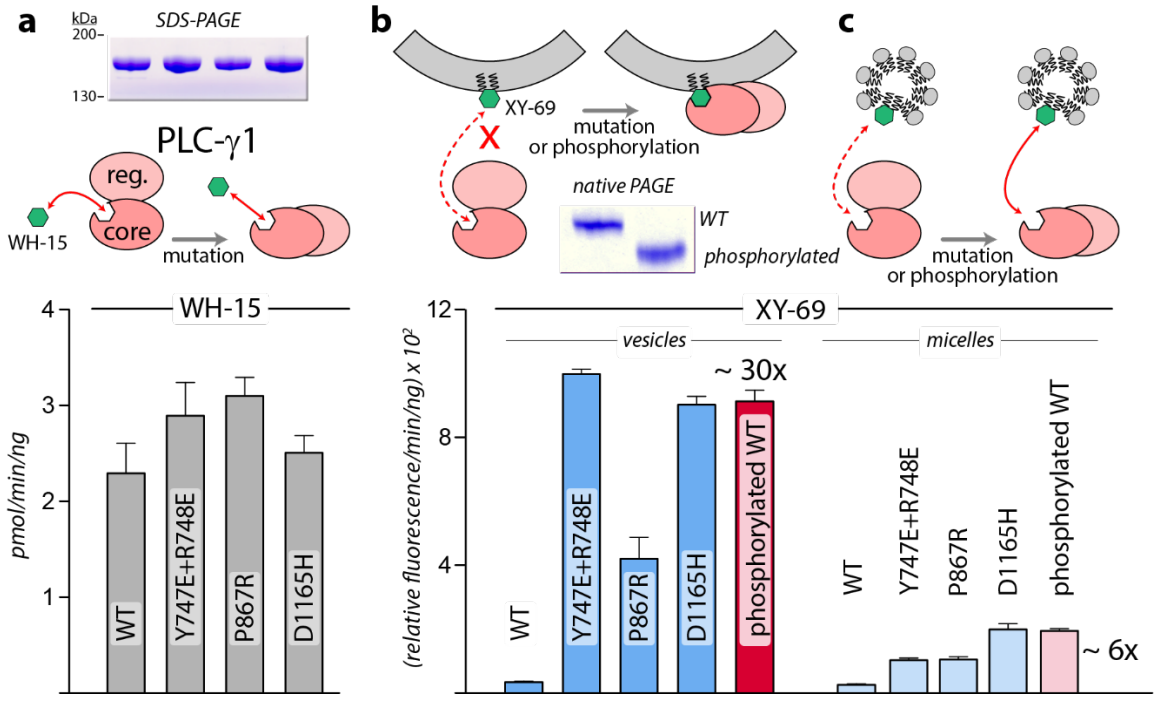

Figure 3.7 – Interfacial regulation of purified forms of PLC-γ1. a, Specific activities measured with the soluble substrate, WH-15 (3 μM). Purified PLC-γ1 variants (2 μg) shown in inset in the same order as bar chart. Data represent the mean ± SEM calculated from three independent experiments. **b-c**, Quantification of phospholipase activity at lipid interfaces. The membrane-associated substrate XY-69 (5 μM) was incorporated into phospholipid vesicles containing 220 μM PE and 20 μM PIP_2 (vesicles) or detergent-mixed micelles containing 0.5% w/v sodium cholate (micelles) prior to the addition of indicated forms of PLC-γ1 (wild-type PLC-γ1, 1 nM; mutant forms, 0.5 nM). Phospholipase activity determined by quantifying XY-69 hydrolysis in real-time and presented as the mean ± SEM of three independent experiments. Phosphorylation of PLC-γ1 by a constitutively active version of the FGFR2 kinase domain confirmed by native PAGE followed by Coomassie Brilliant blue staining (inset).

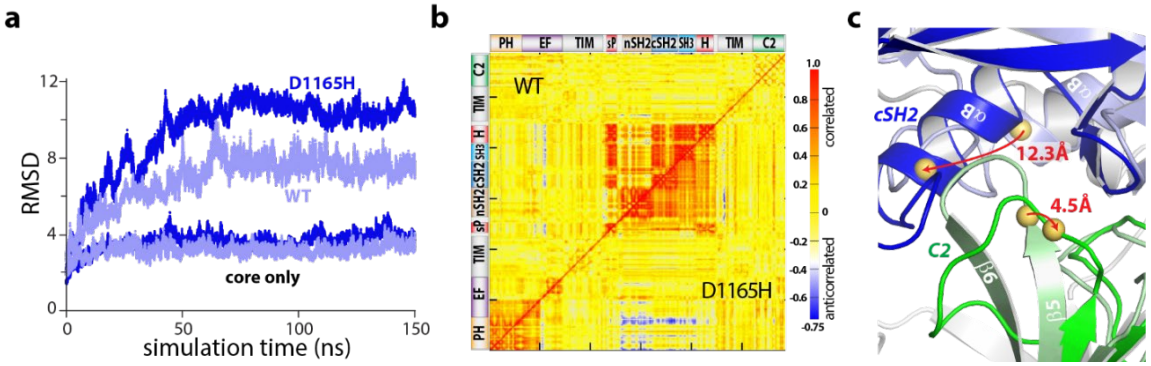

Figure 3.8 – The regulatory domains of PLC-γ1 are dynamic in aMD simulations. a, Root mean square deviations (RMSD) of backbone atoms for the indicated trajectories relative to the starting model of autoinhibited PLC-γ1. For comparison, the equivalent RMSDs for the PLC core ("core only") are also shown. **b**, Correlation matrix for pairs of residues in PLC-γ1 and PLC-γ1(D1165H). Correlated motions were calculated over the first 75 nanoseconds of each simulation. **c**, Superimposition of the average structures of PLC-γ1 and PLC-γ1(D1165H). Structures were calculated over 75-150 nanoseconds of each simulation. Domains in wild-type PLC-γ1 and PLC-γ1(D1165H) are shown in light and dark colors, respectively; the remainder of the proteins are gray. Red arrows indicate displacement of select Cα atoms (yellow spheres).

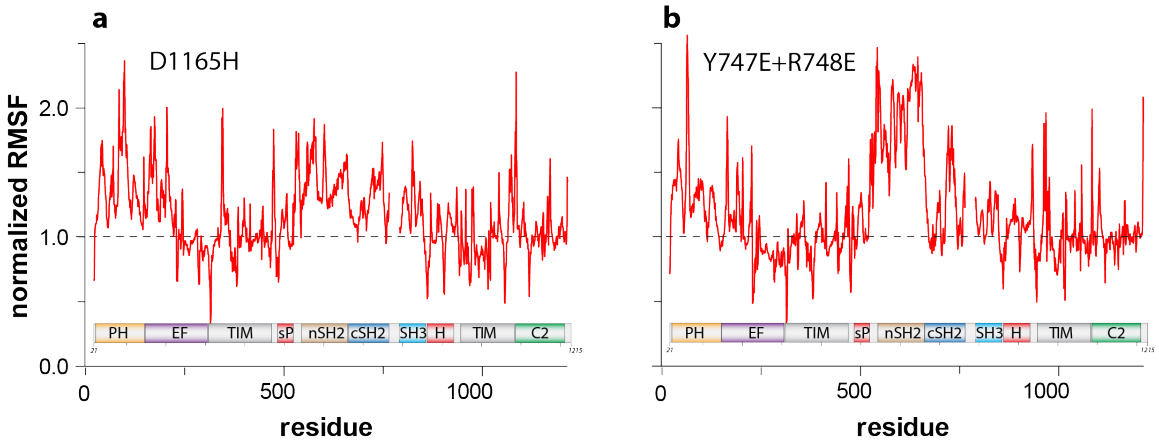

Figure 3.9 – Activated forms of PLC-γ1 have highly mobile regulatory domains. Root mean square fluctuations (RMSF) about the average structure of (**a**) PLC-γ1(D1165H) or (**b**) PLC-γ1(Y747E+R748E) were calculated for each Cα atom and divided by the equivalent RMSF of wild-type PLC-γ1.

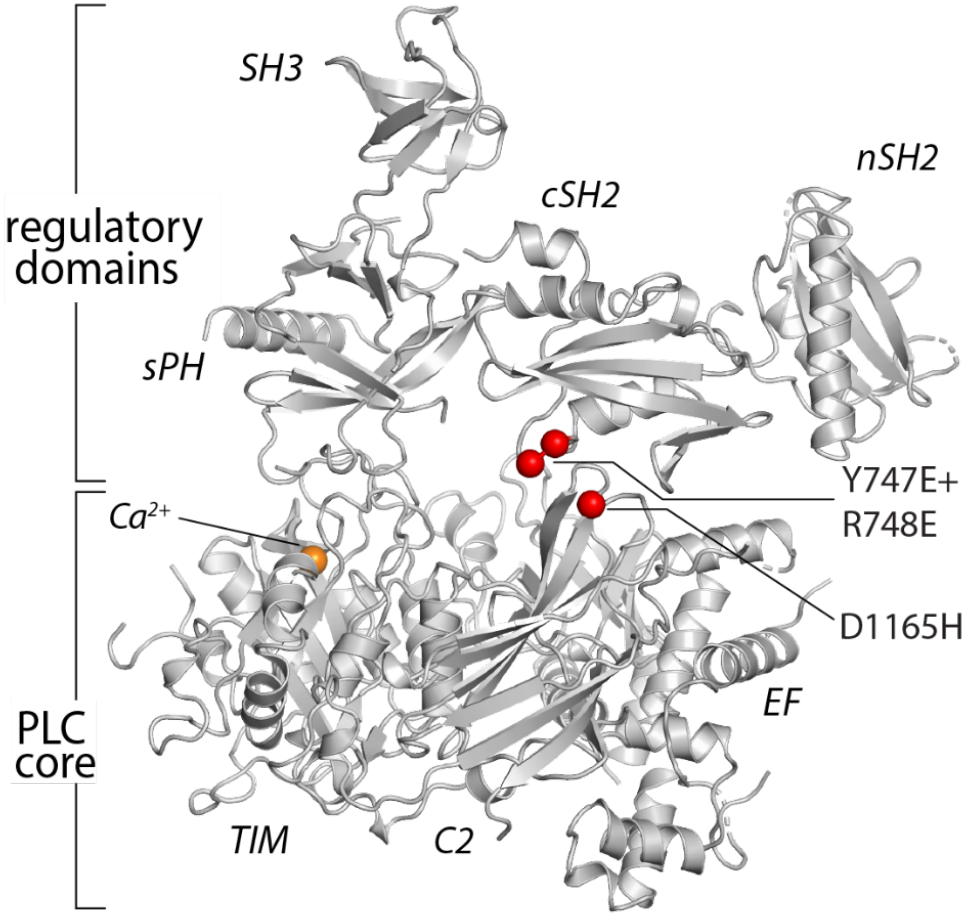

Figure 3.10 – Substitutions of PLC-γ1 analyzed in aMD simulations. The positions of substitutions (red spheres) studied are mapped onto the structure of PLC-γ1.

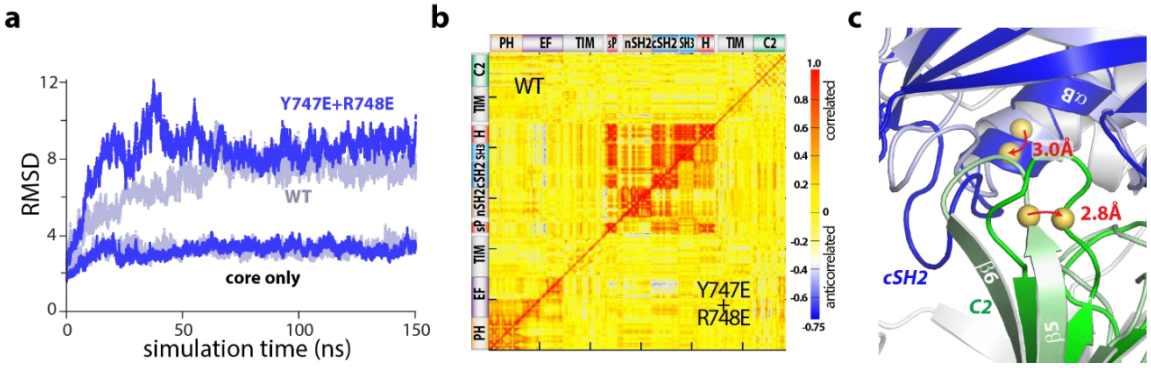

Figure 3.11 – Point mutations in the cSH2 domain recapitulate dynamics. a, Root mean square deviations (RMSD) of backbone atoms for the indicated trajectories relative to the starting model of auto-inhibited PLC-γ1. For comparison, the equivalent RMSDs for the PLC core ("core only") are also shown. **b**, Correlation matrix for pairs of residues in PLC-γ1 and PLC-γ1(Y747E+R748E) calculated over the first 75 nanoseconds of each simulation. **c**, Superimposition of the average structures of PLC-γ1 and PLC-γ1(Y747E+R748E) calculated over 75-150 nanoseconds of each simulation. Domains in wild-type PLC-γ1 and PLC-γ1(Y747E+R748E) are shown in light and dark colors, respectively; the remainder of the proteins are gray. Red arrows indicate displacement of select Cα atoms (yellow spheres).

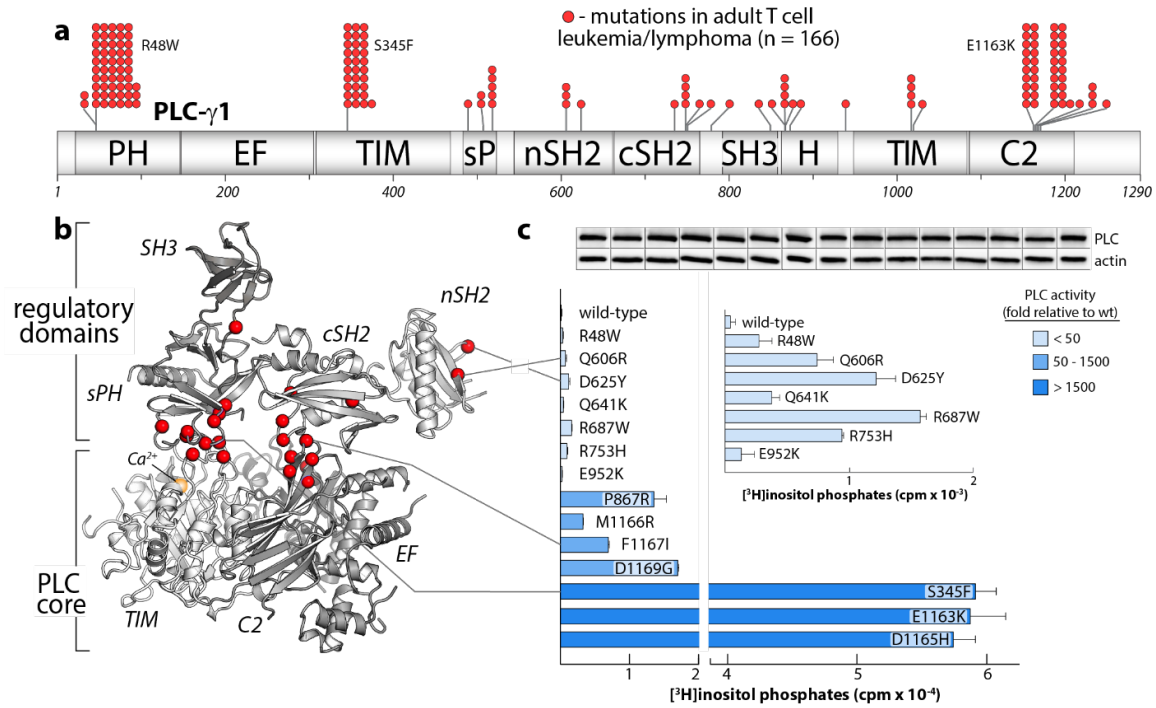

Figure 3.12 – Substitutions of PLC-γ1 found in cancers activate the enzyme. a, Position (n = 26) and frequency of substitutions (red spheres) in PLC-γ1 for a cohort of 370 patients with adult T cell leukemia/lymphoma. **b**, Mutations from a mapped onto the structure of PLC-γ1. c, Basal phospholipase activity of mutant forms of PLC-γ1 in cells. Data represent the mean ± SEM of triplicate samples from a single experiment representative of three independent experiments. Inset shows mutant forms of PLC-γ1 with the lowest relative basal activity. Immunoblots of cell lysates are presented in the same order as the bar graph.

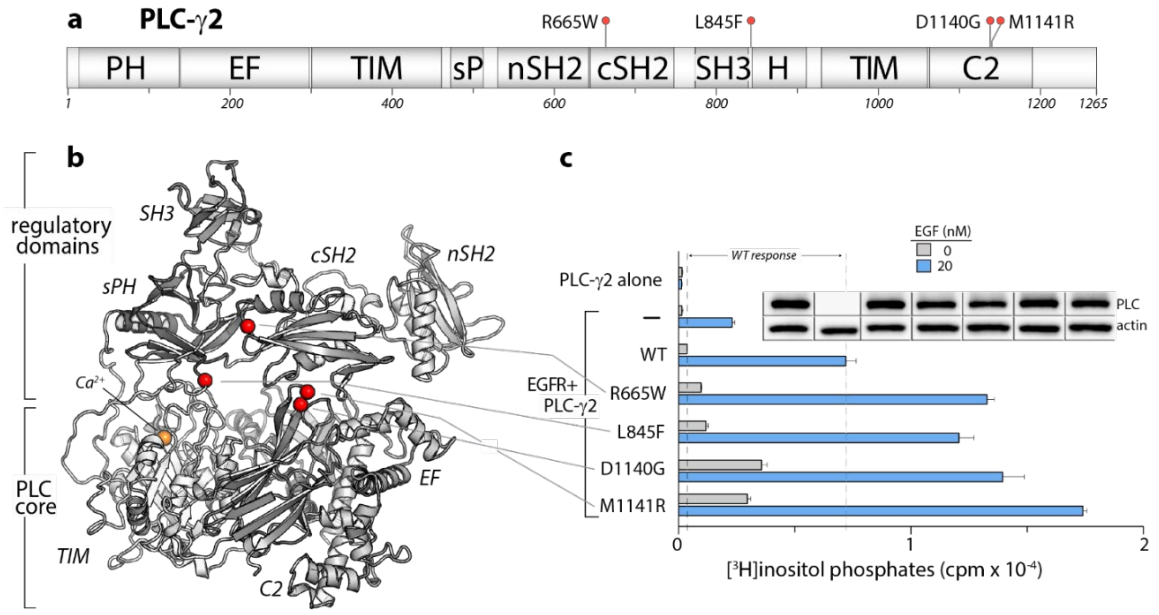

Figure 3.13 – Constitutive activation of PLC-γ2 in cancers. a, Domain architecture of PLC-γ2 drawn to scale. Position of substitutions (red spheres) in PLC-γ2 in patients with chronic lymphocytic leukemia are indicated. **b**, Substitutions (red spheres) mapped onto a homology model of PLC-γ2. **c**, Basal and receptor-dependent activation of PLC-γ2 mutants in cells. Data are presented as the mean ± SEM of triplicate samples from one experiment representative of three independent experiments. Immunoblots of cell lysates are presented in the same order as the bar graph.

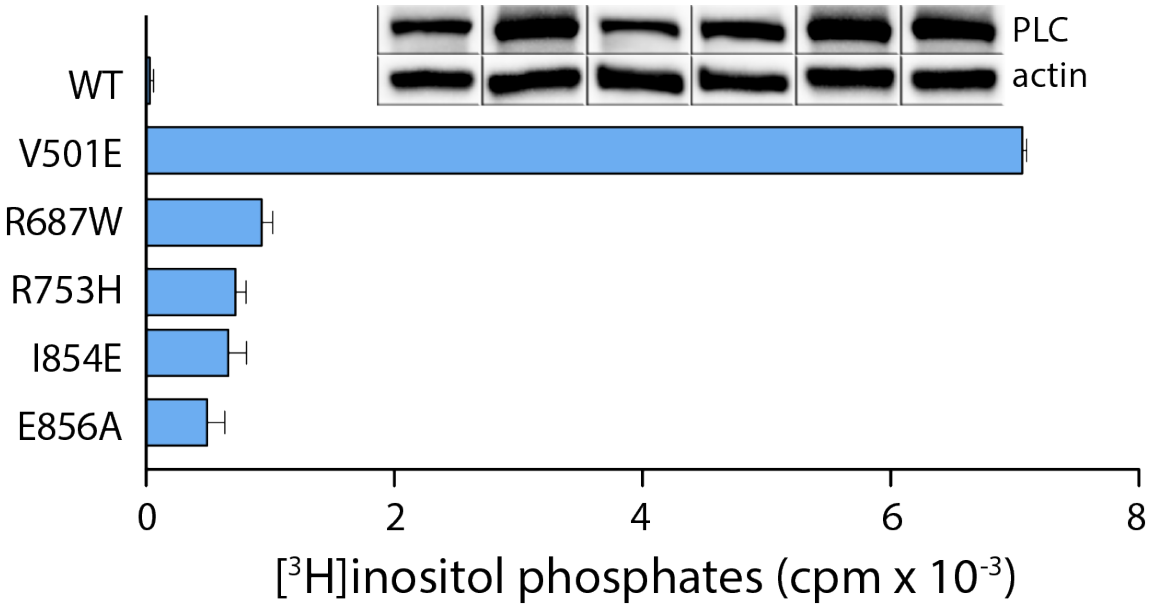

Figure 3.14 – Oncogenic substitutions within the SH3 domain activate PLC-γ1. a, Basal phospholipase activities of the indicated mutant forms of PLC-γ1 were quantified after transient overexpression in cells. Data represent the mean ± SEM of triplicate samples from a single experiment representative of three independent experiments. Immunoblots of cell lysates are presented in the same order as the bar graph.

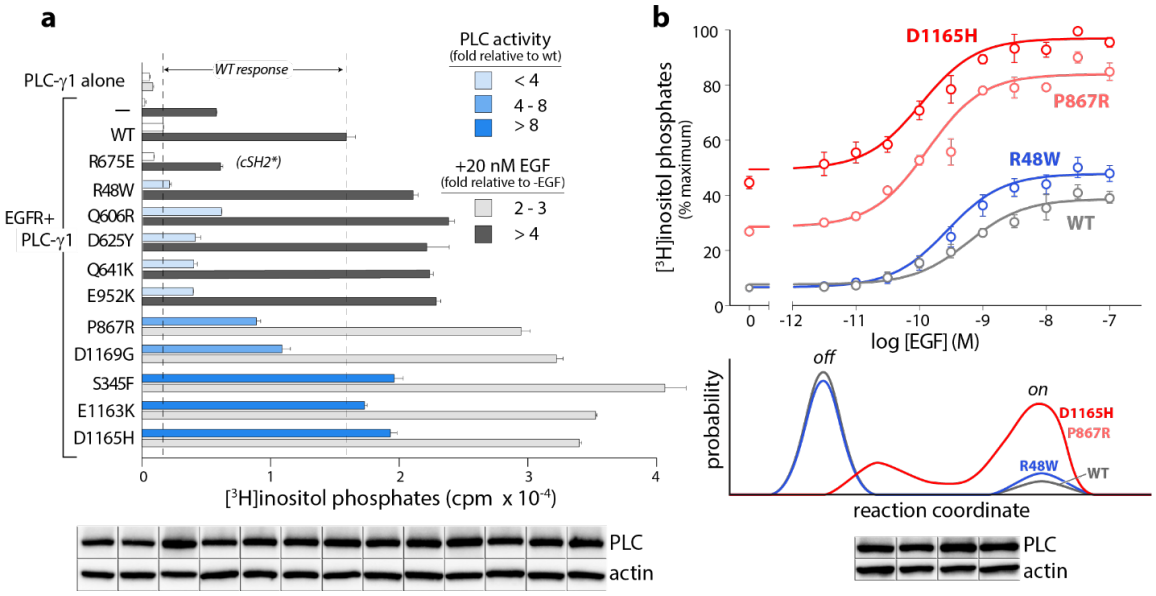

Figure 3.15 – Oncogenic substitutions prime PLC-γ1 for activation by EGFR. a, Receptor-dependent activation of mutant forms of PLC-γ1. A substitution that abolishes phosphorylation-dependent activation of PLC-γ1 is indicated (cSH2*). Data are the mean ± SEM of triplicate samples from one experiment representative of two independent experiments. **b**, EGF concentration-effect curves for wild-type and select mutant forms of PLC-γ1. Data are presented as the mean ± SEM of single data sets pooled from three independent experiments. Hypothetical reaction coordinates for each form of PLC-γ1 are shown below. In both panels, immunoblots of cell lysates transfected with PLC-γ1 are presented in the same order as the bar chart (top to bottom).

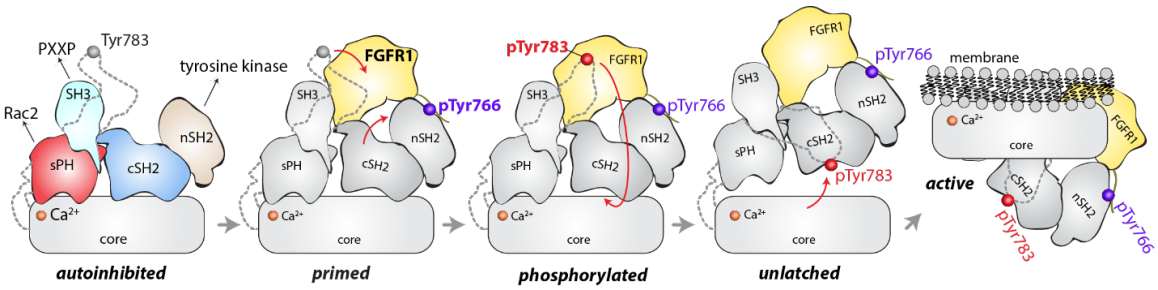

Figure 3.16 – Model for phosphorylation-induced activation of PLC-γ1. In the basal state, the nSH2 domain of PLC-γ1 mediates recruitment of the autoinhibited enzyme to activated receptor tyrosine kinases, e.g. FGFR1. The nSH2 domain binds to phosphorylated Tyr766 (pTyr766) in the C-terminal tail of FGFR1, and its kinase domain acts as a lever to destabilize the interaction between the cSH2 and C2 domains of PLC-γ1, priming the lipase for phosphorylation-dependent activation. PLC-γ1 is subsequently phosphorylated on Tyr783, and the engagement of pTyr783 by the cSH2 domain results in the full dissociation of the cSH2 domain from the C2 domain. Importantly, the phosphorylation of Tyr783 and its subsequent engagement by the cSH2 domain is predicted to induce a large-scale rearrangement of the regulatory domains with respect to the core before the phospholipase can hydrolyze membrane-resident PIP_2.

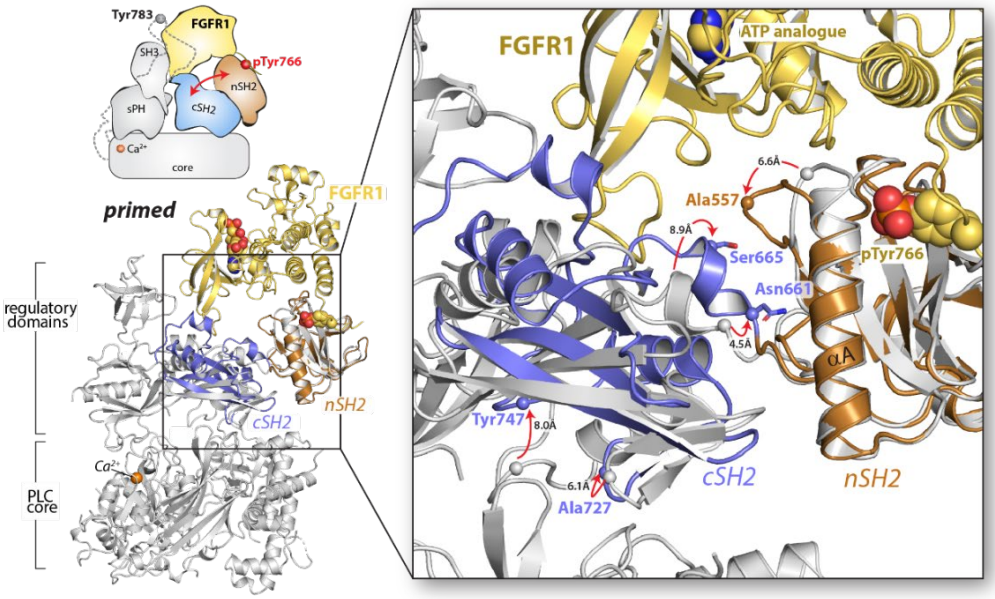

Figure 3.17 – Proposed mechanism for priming of PLC-γ1 by FGFR1. The structure of the SH2 domain array of PLC-γ1 bound to the kinase domain of FGFR1 (nSH2 domain, orange; cSH2 domain, blue; FGFR1 kinase domain, yellow; PDB code: 3GQI) was superimposed on the structure of autoinhibited PLC-γ1 (gray) using the nSH2 domain. Red arrows indicate displacement of select residues (spheres represent Cα atoms).

REFERENCES

1. Harden, T.K., and Sondek, J. (2006). Regulation of phospholipase C isozymes by Ras superfamily GTPases. Annu Rev Pharmacol Toxicol *46*, 355-379.

2. Kadamur, G., and Ross, E.M. (2013). Mammalian phospholipase C. Annu Rev Physiol *75*, 127-154.

3. Asokan, S.B., Johnson, H.E., Rahman, A., King, S.J., Rotty, J.D., Lebedeva, I.P., Haugh, J.M., and Bear, J.E. (2014). Mesenchymal chemotaxis requires selective inactivation of myosin II at the leading edge via a noncanonical PLCγ/PKCα pathway. Dev Cell *31*, 747-760.

4. de Gorter, D.J., Beuling, E.A., Kersseboom, R., Middendorp, S., van Gils, J.M., Hendriks, R.W., Pals, S.T., and Spaargaren, M. (2007). Bruton's tyrosine kinase and phospholipase Cγ2 mediate chemokine-controlled B cell migration and homing. Immunity *26*, 93-104.

5. Jones, N.P., Peak, J., Brader, S., Eccles, S.A., and Katan, M. (2005). PLCg1 is essential for early events in integrin signalling required for cell motility. J Cell Sci *118*, 2695-2706.

6. Mouneimne, G., Soon, L., DesMarais, V., Sidani, M., Song, X., Yip, S.C., Ghosh, M., Eddy, R., Backer, J.M., and Condeelis, J. (2004). Phospholipase C and cofilin are required for carcinoma cell directionality in response to EGF stimulation. J Cell Biol *166*, 697-708.

7. Minichiello, L., Calella, A.M., Medina, D.L., Bonhoeffer, T., Klein, R., and Korte, M. (2002). Mechanism of TrkB-mediated hippocampal long-term potentiation. Neuron *36*, 121-137.

8. Vetter, M.L., Martin-Zanca, D., Parada, L.F., Bishop, J.M., and Kaplan, D.R. (1991). Nerve growth factor rapidly stimulates tyrosine phosphorylation of phospholipase C-γ1 by a kinase activity associated with the product of the trk protooncogene. Proc Natl Acad Sci USA *88*, 5650-5654.

9. Kim, H.K., Kim, J.W., Zilberstein, A., Margolis, B., Kim, J.G., Schlessinger, J., and Rhee, S.G. (1991). PDGF stimulation of inositol phospholipid hydrolysis requires PLC-γ1 phosphorylation on tyrosine residues 783 and 1254. Cell *65*, 435-441.

10. Nishibe, S., Wahl, M.I., Hernandez-Sotomayor, S.M., Tonks, N.K., Rhee, S.G., and Carpenter, G. (1990). Increase of the catalytic activity of phospholipase C-γ1 by tyrosine phosphorylation. Science *250*, 1253-1256.

11. Peters, K.G., Marie, J., Wilson, E., Ives, H.E., Escobedo, J., Del Rosario, M., Mirda, D., and Williams, L.T. (1992). Point mutation of an FGF receptor abolishes phosphatidylinositol turnover and Ca^{2+} flux but not mitogenesis. Nature *358*, 678-681.

12. Takahashi, T., Yamaguchi, S., Chida, K., and Shibuya, M. (2001). A single autophosphorylation site on KDR/Flk-1 is essential for VEGF-A-dependent activation of PLC-γ and DNA synthesis in vascular endothelial cells. EMBO J *20*, 2768-2778.

13. Wahl, M.I., Nishibe, S., Suh, P.G., Rhee, S.G., and Carpenter, G. (1989). Epidermal growth factor stimulates tyrosine phosphorylation of phospholipase C-II independently of receptor internalization and extracellular calcium. Proc Natl Acad Sci USA *86*, 1568-1572.

14. Law, C.L., Chandran, K.A., Sidorenko, S.P., and Clark, E.A. (1996). Phospholipase C-γ1 interacts with conserved phosphotyrosyl residues in the linker region of Syk and is a substrate for Syk. Mol Cell Biol *16*, 1305-1315.

15. Nakanishi, O., Shibasaki, F., Hidaka, M., Homma, Y., and Takenawa, T. (1993). Phospholipase C-γ1 associates with viral and cellular src kinases. J Biol Chem *268*, 10754-10759.

16. Schaeffer, E.M., Debnath, J., Yap, G., McVicar, D., Liao, X.C., Littman, D.R., Sher, A., Varmus, H.E., Lenardo, M.J., and Schwartzberg, P.L. (1999). Requirement for Tec kinases Rlk and Itk in T cell receptor signaling and immunity. Science *284*, 638-641.

17. Yang, Y.R., Choi, J.H., Chang, J.S., Kwon, H.M., Jang, H.J., Ryu, S.H., and Suh, P.G. (2012). Diverse cellular and physiological roles of phospholipase C-γ1. Adv Biol Regul *52*, 138-151.

18. Koss, H., Bunney, T.D., Behjati, S., and Katan, M. (2014). Dysfunction of phospholipase Cγ in immune disorders and cancer. Trends Biochem Sci *39*, 603-611.

19. Kataoka, K., Nagata, Y., Kitanaka, A., Shiraishi, Y., Shimamura, T., Yasunaga, J., Totoki, Y., Chiba, K., Sato-Otsubo, A., Nagae, G.*, et al.* (2015). Integrated molecular analysis of adult T cell leukemia/lymphoma. Nat Genet *47*, 1304-1315.

20. Vaque, J.P., Gomez-Lopez, G., Monsalvez, V., Varela, I., Martinez, N., Perez, C., Dominguez, O., Grana, O., Rodriguez-Peralto, J.L., Rodriguez-Pinilla, S.M.*, et al.* (2014). PLCG1 mutations in cutaneous T-cell lymphomas. Blood *123*, 2034-2043.

21. Woyach, J.A., Furman, R.R., Liu, T.M., Ozer, H.G., Zapatka, M., Ruppert, A.S., Xue, L., Li, D.H., Steggerda, S.M., Versele, M.*, et al.* (2014). Resistance mechanisms for the Bruton's tyrosine kinase inhibitor ibrutinib. New Engl J Med *370*, 2286-2294.

22. Behjati, S., Tarpey, P.S., Sheldon, H., Martincorena, I., Van Loo, P., Gundem, G., Wedge, D.C., Ramakrishna, M., Cooke, S.L., Pillay, N.*, et al.* (2014). Recurrent PTPRB and PLCG1 mutations in angiosarcoma. Nat Genet *46*, 376-379.

23. Ombrello, M.J., Remmers, E.F., Sun, G., Freeman, A.F., Datta, S., Torabi-Parizi, P., Subramanian, N., Bunney, T.D., Baxendale, R.W., Martins, M.S.*, et al.* (2012). Cold urticaria, immunodeficiency, and autoimmunity related to PLCG2 deletions. New Engl J Med *366*, 330-338.

24. Zhou, Q., Lee, G.S., Brady, J., Datta, S., Katan, M., Sheikh, A., Martins, M.S., Bunney, T.D., Santich, B.H., Moir, S.*, et al.* (2012). A hypermorphic missense mutation in PLCG2, encoding phospholipase Cγ2, causes a dominantly inherited autoinflammatory disease with immunodeficiency. Am J Hum Genet *91*, 713-720.

25. de Lange, K.M., Moutsianas, L., Lee, J.C., Lamb, C.A., Luo, Y., Kennedy, N.A., Jostins, L., Rice, D.L., Gutierrez-Achury, J., Ji, S.G.*, et al.* (2017). Genome-wide association study implicates immune activation of multiple integrin genes in inflammatory bowel disease. Nat Genet *49*, 256-261.

26. Gbadegesin, R.A., Adeyemo, A., Webb, N.J., Greenbaum, L.A., Abeyagunawardena, A., Thalgahagoda, S., Kale, A., Gipson, D., Srivastava, T., Lin, J.J.*, et al.* (2015). HLA-DQA1 and PLCG2 are candidate risk loci for childhood-onset steroid-sensitive nephrotic syndrome. J Am Soc Nephrol *26*, 1701-1710.

27. Parker, L., Bahat, H., Appel, M.Y., Baum, D.V., Forer, R., Pillar, N., Goldberg, M., and Goldman, M. (2019). Phospholipase C-γ2 activity in familial steroid-sensitive nephrotic syndrome. Pediatr Res *85*, 719-723.

28. Magno, L., Lessard, C.B., Martins, M., Lang, V., Cruz, P., Asi, Y., Katan, M., Bilsland, J., Lashley, T., Chakrabarty, P.*, et al.* (2019). Alzheimer's disease phospholipase C-γ2 (PLCG2) protective variant is a functional hypermorph. Alzheimers Res Ther *11*, 16.

29. Sims, R., van der Lee, S.J., Naj, A.C., Bellenguez, C., Badarinarayan, N., Jakobsdottir, J., Kunkle, B.W., Boland, A., Raybould, R., Bis, J.C.*, et al.* (2017). Rare coding variants in PLCG2, ABI3, and TREM2 implicate microglial-mediated innate immunity in Alzheimer's disease. Nat Genet *49*, 1373-1384.

30. Gresset, A., Hicks, S.N., Harden, T.K., and Sondek, J. (2010). Mechanism of phosphorylation-induced activation of phospholipase C-γ isozymes. J Biol Chem *285*, 35836-35847.

31. Bae, J.H., Lew, E.D., Yuzawa, S., Tome, F., Lax, I., and Schlessinger, J. (2009). The selectivity of receptor tyrosine kinase signaling is controlled by a secondary SH2 domain binding site. Cell *138*, 514-524.

32. Hajicek, N., Charpentier, T.H., Rush, J.R., Harden, T.K., and Sondek, J. (2013). Autoinhibition and phosphorylation-induced activation of phospholipase C-γ isozymes. Biochem *52*, 4810-4819.

33. Sherman, E., Barr, V.A., Merrill, R.K., Regan, C.K., Sommers, C.L., and Samelson, L.E. (2016). Hierarchical nanostructure and synergy of multimolecular signalling complexes. Nat Commun *7*, 12161.

34. Walliser, C., Retlich, M., Harris, R., Everett, K.L., Josephs, M.B., Vatter, P., Esposito, D., Driscoll, P.C., Katan, M., Gierschik, P.*, et al.* (2008). rac regulates its effector phospholipase Cγ2 through interaction with a split pleckstrin homology domain. J Biol Chem *283*, 30351-30362.

35. Hicks, S.N., Jezyk, M.R., Gershburg, S., Seifert, J.P., Harden, T.K., and Sondek, J. (2008). General and versatile autoinhibition of PLC isozymes. Mol Cell *31*, 383-394.

36. Everett, K.L., Buehler, A., Bunney, T.D., Margineanu, A., Baxendale, R.W., Vatter, P., Retlich, M., Walliser, C., Manning, H.B., Neil, M.A.*, et al.* (2011). Membrane environment exerts an important influence on rac-mediated activation of phospholipase Cγ2. Mol Cell Biol *31*, 1240-1251.

37. Poulin, B., Sekiya, F., and Rhee, S.G. (2005). Intramolecular interaction between phosphorylated tyrosine-783 and the C-terminal Src homology 2 domain activates phospholipase C-γ1. Proc Natl Acad Sci USA *102*, 4276-4281.

38. Huang, Z., Marsiglia, W.M., Basu Roy, U., Rahimi, N., Ilghari, D., Wang, H., Chen, H., Gai, W., Blais, S., Neubert, T.A.*, et al.* (2016). Two FGF receptor kinase molecules act in concert to recruit and transphosphorylate phospholipase Cγ. Mol Cell *61*, 98-110.

39. Gibson, D.G., Young, L., Chuang, R.Y., Venter, J.C., Hutchison, C.A., 3rd, and Smith, H.O. (2009). Enzymatic assembly of DNA molecules up to several hundred kilobases. Nat Methods *6*, 343-345.

40. Stols, L., Gu, M., Dieckman, L., Raffen, R., Collart, F.R., and Donnelly, M.I. (2002). A new vector for high-throughput, ligation-independent cloning encoding a tobacco etch virus protease cleavage site. Protein Expr Purif *25*, 8-15.

41. Otwinowski, Z., and Minor, W. (1997). Processing of X-ray diffraction data collected in oscillation mode. Methods Enzymol *276*, 307-326.

42. Adams, P.D., Afonine, P.V., Bunkoczi, G., Chen, V.B., Davis, I.W., Echols, N., Headd, J.J., Hung, L.W., Kapral, G.J., Grosse-Kunstleve, R.W., McCoy, A.J., Moriarty, N.W., Oeffner, R., Read, R.J., Richardson, D.C., Richardson, J.S., Terwilliger, T.C., and Zwart, P.H. (2010). PHENIX: a comprehensive Python-based system for macromolecular structure solution. Acta Crystallogr D Biol Crystallogr *66*, 213-221.

43. Terwilliger, T.C., Grosse-Kunstleve, R.W., Afonine, P.V., Moriarty, N.W., Zwart, P.H., Hung, L.W., Read, R.J., and Adams, P.D. (2008). Iterative model building, structure refinement and density modification with the PHENIX AutoBuild wizard. Acta Crystallogr D Biol Crystallogr *64*, 61-69.

44. Emsley, P., Lohkamp, B., Scott, W.G., and Cowtan, K. (2010). Features and development of Coot. Acta Crystallogr D Biol Crystallogr *66*, 486-501.

45. Chen, V.B., Arendall, W.B., 3rd, Headd, J.J., Keedy, D.A., Immormino, R.M., Kapral, G.J., Murray, L.W., Richardson, J.S., and Richardson, D.C. (2010). MolProbity: all-atom structure validation for macromolecular crystallography. Acta Crystallogr D Biol Crystallogr *66*, 12-21.

46. Waldo, G.L., Ricks, T.K., Hicks, S.N., Cheever, M.L., Kawano, T., Tsuboi, K., Wang, X., Montell, C., Kozasa, T., Sondek, J., and Harden, T.K. (2010). Kinetic

scaffolding mediated by a phospholipase C-β and Gq signaling complex. Science *330*, 974-980.

47. Charpentier, T.H., Waldo, G.L., Barrett, M.O., Huang, W., Zhang, Q., Harden, T.K., and Sondek, J. (2014). Membrane-induced allosteric control of phospholipase C-β isozymes. J Biol Chem *289*, 29545-29557.

48. Huang, W., Wang, X., Endo-Streeter, S., Barrett, M., Waybright, J., Wohlfeld, C., Hajicek, N., Harden, T.K., Sondek, J., and Zhang, Q. (2018). A membrane-associated, fluorogenic reporter for mammalian phospholipase C isozymes. J Biol Chem *293*, 1728-1735.

49. Marti-Renom, M.A., Stuart, A.C., Fiser, A., Sanchez, R., Melo, F., and Sali, A. (2000). Comparative protein structure modeling of genes and genomes. Annu Rev Biophys Biomol Struct *29*, 291-325.

50. Zimmermann, L., Stephens, A., Nam, S., Rau, D., Kübler, J., Lozajic, M., Gabler, F., Söding, J., Lupas, A., and Alva, V. (2017). A completely reimplemented MPI bioinformatics toolkit with a new HHpred server at its core. J Mol Biol.

51. Lyon, A.M., Tesmer, V.M., Dhamsania, V.D., Thal, D.M., Gutierrez, J., Chowdhury, S., Suddala, K.C., Northup, J.K., and Tesmer, J.J. (2011). An autoinhibitory helix in the C-terminal region of phospholipase C-β mediates Ga_q activation. Nat Struct Mol Biol *18*, 999-1005.

52. Gagné, S.M., Tsuda, S., Li, M.X., Smillie, L.B., and Sykes, B.D. (1995). Structures of the troponin C regulatory domains in the apo and calcium-saturated states. Nat Struct Biol *2*, 784-789.

53. Case, D.A., Cerutti, D.S., Cheatham, I., T. E., Darden, T.A., Duke, R.E., Giese, T.J., Gohlke, H., Goetz, A.W., Greene, D., Homeyer, N., Izadi, S., Kovalenko, A., Lee, T.S., LeGrand, S., Li, P., Lin, C., Liu, J., Luchko, T., Luo, R., Mermelstein, D., Merz, K.M., Monard, G., Nguyen, H., Omelyan, I., Onufriev, A., Pan, F., Qi, R., Roe, D.R., Roitberg, A., Sagui, C., Simmerling, C.L., Botello-Smith, W.M., Swails, J., Walker, R.C., Wang, J., Wolf, R.M., Wu, X., Xiao, L., York, D.M., and Kollman, P.A. (2017). AMBER 2017. University of California, San Francisco.

54. Maier, J.A., Martinez, C., Kasavajhala, K., Wickstrom, L., Hauser, K.E., and Simmerling, C. (2015). ff14SB: improving the accuracy of protein side chain and backbone parameters from ff99SB. J Chem Theory Comput *11*, 3696-3713.

55. Pierce, L.C., Salomon-Ferrer, R., Augusto, F.d.O.C., McCammon, J.A., and Walker, R.C. (2012). Routine access to millisecond time scale events with accelerated molecular dynamics. J Chem Theory Comput *8*, 2997-3002.

56. Falasca, M., Logan, S.K., Lehto, V.P., Baccante, G., Lemmon, M.A., and Schlessinger, J. (1998). Activation of phospholipase Cγ by PI 3-kinase-induced PH domain-mediated membrane targeting. EMBO J *17*, 414-422.

57. Ellis, M.V., James, S.R., Perisic, O., Downes, C.P., Williams, R.L., and Katan, M. (1998). Catalytic domain of phosphoinositide-specific phospholipase C (PLC).

Mutational analysis of residues within the active site and hydrophobic ridge of PLCd1. J Biol Chem *273*, 11650-11659.

58. Ananthanarayanan, B., Das, S., Rhee, S.G., Murray, D., and Cho, W. (2002). Membrane targeting of C2 domains of phospholipase C-δ isoforms. J Biol Chem *277*, 3568-3575.

59. Lomasney, J.W., Cheng, H.F., Kobayashi, M., and King, K. (2012). Structural basis for calcium and phosphatidylserine regulation of phospholipase C δ1. Biochem *51*, 2246-2257.

60. Nishida, M., Sugimoto, K., Hara, Y., Mori, E., Morii, T., Kurosaki, T., and Mori, Y. (2003). Amplification of receptor signalling by Ca^{2+} entry-mediated translocation and activation of PLCγ2 in B lymphocytes. EMBO J *22*, 4677-4688.

61. Bunney, T.D., Esposito, D., Mas-Droux, C., Lamber, E., Baxendale, R.W., Martins, M., Cole, A., Svergun, D., Driscoll, P.C., and Katan, M. (2012). Structural and functional integration of the PLCγ interaction domains critical for regulatory mechanisms and signaling deregulation. Structure *20*, 2062-2075.

62. Lemmon, M.A., and Schlessinger, J. (2010). Cell signaling by receptor tyrosine kinases. Cell *141*, 1117-1134.

63. Rouquette-Jazdanian, A.K., Sommers, C.L., Kortum, R.L., Morrison, D.K., and Samelson, L.E. (2012). LAT-independent Erk activation via Bam32-PLC-γ1-Pak1 complexes: GTPase-independent Pak1 activation. Mol Cell *48*, 298-312.

64. Timsah, Z., Ahmed, Z., Lin, C.C., Melo, F.A., Stagg, L.J., Leonard, P.G., Jeyabal, P., Berrout, J., O'Neil, R.G., Bogdanov, M.*, et al.* (2014). Competition between Grb2 and Plcg1 for FGFR2 regulates basal phospholipase activity and invasion. Nat Struct Mol Biol *21*, 180-188.

65. DeBell, K.E., Stoica, B.A., Veri, M.C., Di Baldassarre, A., Miscia, S., Graham, L.J., Rellahan, B.L., Ishiai, M., Kurosaki, T., and Bonvini, E. (1999). Functional independence and interdependence of the Src homology domains of phospholipase C-γ1 in B-cell receptor signal transduction. Mol Cell Biol *19*, 7388-7398.

66. Poulin, B., Sekiya, F., and Rhee, S.G. (2000). Differential roles of the Src homology 2 domains of phospholipase C-γ1 (PLC-γ1) in platelet-derived growth factor-induced activation of PLC-g1 in intact cells. J Biol Chem *275*, 6411-6416.

67. Deng, L., Velikovsky, C.A., Swaminathan, C.P., Cho, S., and Mariuzza, R.A. (2005). Structural basis for recognition of the T cell adaptor protein SLP-76 by the SH3 domain of phospholipase Cγ1. J Mol Biol *352*, 1-10.

68. Tvorogov, D., and Carpenter, G. (2002). EGF-dependent association of phospholipase C-γ1 with c-Cbl. Exp Cell Res *277*, 86-94.

69. Braiman, A., Barda-Saad, M., Sommers, C.L., and Samelson, L.E. (2006). Recruitment and activation of PLCg1 in T cells: a new insight into old domains. EMBO J *25*, 774-784.

70. Knyazhitsky, M., Moas, E., Shaginov, E., Luria, A., and Braiman, A. (2012). Vav1 oncogenic mutation inhibits T cell receptor-induced calcium mobilization through inhibition of phospholipase Cγ1 activation. J Biol Chem *287*, 19725-19735.

71. Wang, J., Sohn, H., Sun, G., Milner, J.D., and Pierce, S.K. (2014). The autoinhibitory C-terminal SH2 domain of phospholipase C-γ2 stabilizes B cell receptor signalosome assembly. Sci Signal *7*, ra89.

72. Piechulek, T., Rehlen, T., Walliser, C., Vatter, P., Moepps, B., and Gierschik, P. (2005). Isozyme-specific stimulation of phospholipase C-γ2 by Rac GTPases. J Biol Chem *280*, 38923-38931.

73. Walliser, C., Retlich, M., Harris, R., Everett, K.L., Josephs, M.B., Vatter, P., Esposito, D., Driscoll, P.C., Katan, M., Gierschik, P.*, et al.* (2008). rac regulates its effector phospholipase Cγ2 through interaction with a split pleckstrin homology domain. J Biol Chem *283*, 30351-30362.

74. Walliser, C., Hermkes, E., Schade, A., Wiese, S., Deinzer, J., Zapatka, M., Desire, L., Mertens, D., Stilgenbauer, S., and Gierschik, P. (2016). The phospholipase Cγ2 mutants R665W and L845F identified in ibrutinib-resistant chronic lymphocytic leukemia patients are hypersensitive to the Rho GTPase Rac2 protein. J Biol Chem *291*, 22136-22148.

75. Serrano, C.J., Graham, L., DeBell, K., Rawat, R., Veri, M.C., Bonvini, E., Rellahan, B.L., and Reischl, I.G. (2005). A new tyrosine phosphorylation site in PLC-γ1: the role of tyrosine 775 in immune receptor signaling. J Immunol *174*, 6233-6237.

76. Humphries, L.A., Dangelmaier, C., Sommer, K., Kipp, K., Kato, R.M., Griffith, N., Bakman, I., Turk, C.W., Daniel, J.L., and Rawlings, D.J. (2004). Tec kinases mediate sustained calcium influx via site-specific tyrosine phosphorylation of the phospholipase Cγ Src homology 2-Src homology 3 linker. J Biol Chem *279*, 37651-37661.

77. Ozdener, F., Dangelmaier, C., Ashby, B., Kunapuli, S.P., and Daniel, J.L. (2002). Activation of phospholipase Cγ2 by tyrosine phosphorylation. Mol Pharmacol *62*, 672-679.

78. Rodriguez, R., Matsuda, M., Perisic, O., Bravo, J., Paul, A., Jones, N.P., Light, Y., Swann, K., Williams, R.L., and Katan, M. (2001). Tyrosine residues in phospholipase Cγ2 essential for the enzyme function in B-cell signaling. J Biol Chem *276*, 47982-47992.

79. Watanabe, D., Hashimoto, S., Ishiai, M., Matsushita, M., Baba, Y., Kishimoto, T., Kurosaki, T., and Tsukada, S. (2001). Four tyrosine residues in phospholipase C-γ2, identified as Btk-dependent phosphorylation sites, are required for B cell antigen receptor-coupled calcium signaling. J Biol Chem *276*, 38595-38601.

80. Huang, W., Hicks, S.N., Sondek, J., and Zhang, Q. (2011). A fluorogenic, small molecule reporter for mammalian phospholipase C isozymes. ACS Chem Biol *6*, 223-228.

81. Burger, J.A., Landau, D.A., Taylor-Weiner, A., Bozic, I., Zhang, H., Sarosiek, K., Wang, L., Stewart, C., Fan, J., Hoellenriegel, J.*, et al.* (2016). Clonal evolution in patients with chronic lymphocytic leukaemia developing resistance to BTK inhibition. Nat Commun *7*, 11589.

82. Choi, J., Goh, G., Walradt, T., Hong, B.S., Bunick, C.G., Chen, K., Bjornson, R.D., Maman, Y., Wang, T., Tordoff, J.*, et al.* (2015). Genomic landscape of cutaneous T cell lymphoma. Nat Genet *47*, 1011-1019.

83. da Silva Almeida, A.C., Abate, F., Khiabanian, H., Martinez-Escala, E., Guitart, J., Tensen, C.P., Vermeer, M.H., Rabadan, R., Ferrando, A., and Palomero, T. (2015). The mutational landscape of cutaneous T cell lymphoma and Sezary syndrome. Nat Genet *47*, 1465-1470.

84. Kiel, M.J., Sahasrabuddhe, A.A., Rolland, D.C., Velusamy, T., Chung, F., Schaller, M., Bailey, N.G., Betz, B.L., Miranda, R.N., Porcu, P.*, et al.* (2015). Genomic analyses reveal recurrent mutations in epigenetic modifiers and the JAK-STAT pathway in Sézary syndrome. Nat Commun *6*, 8470.

85. Everett, K.L., Bunney, T.D., Yoon, Y., Rodrigues-Lima, F., Harris, R., Driscoll, P.C., Abe, K., Fuchs, H., de Angelis, M.H., Yu, P.*, et al.* (2009). Characterization of phospholipase Cγ enzymes with gain-of-function mutations. J Biol Chem *284*, 23083-23093.

86. Wilson, T.R., Fridlyand, J., Yan, Y., Penuel, E., Burton, L., Chan, E., Peng, J., Lin, E., Wang, Y., Sosman, J.*, et al.* (2012). Widespread potential for growth-factor-driven resistance to anticancer kinase inhibitors. Nature *487*, 505-509.

87. Groesch, T.D., Zhou, F., Mattila, S., Geahlen, R.L., and Post, C.B. (2006). Structural basis for the requirement of two phosphotyrosine residues in signaling mediated by Syk tyrosine kinase. J Mol Biol *356*, 1222-1236.

88. Arteaga, C.L., Johnson, M.D., Todderud, G., Coffey, R.J., Carpenter, G., and Page, D.L. (1991). Elevated content of the tyrosine kinase substrate phospholipase C-γ1 in primary human breast carcinomas. Proc Natl Acad Sci USA *88*, 10435-10439.

89. Peles, E., Levy, R.B., Or, E., Ullrich, A., and Yarden, Y. (1991). Oncogenic forms of the neu/HER2 tyrosine kinase are permanently coupled to phospholipase Cγ. EMBO J *10*, 2077-2086.

90. Straussman, R., Morikawa, T., Shee, K., Barzily-Rokni, M., Qian, Z.R., Du, J., Davis, A., Mongare, M.M., Gould, J., Frederick, D.T.*, et al.* (2012). Tumour micro-environment elicits innate resistance to RAF inhibitors through HGF secretion. Nature *487*, 500-504.

91. Guittard, G., Dios-Esponera, A., Palmer, D.C., Akpan, I., Barr, V.A., Manna, A., Restifo, N.P., and Samelson, L.E. (2018). The Cish SH2 domain is essential for PLC-γ1 regulation in TCR stimulated $CD8^+$ T cells. Sci Rep *8*, 5336

CHAPTER IV: ALLOSTERIC REGULATION OF THE PLC-γ ISOZYMES[3]

Background

Cells maintain homeostasis by responding to a multitude of extracellular ligands including neurotransmitters, hormones, and growth factors. These extracellular ligands bind to cell-surface receptors that amplify and relay signals from the outside to the inside of the cell through the creation of second messengers (1). One such example is the creation of 1,2-diacyglycerol (DAG) and inositol 1,4,5-trisphosphate (IP_3) from the hydrolysis of membrane-embedded phosphatidylinositol 4,5-bisphosphate (PIP_2) by the phosphoinositide-specific phospholipase C (PLC) isozymes (2, 3). The regulated activation of this signaling pathway is fundamental for the control of diverse biological processes including cell growth, proliferation, differentiation, and migration (2, 3).

The thirteen mammalian PLC isozymes are grouped into six subgroups (-β, -γ, -δ, -ε, -ζ, -η) based on sequence similarity; they share a highly conserved catalytic core comprised of an N-terminal pleckstrin homology (PH) domain, two pairs of EF hands, a catalytic triosephosphate isomerase (TIM) barrel, and a C-terminal C2 domain (2, 3). In the majority of mammalian PLCs, enzymatic activity is basally autoinhibited by a mostly disordered and negatively charged linker that prevents membrane association via electrostatic repulsion (2-4). In contrast, the two PLC-γ isozymes (-γ1 and -γ2) possess an elaborate linker that includes additional regulatory domains: a split PH (sPH) domain, two Src-homology 2 (SH2) domains in tandem, and an SH3 domain (3, 5).

[3] A version of this chapter was submitted as an article for publication in Journal of Biological Chemistry. The original citation is as follows: Siraliev-Perez, E., Hoffman, R., Stariha, J., Zhang, Q., Hajicek, N., Burke, J., and Sondek, J. (2020) "Dynamics of allosteric activation of the PLC-γ isozymes" *Journal of Biological Chemistry* (submitted)

The PLC-γ isozymes are unique because they require tyrosine phosphorylation for activation (6-8). Depending on the cell context, the PLC-γ isozymes are phosphorylated by soluble tyrosine kinases associated with immune receptors as well as by receptor tyrosine kinases (RTKs) for a variety of growth factors including members of the fibroblast growth factor receptor (FGFR) family (2, 3, 5, 9). Phosphorylation-dependent activation of the PLC-γ isozymes downstream of a multitude of extracellular ligands is necessary for the proper development of a mature vascular system, directed cell migration, and mounting of an immune response (10).

Aberrant PLC-γ isozyme signaling has been identified in a variety of human diseases including cancers and immune disorders. For example, PLC-γ1 is overexpressed in human cancers such as breast (11, 12), prostate (12), and colon cancers (13, 14). With the advent of genome-wide sequencing, studies have identified acquired mutations in both PLC-γ1 and PLC-γ2 in several immunoproliferative malignancies. For example, PLC-γ1 is the most frequently mutated protein in approximately 40% of patients with adult T cell leukemia/lymphoma where hotspots of mutation where found wide-spread throughout the entire primary sequence of the protein (15). Moreover, variants of PLC-γ2 arise in approximately 30% of patients with relapsed chronic lymphocytic leukemia after treatment with ibrutinib, a covalent inhibitor of Bruton's tyrosine kinase (16).

We recently described the first crystal structure of essentially full-length PLC-γ1 in the autoinhibited state (17). The structure, together with biochemical and computational studies, provides insights into the regulated activation of the PLC-γ isozymes. The structure illustrates how the regulatory domains sit on top of the catalytic core to form two interfaces: residues of the sPH domain interdigitate with hydrophobic residues of the TIM barrel and the C-terminal SH2 domain (cSH2) clasps the C2 domain. This arrangement is poised to autoinhibit phospholipase activity while simultaneously integrating

phosphorylation-dependent activation and scaffolding properties of the regulatory domains. In addition, we demonstrated that most cancer-associated substitutions reside within the two interfaces between the regulatory domains and the catalytic core to elevate phospholipase activity in cells and with purified components.

Based on these results, we developed a high-resolution model for the regulated activation of PLC-γ isozymes. In this model, kinases bind to the nSH2 domain, phosphorylate one or more tyrosines within the regulatory domains, and these phosphorylated tyrosines then bind to the cSH2 domain to unlatch this domain from the catalytic core. Unlatching presumably initiates a rearrangement of the regulatory domains relative to the catalytic core that liberates the active site to bind membranes (17, 18).

The structure also provides unrealized opportunities to understand the dynamic regulation of the PLC-γ isozymes at atomic resolution. In particular, hydrogen-deuterium exchange mass spectrometry (HDX-MS) coupled with structural information has proven useful for mapping regions of large proteins that dynamically respond to mutations (19), the binding of additional proteins (20), or changes in solvent conditions as exemplified by the interaction of proteins with membranes (19, 21). Since an overall goal of our work has been to understand how PLC-γ isozymes operate at membranes, we used HDX-MS to define the exchange kinetics of PLC-γ1 as it interacts with the kinase domain of FGFR1 and liposomes containing PIP_2.

In this report we show that binding of the phosphorylated kinase domain of FGFR1 to PLC-γ1 allosterically disrupts autoinhibition and that kinases and membranes can cooperate to activate PLC-γ1, likely via stabilization of the ensemble of active PLC-γ1.

Materials and Methods

Molecular cloning

PLC-γ1 – Transfer vector (pFB-LIC2) encoding wild-type rat PLC-γ1 (residues 21-1215) and PLC-γ1 (D1165H) have been previously described (17). The H335A mutation that renders PLC-γ1 catalytically inactive was introduced into the transfer vector encoding wild-type PLC-γ1 (residues 21-1215) or PLC-γ1 (D1165H) using standard primer-mediated mutagenesis (Agilent Technologies; QuikChange site-directed mutagenesis manual). Mutagenesis was confirmed by automated DNA sequencing of the open reading frame. These constructs are referred as PLC-γ1 (H335A) and PLC-γ1 (H335A+D1165H), respectively.

FGFR1K – Plasmid DNA encoding the kinase domain (residues 458-774) of human fibroblast growth factor receptor 1 (FGFR1) with four substitutions (Y463F, Y583F, Y585F, Y730F) was synthesized by Genewiz (South Plainfield, NJ). The plasmid DNA encoding this variant of FGFR1K was then sub cloned from a pUC57-Amp vector to a modified pFastBac-HT vector (pFB-LIC2) using ligation-independent cloning (LIC) strategy (27). The baculovirus expression vector, pFB-LIC2, incorporates a His6 tag and a tobacco etch virus (TEV) protease site at the amino terminus of the expressed protein. This variant of FGFR1K is referred as FGFR1K (4Y/F). Two substitutions that render the kinase catalytically inactive (Y653F+Y654F) were introduced into the original transfer vector encoding FGFR1K (4Y/F) using standard primer-mediated mutagenesis s (Agilent Technologies; QuikChange site-directed mutagenesis manual). The Y766F substitution was introduced separately into the original transfer vector encoding FGFR1K (4Y/F) using standard primer-mediated mutagenesis. This substitution eliminates the PLC-γ1 binding site at the C-terminal tail of the kinase domain and is referred as FGFR1K (5Y/F). All FGFR1K variants were verified by automated DNA sequencing of the open reading frame.

Protein expression and purification

PLC-γ1 – Expression and purification of PLC-γ1 variants have been previously described (17) and was employed here with minor modifications. Briefly, four liters of High Five (*T. ni*) cells at a density of approximately 2.0 x 10^6 cells/mL were infected with amplified baculovirus stock (10 - 15mL/L) encoding individual PLC-γ1 variants. Cells were harvested approximately 48 hr. post-infection by centrifugation at 6,000 rpm in a Beckman JA-10 rotor at 4°C. Cell pellet was resuspended in 200 mL of buffer N1 (20 mM HEPES (pH 7.5), 300 mM NaCl, 10 mM imidazole, 10% v/v glycerol, and 0.1 mM EDTA) supplemented with 10 mM 2-mercaptoethanol (BME) and four EDTA-free cOmplete protease inhibitor tablets (Roche Applied Science) prior to lysis using the Nano DeBEE High Pressure Homogenizer (BEE International). Lysate was centrifuged at 50,000 rpm for 1 hr. in a Beckman Ti70 rotor. The supernatant was filtered through a 0.45 μm polyethersulfone (PES) low protein-binding filter and loaded onto a 5 mL HisTrap HP immobilized metal affinity chromatography (IMAC) column equilibrated in buffer N1. The column was washed with 15 column volumes (CV) of buffer N1, followed by 15 CV of 2.5% buffer N2 (buffer N1 + 1 M imidazole). Bound proteins were eluted with 40% buffer N2. Fractions containing PLC-γ1 were pooled and dialyzed overnight in the presence of 2% (w/w) TEV protease to remove the His6 tag in a buffer solution containing 20 mM HEPES (pH 7.5), 300 mM NaCl, 10% v/v glycerol, 1 mM dithiothreitol (DTT), 1 mM EDTA. The sample was subsequently diluted 2-fold with buffer N1 and applied to a 5 mL HisTrap HP column. Flow-through fractions containing cleaved PLC-γ1 were pooled, diluted 4-fold with buffer Q1 (20 mM HEPES (pH 7.5) and 2 mM DTT), and loaded onto an 8 mL SourceQ anion exchange column equilibrated in 10% buffer Q2 (buffer Q1 + 1 M NaCl). Bound proteins were eluted in a linear gradient of 10% - 60% buffer Q2 over 50 CV. Fractions containing PLC-γ1 were pooled, concentrated using a GE Healthcare VivaSpin 50K

molecular weight cut-off (MWCO) centrifugal concentrator and applied to a 16 mm x 700 mm HiLoad Superdex 200 size exclusion column equilibrated in a buffer solution containing 20 mM HEPES (pH 7.5), 150 mM NaCl, 5% v/v glycerol, and 2 mM DTT. Pure PLC-γ1 was concentrated to a final concentration of 40 - 80 mg/mL, aliquoted, snap-frozen in liquid nitrogen, and stored at -80°C until use.

FGFR1K – Expression and purification of FGFR1K (6Y/F) follows that of PLC-γ1 variants with the following modifications. After removal of His6 tag by TEV protease and subsequent 5 mL HisTrap HP IMAC column, the sample was concentrated using a GE Healthcare VivaSpin 10K MWCO centrifugal concentrator. Concentrated sample was applied to a 16 mm x 700 mm HiLoad Superdex 200 size exclusion column equilibrated in buffer containing 20 mM HEPES (pH 7.5), 200 mM NaCl, 5% (v/v) glycerol, and 2 mM DTT. Fractions containing pure FGFR1K (6Y/F) were concentrated to a final concentration of 20 - 30 mg/mL, aliquoted, snap-frozen in liquid nitrogen, and stored at -80°C until use. The FGFR1K (5Y/F) variant was expressed as described above and the purification protocol terminates after the first 5 mL HisTrap HP IMAC column. This variant of FGFR1K retains the His6 tag.

In vitro phosphorylation of FGFR1K

Equimolar concentrations (100 μM) of purified FGFR1K (6Y/F) were incubated with purified His6-tagged FGFR1K (5Y/F) in 20 mM HEPES (pH 7.5), 50 mM NaCl, 25 mM $MgCl_2$, 50 ng/mL fatty-acid free bovine serum albumin (FAF BSA), 10 mM ATP, and 2 mM DTT. The phosphorylation reaction was terminated after 100 minutes and phosphorylation of the kinase was confirmed via native PAGE followed by staining with Coomassie Brilliant Blue. Sample was loaded onto a 1mL HisTrap HP IMAC to separate kinases using a 200 μL sample loop. The sample loop was washed with 2 mL of buffer N1 (20 mM HEPES pH 7.5, 100 mM NaCl, 10 mM $MgCl_2$, and 2 mM DTT). The column was washed with 5 CV of

buffer N1, followed by 5 CV of 40% buffer N2 (buffer N1 + 1 M imidazole), and 5 CV of 100% buffer N2. Flow-through fractions containing phosphorylated FGFR1K (6Y/F) were pooled and concentrated using a GE Healthcare Vivaspin 6 10K MWCO, aliquoted, snap-frozen in liquid nitrogen, and stored at -80°C until use.

LC-MS/MS of phosphorylated FGFR1K

Phosphorylated FGFR1K was diluted and loaded onto a native PAGE followed by staining with Coomassie Brilliant Blue. Gel bands were excised and digested with trypsin overnight. Peptides were extracted, then analyzed by LC/MS/MS using the Thermo Easy nLC 1200-QExactive HF. Data were searched against a Uniprot Sf9 database including the sequence for FGFR1K using Sequest within Proteome Discoverer 2.1. All data were filtered using a false discovery rate (FDR) of 5%.

Formation of PLC-γ1:FGFR1K complex

Phosphorylated FGFR1K was generated as described above. Either PLC-γ1 (H335A) or PLC-γ1(H335A+D1165H) was added in a 2-fold molar excess relative to kinase. The sample was immediately loaded onto a 10 mm × 300 mm Superdex 200 GL size exclusion column equilibrated with 20 mM HEPES (pH 7.5), 100 mM NaCl, 10 mM $MgCl_2$, and 2 mM DTT. Pure complex was pooled and concentrated using a GE Healthcare Vivaspin 6 10K MWCO, aliquoted, snap-frozen in liquid nitrogen, and stored at -80°C until use. Formation of the complex was confirmed via SDS-PAGE followed by staining with Coomassie Brilliant Blue.

In vitro quantification of phospholipase activity

XY-69 fluorogenic assay – Liposomes with a final PE:PIP_2 content of 80:20 were generated by mixing 750 nM XY-69 (24), 192 μM of liver phosphatidylethanolamine (PE, Avanti Polar Lipids), 48 μM brain phosphatidylinositol 4,5-bisphosphate (PIP_2, Avanti Polar

Lipids) in 12 x 75 mm borosilicate tubes. Lipids were dried under a nitrogen stream followed by high vacuum (0.5 mtorr). Dried lipid mixture was suspended in 20 mM HEPES (pH 7.5) using a probe microtip sonicator of 5/64" at 20% output for 3 cycles of 5 sec ON, 15 sec OFF. Concurrently, the PLC-γ1 proteins were diluted in a buffer containing 20 mM HEPES (pH 7.5), 50 mM NaCl, 2 mM DTT, and 1 mg/mL FAF BSA. The 6X assay buffer containing 80 mM HEPES (pH 7.5), 420 mM KCl, 10 mM DTT, 18 mM EGTA, and 14.1 mM $CaCl_2$ (~390 nM free Ca^{2+}) was added to the resuspended lipid mixture in a 1:4 ratio. To a non-binding surface (NBS)-treated Corning 384-well plate, 2 μL of diluted PLC-γ1 proteins were added. PLC-γ1 variants (WT or D1165H) were either alone or in the presence of a two-fold molar excess of unphosphorylated or phosphorylated FGFR1K relative to PLC-γ1. To initiate the assay, 10 μL of the lipid and assay buffer mixture was added. The plates were incubated at 30°C and data was recorded for 30 min at intervals of 1 min using excitation and emission wavelengths of 485 nm and 520 nm, respectively. Fluorescence intensity was normalized to a blank reaction lacking phospholipase, and initial rates of XY-69 hydrolysis were calculated from the slope of the linear portion of the curve. Final concentrations of XY-69, PIP_2, and PE were 5 μM, 48 μM, and 192 μM, respectively.

WH-15 fluorogenic assay – Assays with the soluble substrate WH-15 were performed as described previously (25) with the following modifications. WH-15 was diluted to a final concentration of 5 μM in assay buffer containing 50 mM HEPES (pH 7.5), 70 mM KCl, 3 mM EGTA, 2.97 mM $CaCl_2$ (~10 μM free Ca^{2+}), 50 μg/mL FAF BSA, and 2 mM DTT. Basal fluorescence was equilibrated for approximately 10 minutes before addition of PLC-γ1 (D1165) alone or in the presence of a two-fold molar excess of unphosphorylated or phosphorylated FGFR1K (6Y/F) relative to PLC-γ1 (1nM, final concentration). Data was recorded for 1 hr. at intervals of 30 sec using excitation and

emission wavelengths of 488 nm and 520 nm, respectively. Fluorescence intensity was normalized to the reaction lacking phospholipase, and initial rates of WH-15 hydrolysis were calculated from the slope of the linear portion of the curve.

Liposome floatation assay

Liposomes with a final content of 90% PE and 10% PIP_2 were prepared as described above and resuspended in 20 mM HEPES (pH 7.5). Concurrently PLC-γ1 (H335A), alone or in complex with phosphorylated FGFR1K (6Y/F) were diluted in assay buffer containing 100 mM HEPES (pH 7.5), 150 mM NaCl, 10 mM KCl, 10 μM $CaCl_2$, 0.5 mM tris(2-carboxyethyl)phosphine (TCEP). PLC-γ1 and liposomes were mixed and incubated on ice for 2 min. Immediately after mixing, 100 μL of assay buffer with 75% sucrose were added to the protein-lipid mixture to a final concentration of 30% sucrose in 250 μL total volume. The samples were overlaid with 200 μL of assay buffer with 25% sucrose and 50 μL of assay buffer. Samples were centrifuged at 55,000 rpm in a TLS-55 rotor for 1 hr at 4°C. After centrifugation, three fractions were collected: bottom (B, 250 μL), middle (M, 150 μL), and top (T, 100 μL). Samples (30 μL) of each fraction were mixed with 7 μL of 6X SDS sample buffer and analyzed by SDS-PAGE followed by staining with Coomassie Brilliant Blue.

Hydrogen Deuterium eXchange-Mass Spectrometry

Sample preparation – Exchange reactions were carried out at 18°C in 20 μL volumes with a final concentration of 1.25 μM PLC-γ1 (H335A), PLC-γ1 (H335A+D1165H), PLC-γ1 (H335A)-FGFR1K complex, or PLC-γ1 (H335A+D1165H)-FGFR1K complex. A total of eight conditions were assessed: four in the presence of liposomes containing 90% phosphatidylethanolamine (PE) and 10% phosphatidylinositol 4,5-bisphosphate (PIP_2) and four in the absence of liposomes. The conditions were as follows:

- PLC-γ1(H335A) alone
- PLC-γ1(H335A+D1165H) alone
- PLC-γ1(H335A)-FGFR1K
- PLC-γ1(H335A+D1165H)-FGFR1K
- PLC-γ1(H335A) + liposomes
- PLC-γ1(H335A+D1165H) + liposomes
- PLC-γ1(H335A)-FGFR1K + liposomes
- PLC-γ1(H335A+D1165H)-FGFR1K + liposomes

For conditions containing lipid, liposomes were present at a final concentration of 320 μM. Prior to the addition of D_2O, 2.0 μL of liposomes (or liposome buffer [20 mM HEPES pH 7.5, 100 mM KCl]) was added to 1.5 μL of protein, and the solution was left to incubate at 18°C for 2 min. The hydrogen-deuterium exchange reaction was initiated by the addition of 16.5 μL D_2O buffer (88% D_2O, 150 mM NaCl, 100 mM HEPES pH 7.0, 10 μM $CaCl_2$, 0.5 mM TCEP pH 7.5) to 3.5 μL protein or protein-liposome solution for a final D_2O concentration of 72%. Exchange was carried out over five time points (3, 30, 300, 3000, and 10000 sec) and terminated by the addition of 50 μL ice-cold acidic quench buffer (0.8 M guanidine-HCl, 1.2% formic acid). After quenching, samples were immediately frozen in liquid nitrogen and stored at -80°C. All reactions were carried out in triplicate.

Protein digestion and MS/MS data collection – Protein samples were rapidly thawed and injected onto an integrated fluidics system containing a HDx-3 PAL liquid handling robot and climate-controlled chromatography system (LEAP Technologies), a Dionex Ultimate 3000 UHPLC system, as well as an Impact HD QTOF Mass spectrometer (Bruker). The protein was run over two immobilized pepsin columns (Applied Biosystems; Poroszyme™ Immobilized Pepsin Cartridge, 2.1 mm x 30 mm; Thermo-Fisher 2-3131-00;

at 10°C and 2°C respectively) at 200 μL/min for 3 minutes. The resulting peptides were collected and desalted on a C18 trap column (Acquity UPLC® BEH^{TM} C18 1.7μm column (2.1 x 5 mm); Waters 186002350). The trap was subsequently eluted in line with a C18 reverse-phase separation column (Acquity 1.7 μm particle, 100 × 1 mm^2 C18 UPLC column, Waters 186002352), using a gradient of 5-36% B (Buffer A 0.1% formic acid; Buffer B 100% acetonitrile) over 16 minutes. Mass spectrometry experiments were performed on an Impact II QTOF (Bruker) acquiring over a mass range from 150 to 2200 *m/z* using an electrospray ionization source operated at a temperature of 200 °C and a spray voltage of 4.5 kV.

Peptide identification – Peptides were identified using data-dependent acquisition following tandem MS/MS experiments (0.5 s precursor scan from 150-2000 m/z; twelve 0.25 s fragment scans from 150-2000 m/z). MS/MS datasets were analyzed using PEAKS7 (PEAKS), and a false discovery rate was set at 1% using a database of purified proteins and known contaminants.

Mass analysis of peptide centroids and measurement of deuterium incorporation – HD-Examiner Software (Sierra Analytics) was used to automatically calculate the level of deuterium incorporation into each peptide. All peptides were manually inspected for correct charge state, correct retention time, appropriate selection of isotopic distribution, etc. Deuteration levels were calculated using the centroid of the experimental isotope clusters. Results for these proteins are presented as relative levels of deuterium incorporation and the only control for back exchange was the level of deuterium present in the buffer (72%). Changes in any peptide at any time point greater than specified cut-offs (5% and 0.4 Da) and with an unpaired, two-tailed t-test value of $p<0.01$ were considered significant.

Results

PLC-γ1 forms a stable complex with the phosphorylated kinase domain of FGFR1

To undertake the experiments, it was first necessary to ensure that PLC-γ1 was amenable to HDX-MS and that conditions could be defined allowing PLC-γ1 to interact with liposomes during the exchange process. These preliminary experiments were undertaken in two steps. First, purified PLC-γ1 (Fig. 1A) was subjected to deuterium exchange over a wide range of times (t = 3, 30, 300, 3000 seconds) and amounts of exchange quantified. These initial measurements demonstrated that exchange was measured with greater than 90% coverage and levels of exchange varied substantially from regions with minimal incorporation at the longest time points to regions with rapid and almost total exchange.

In the second set of preliminary experiments, it was necessary to design and ensure a system that would allow PLC-γ1 to interact with PIP_2-containing liposomes over the time course of the exchange reaction without alterations to the liposomes. This outcome was accomplished by introducing a single substitution (H335A) into PLC-γ1 of a catalytic residue necessary for PIP_2 hydrolysis (Fig. 1B). Although several substitutions of active site residues are known to render PLCs catalytically inactive, His335 was specifically chosen for its role in the enzymatic process. That is, His335 coordinates the incoming water molecule required for PIP_2 hydrolysis; it is required during the transition state but should have little effect on the affinity of PLC-γ1 for PIP_2 as a substrate. His335 also does not ligate the calcium ion cofactor and for this reason is unlikely to globally perturb the structure of the active site.

Consequently, PLC-γ1 (H335A) was purified and its lack of catalytic activity verified using a fluorescent substrate embedded within liposomes (Fig. 2A). In addition, a flotation assay was used to show that PLC-γ1 (H335A) and wild-type PLC-γ1 bound PIP_2-

containing liposomes with approximately equal propensity (~20%) (Fig. 2B). For these measurements, proteins were initially treated to chelate calcium and free calcium concentrations were maintained below 400 nM to prevent PIP_2 hydrolysis by wild-type PLC-γ1. Finally, and perhaps most importantly, PLC-γ1 (H335A) preserved the exchange profile determined initially for wild-type PLC-γ1 indicating that H335A did not perturb the overall structure of the protein and that PLC-γ1 (H335A) was a suitable surrogate for wild-type PLC-γ1 (Fig 2C).

To measure deuterium incorporation in PLC-γ1 (H335A) upon binding the phosphorylated kinase domain of the fibroblast growth factor receptor 1 (FGFR1K; residues 458-774), six tyrosines in FGFR1K were mutated to phenylalanine to both render the kinase catalytically inactive and to ensure it was primarily phosphorylated at Tyr766 upon incubation with the equivalent, active kinase (Fig. 3A-B). Tyrosine 766 is a major site of phosphorylation in FGFR1 used to recruit PLC-γ1 to membranes in cells. Phosphorylated Tyr766 of FGFR1K is also the major site of interaction between the kinase domain and the tandem SH2 array of PLC-γ1 in a crystal structure of these fragments in complex (22). Once phosphorylated at Tyr766, catalytically inactive FGFR1K was separated from active kinase, incubated with PLC-γ1 (H335A), and the resulting 1:1 complex purified by gel exclusion chromatography (Fig. 1C, 2C-D, 4A). Phosphorylated FGFR1K bound to PLC-γ1 (H335A) was stable for up to 8 hours based on subsequent gel exclusion chromatography (Fig. 4B) and it was this complex that was used to assess changes in the exchange profile of PLC-γ1 (H335A) upon engagement of kinase and in the presence of PIP_2-containing liposomes.

FGFR1K potentially disrupts autoinhibition

In comparison to PLC-γ1 in isolation, PLC-γ1 (H335A) bound to phosphorylated FGFR1K exhibited widespread changes in its exchange profile (Fig. 5A, 6A). At one end of the spectrum, reduced exchange centered on the nSH2 domain. It is this domain that directly engages phosphorylated Tyr766 in the crystal structure of the kinase domain of FGFR1 bound to the tandem SH2 domains of PLC-γ1 (22). Consequently, the most straightforward interpretation of the reduced exchange in the complex is that it reflects the major site of interaction between phosphorylated Tyr766 of FGFR1 and PLC-γ1. This interpretation is also consistent with previously published reports (9). At the other end of the spectrum, increased exchange manifested throughout much of PLC-γ1. Most notably, increased exchange was widespread within the interface between the regulatory domains and the catalytic core as highlighted by the hydrophobic ridge of the TIM barrel and where this ridge contacts the sPH domain. Based on the superposition of the structure of essentially full-length PLC-γ1 with the complex of the two SH2 domains of PLC-γ1 bound to FGFR1K, the kinase does not directly impinge either the TIM barrel or the sPH domain. Therefore, while intriguing, it is difficult to speculate on the mechanistic details that promote increased exchange in these regions (Fig. 7).

In contrast to the widespread changes in the exchange profile of PLC-γ1 upon engagement of FGFR1, PIP_2-containing liposomes incubated with PLC-γ1 (H335A) produced minimal changes in exchange (Fig. 5B, 6B). This is best emphasized by comparisons of the absolute number of deuterons exchanged per peptide of PLC-γ1 (H335A) (Fig. 5B, lower panel). Liposomes rarely altered exchange levels in PLC-γ1 (H335A) by more than one deuteron, whereas phosphorylated FGFR1K produced exchange well beyond this level in several regions of PLC-γ1 (H335A). In this respect, PIP_2-containing liposomes designed to approximate cellular membranes are relatively

ineffectual at altering the conformational dynamics of PLC-γ1. This result is consistent with the tight basal autoinhibition of purified PLC-γ1 when presented with PIP_2 in liposomes as well as endogenous PLC-γ1 in unstimulated cells (12).

The simultaneous incubation of PLC-γ1 (H335A) with both phosphorylated FGFR1K and PIP_2-containing liposomes resulted in an exchange profile that essentially recapitulated the profile obtained for PLC-γ1 (H335A) in complex with phosphorylated FGFRK1K alone (Fig. 5C). Absolute exchange was slightly elevated, but the overall deuterium incorporation pattern was essentially preserved. Overall, these results suggest that autoinhibited PLC-γ1 is refractory to activation by membranes, but that in contrast, kinase engagement as exemplified by FGFR1K will produce widespread increases in the conformational flexibility at the interface between the regulatory domains of PLC-γ1 and its catalytic core. In this respect, kinase engagement might act as an allosteric step to prime the phospholipase for subsequent activation.

Oncogenic substitution of PLC-γ1 mimics kinase engagement

The PLC-γ1 interface between its regulatory domains and catalytic core is frequently mutated in certain cancers and immune disorders (15-16). We have previously proposed that these mutations likely disrupt this interface leading to elevated, basal phospholipase activity. If true, oncogenic substitutions at this interface in PLC-γ1 might recapitulate changes in deuterium exchange in PLC-γ1 observed upon binding phosphorylated FGFR1K and this idea was tested using HDX-MS and PLC-γ1 (D1165H) (Fig. 8). Asp1165 resides in a loop between strands β5 and β6 of the C2 domain; it is required to stabilize extensive interactions between the C2 and cSH2 domains. These interactions are required to maintain PLC-γ1 in an autoinhibited state since the basal activity of PLC-γ1 (D1165H) is ~1,500-fold higher than the wild-type phospholipase (17).

In comparison to PLC-γ1 (H335A), PLC-γ1 (H335A+D1165H) exhibited increased deuterium exchange throughout the interface between the regulatory domains and the catalytic core. In the immediate vicinity of D1165H, deuterium exchange increased within the β6 strand of the C2 domain suggesting that Asp1165 serves to support the position of the β6 strand. This idea is consistent with previous molecular dynamics simulations of PLC-γ1 that highlighted an unravelling of the β6 strand upon introduction of D1165H (17). The previous molecular dynamics simulations also highlighted a relatively large (~10 Å) movement of the cSH2 upon collapse of the β6 strand, and this movement may be reflected in the increased exchange of the αB helix and BG loop of the cSH2 domain. Other regions of increased exchange are more distant and include portions of the first EF hand, sPH domain, and TIM barrel. Overall, regions of increased exchange in catalytically-inactive PLC-γ1 (D1165H) overlap well with regions of increased exchange in PLC-γ1 (H335A) when it engages phosphorylated FGFR1K (Fig. 5A). This comparison further supports the notion that kinase engagement may enhance lipase activity, possibly through molecular mechanisms mimicked by oncogenic substitutions—namely a loosening of the interface between the regulatory domains and the catalytic core. Indeed, it should be noted that regions of increased exchange are more extensive in the complex of PLC-γ1 and FGFR1K suggesting that kinase engagement may more robustly activate PLC-γ1 relative to oncogenic mutations. Finally, it should also be mentioned that D1165H produced no regions of decreased exchange in PLC-γ1. This lack is consistent with the contention that FGFR1K binds to the nSH2 domain of PLC-γ1 to reduce exchange in this region.

Oncogenic substitution uncovers functional cooperativity within PLC-γ1

Constitutively active variants of PLC-γ1 have untapped reserves of lipase activity. For example, although PLC-γ1 (D1165H) possesses exceptionally high basal lipase

activity, this activity can be further enhanced in cells by the epidermal growth factor receptor (17) suggesting that normal cellular regulation is preserved in constitutively active forms of PLC-γ1. To test this idea, changes in the hydrogen-deuterium exchange profile of PLC-γ1 (H335A+D1165H) were determined in response to phosphorylated FGFR1K, liposomes, or both (Fig 9). In comparison to the identical measurements described earlier using PLC-γ1 (H335A) (Fig. 5), these measurements turned out to be particularly revealing for several reasons.

First, phosphorylated FGFR1K produced almost identical changes in the exchange profiles of the two forms of PLC-γ1; compare figures 5A and 9A (see also Fig. 10A). Not only does this result attest to the reproducibility of the experimental design, it strongly suggests that wild-type and constitutively active forms of PLC-γ1 respond similarly to engagement of kinases.

Second, and in contrast to effects mediated by phosphorylated FGFR1K, liposomes produced much more extensive and wide-spread changes in the exchange profile of the PLC-γ1 (H335A+D1165H) (Fig. 9B, 10B) compared to PLC-γ1 (H335A) (Fig. 5B). Of note, the entire first EF hand as well the start of the second EF hand now have increased exchange in PLC-γ1 (H335A+D1165H), whereas before for PLC-γ1 (H335A), the exchange kinetics of all EF hands were essentially unchanged upon addition of liposomes. Similarly, the addition of liposomes increased exchange in all regulatory domains of the D1165H form of PLC-γ1 but only a minor subset of these regions experienced increased exchange under identical conditions for PLC-γ1 (H335A). In particular, the entire second half of the sPH domain of the constitutively active mimetic exhibited increased exchange with liposomes while no portion of this domain showed increased exchange for the basally inhibited form.

Perhaps even more intriguing, liposomes also led to decreased exchange within PLC-γ1 (H335A+D1165H) while there were no regions of decreased exchange under identical conditions for PLC-γ1 (H335A). These regions of decreased exchange are primarily in the TIM barrel: β2-β2' and β7 strands as well as the subsequent loops comprising the majority of the hydrophobic ridge—known to insert into membranes during catalysis of membrane-resident PIP_2 by PLCs (23). A second region of decreased exchange encompasses α1 of the sPH domain and the adjoining linker connecting to the second half of the TIM barrel. This linker region is disordered in the crystal structure of full-length PLC-γ1 (17).

Overall, the exchange results with liposomes indicate that the oncogenic substitution, D1165H, leads to a much more conformationally flexible PLC-γ1 that more readily interacts with lipid bilayers, presumably in a fashion that mirrors interfacial catalysis by PLC isozymes. This process would require a large movement by the regulatory domains, which is represented by the icon in Figure 9B and consistent with the exchange data.

Finally, the exchange profile of PLC-γ1 (H335A+D1165H) upon the addition of both phosphorylated FGFR1K and liposomes approximately resembles the composite profile of each component alone with two interesting caveats. First, the end of the cSH2 domain (βG) and a portion of the subsequent linker possess decreased exchange that cannot be accounted by a composite profile. This difference presumably reflects structural changes in PLC-γ1 (H335A+D1165H) that arise due to cooperative interactions among the PLC isozyme, FGFR1K, and liposomes. This presumption is reinforced by the second caveat: in the presences of both FGFR1K and liposomes, total exchange in specific portions of PLC-γ1 (H335A+D1165H) increase approximately 2-fold relative to exchange observed for either component alone (Fig. 9C, lower panel; Fig. 11). These regions include most of

the first and second EF hands as well as a large segment of the second half of the TIM barrel spanning strands β6 and β7 and including helices α5 and α5'.

Phosphorylated FGFR1K increases PLC-γ1 specific activity

The hydrogen-deuterium exchange kinetics described above strongly suggest that the initial engagement of PLC-γ isozymes by kinases may be sufficient to enhance phospholipase activity irrespective of subsequent phosphorylation. This idea was tested using a fluorescent analog of PIP_2, XY-69 (24), embedded in lipid vesicles (Fig. 12). PLCs readily hydrolyze XY-69 leading to increased fluorescence that can be followed in real-time. As shown previously, when XY-69 in lipid vesicles is mixed with PLC-γ1, the specific activity of the phospholipase is low, indicative of basal autoinhibition (17, 24). This activity remained unchanged upon pre-incubation of PLC-γ1 with catalytically-inactive FGFR1K that was not phosphorylated. In contrast, when PLC-γ1 was pre-incubated with catalytically-inactive FGFR1K phosphorylated at Tyr766 to promote complex formation with PLC-γ1, specific lipase activity of PLC-γ1 increased approximately three-fold. These results indicate that kinase engagement by PLC-γ1 is sufficient to enhance lipase activity and support the proposition that PLC-γ1 is allosterically modulated by FGFR1K upon complex formation and irrespective of the phosphorylation state of the lipase.

Similar results were observed with PLC-γ1 (D1165H). In particular, addition of catalytically-inactive, phosphorylated FGFR1K increased the basal lipase activity of PLC-γ1 (D1165H) approximately two-fold. The basal capacity of PLC-γ1 (D1165H) to hydrolyze vesicle-embedded XY-69 was substantially higher than the equivalent activity of wild-type PLC-γ1, but this result has been previously published and comports with the higher constitutive activity of PLC-γ1 (D1165H) in cells (17). Interestingly, the addition of catalytically-inactive but non-phosphorylated FGFR1K also led to a significant increase in

the specific activity of PLC-γ1 (D1165H). We are unable to readily account for this observation, but it should be noted that the crystal structure of phosphorylated FGFR1K bound to the two SH2 domains of PLC-γ1 highlights a secondary interface outside of the canonical pTyr-binding site that contributes to the affinity of the complex. Therefore, unphosphorylated FGFR1K may have sufficient affinity for PLC-γ1 such that it is able to enhance the lipase activity of constitutively active PLC-γ1 (D1165H) but not the more basally autoinhibited, wild-type form.

Finally, WH-15 is a soluble, fluorescent substrate of PLCs that is insensitive to the autoregulation of the PLC-γ isozymes (25, 26). Its hydrolysis by PLC-γ1 (D1165H) is insensitive to either form of FGFR1K used above (Fig. 5B) and these results further support the idea that the complex of FGFR1K and PLC-γ1 diminishes autoregulation by loosening the conformational ensemble of the autoinhibited form of PLC-γ1.

Discussion

Model for PLC-γ isozyme activation - We previously described the crystal structure of autoinhibited PLC-γ1. The structure illustrates how the regulatory domains sit on top of the catalytic core to mediate autoinhibition by effectively blocking access to the active site. In addition, the regulatory domains are arranged to integrate inputs from signaling and adaptor proteins. One such example is the nSH2 domain of PLC-γ1 which docks to active kinases. Subsequently, the PLC-γ isozymes are directly activated by tyrosine phosphorylation. The HDX-MS studies presented here suggest that binding of phosphorylated FGFR1K to PLC-γ1 led to a decrease in deuteration only at the nSH2 domain. This decrease in deuteration highlights the nSH2 domain as the major site of interaction between PLC-γ isozymes and active kinases. The observed decrease in deuteration may be the manifestation of both binding of pY766 of FGFR1K to the canonical pTyr-binding pocket and the subsequent conformational changes elicited by the binding event. This idea is supported by comparison of the structure of full-length PLC-γ1 and the structure of the tandem SH2 domains bound to phosphorylated FGFR1K. This comparison illustrates conformational changes within the SH2 domain including the inward movement of the loop preceding helix αA towards the cSH2 domain, suggesting that conformational changes at the nSH2 domain may elicit conformational changes elsewhere that disrupt the interface between the catalytic core and the regulatory domains. This idea is supported by the widespread changes in deuterium incorporation throughout the rest of the protein including portions of the sPH domain and the EF hands. Subsequent biochemical assays with the membrane-embedded substrate, XY-69, show that the kinase domain of FGFR1 elevates phospholipase activity. Together, these data suggest that kinases act as allosteric modulators by shifting the equilibrium from a predominantly autoinhibited PLC-γ isozyme to a more active conformation. These findings are likely generalizable given that

PLC-γ isozyme activity is controlled by a several tyrosine kinases depending on cell context.

The allosteric effect of FGFR1K is enhanced in the presence of PIP_2-containing liposomes. For instance, the deuterium exchange profile of PLC-γ1 (D1165H) bound to phosphorylated FGFR1K and in the presence of liposomes showcases a decrease in deuteration within the loop containing tyrosine residues required for phosphorylation-dependent activation of PLC-γ isozymes, e.g. Tyr783. Deuteration within this region is absent in the kinase-bound state, suggesting that membranes cooperate to optimally orient PLC-γ isozymes for phosphorylation-dependent activation by tyrosine kinases.

One of the predominant sites of increased deuteration upon kinase binding is the sPH domain. The elevation in deuterium incorporation can be a manifestation of conformational changes associated with binding to adaptor proteins including the small GTPase Rac1. It has been proposed that Rac1 stabilizes the ensemble of active PLC-γ isozyme instead of disrupting the autoinhibited state.

Subsequent to phosphorylation-dependent activation, the PLC-γ isozymes insert into membranes via hydrophobic residues that line the catalytic cavity. This region has a decrease in deuterium incorporation in PLC-γ1(H335A+D1165H) in the presence of PIP_2-containing liposomes. Surprisingly, liposomes also lead to widespread increases in deuterium incorporation predominantly within the regulatory domains suggesting that liposomes induce conformational changes that may stabilize the active ensemble of PLC-γ isozymes at the membrane. Presumably, these membrane-associated confirmations are stabilized by the EF hands that, in the open state, have access to membranes.

Together, with the structural and biochemical studies, these data evoke a mechanism for the regulated activation of PLC-γ isozymes. In the basal state, PLC-γ isozymes are autoinhibited. In the presence of an extracellular signal, active tyrosine

kinases phosphorylate PLC-γ1 and prime their phosphorylation-dependent activation by shifting the dynamic equilibrium to a more active conformation. Subsequently, active kinases phosphorylate PLC-γ1 within the regulatory domains, e.g. Tyr783. These phosphorylated tyrosines bind the cSH2 domain and compete the interactions between this domain and the catalytic core. Once active, PLC-γ isozymes insert into membranes to hydrolyze the preferred substrate, PIP_2. Simultaneously, membranes cooperate with active kinases to stabilize the ensemble of active PLC-γ1.

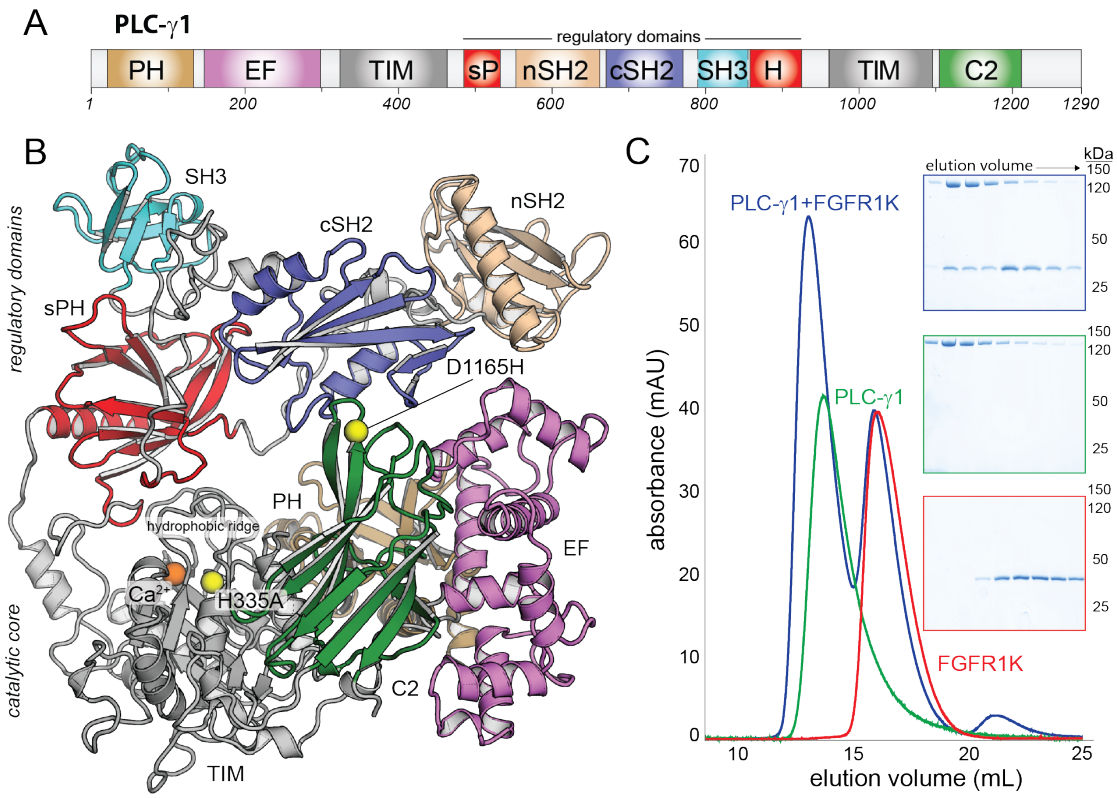

Figure 4.1 – PLC-γ1 forms a stable complex with phosphorylated FGFR1K. A, Domain architecture of full-length PLC-γ1 drawn to scale. Purified PLC-γ1 (residues 21-1215) lacks disordered, non-conserved portions at both N- and C-termini. **B**, Crystal structure of autoinhibited PLC-γ1 (PDB ID: 6PBC) with loops modeled. Domains colored as in **A**. The calcium ion cofactor (orange sphere) marks the active site. Mutations (H335A and D1165H) are indicated with yellow spheres. **C**, Size exclusion chromatography of phosphorylated FGFR1K (red curve), PLC-γ1 (green curve), or a pre-incubated mixture of the two proteins (blue curve). Eluted fractions were subjected to SDS-PAGE followed by staining with Coomassie Brilliant Blue (inset).

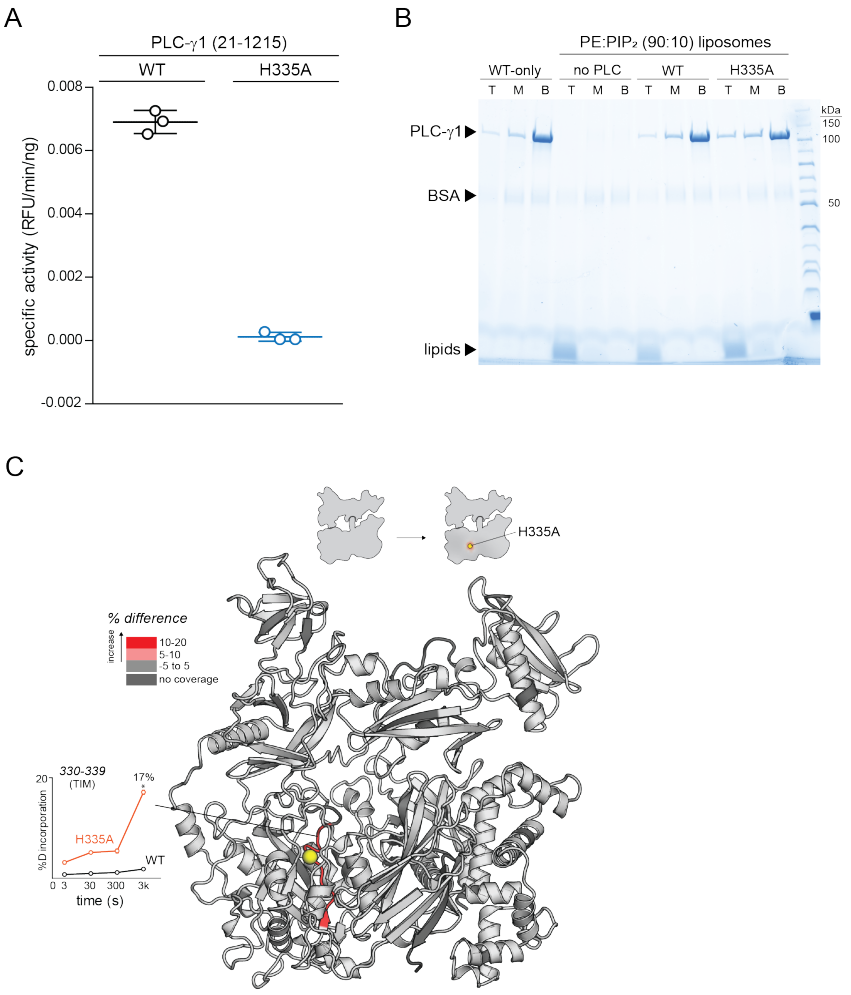

Figure 4.2 – PLC-γ1 (H335A) is catalytically inactive and binds liposomes. A, Specific activities measured with the membrane-embedded substrate XY-69. XY-69 (0.5μM) was incorporated into PE:PIP_2 (80:20) liposomes prior to addition of indicated variants of PLC-γ1 (10nM WT; 10 nM H335A). Phospholipase activity was determined by quantifying XY-69 hydrolysis in real-time and presented as the mean ± SD of three independent experiments (n=3), each with three or more technical replicates. Statistical significance was determined with a one-way ANOVA followed by Tukey's post-hoc test and represented as *** $p > 0.001$. **B**, Membrane floatation assay with wild-type (WT) PLC-γ1 and PLC-γ1 (H335A). Proteins were incubated with liposomes of PE:PIP_2:NBD-PE (89.8:10:0.2) and centrifuged in a sucrose gradient (30-0%). After centrifugation, top (T), middle (M), and bottom (B) fractions were collected. Samples were loaded onto an SDS-PAGE followed by staining with Coomassie Brilliant Blue. **C**, Deuterium incorporation was measured for PLC-γ1 (H335A) and differences in deuterium incorporation were calculated relative to wild-type PLC-γ1. Site of the H335A substitution is denotated by a yellow sphere. Peptides that showed H/D exchange differences (by the following criteria: >5% and >0.4 Da difference in exchange at any timepoint, with an unpaired student t-test value <0.01) are mapped onto the structure. The percent deuterium incorporation for this region is graphed over a series of time points (3, 30, 300, 3000 sec) and shown next to the structure as mean ± SD (n = 3), with most SD smaller than the size of the point. The highest percent of deuterium incorporation is shown above the curve. An asterisk (*) indicates a difference >0.4 Da for the corresponding time point.

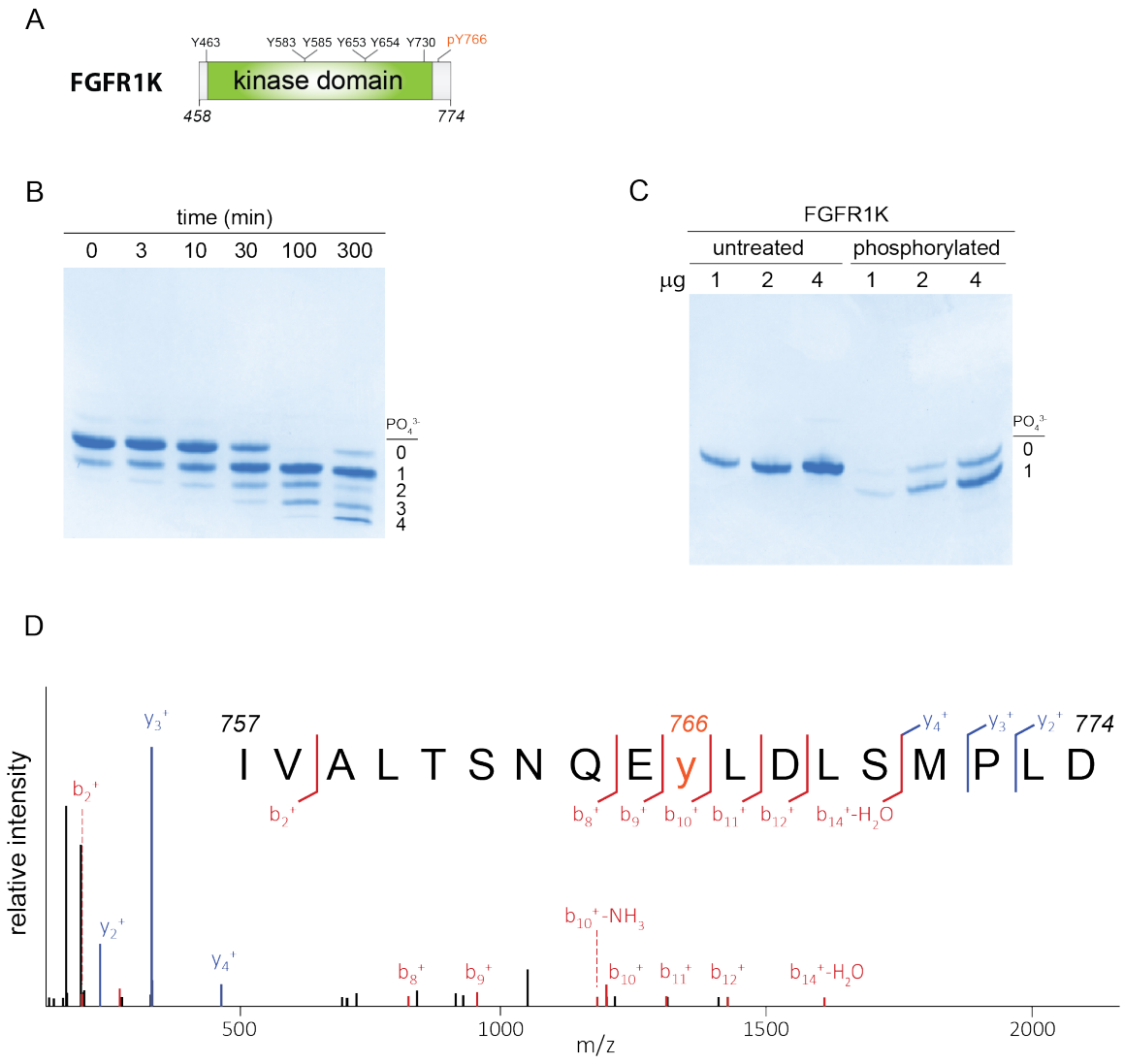

Figure 4.3 – FGFR1K is phosphorylated only on Tyr766. A, Schematic diagram of the kinase domain (residues 458-774) of the fibroblast growth factor receptor 1 (FGFR1K). This variant includes six tyrosines mutated to phenylalanine (Y463F, Y583F, Y585F, Y653F, Y654F, Y730F) to eliminate most sites of phosphorylation and to render the kinase catalytically inactive. **B**, Purified FGFR1K (100µM) was phosphorylated using equimolar concentrations of the equivalent fragment of FGFR1K that had not been mutated. Progression of the phosphorylation reaction was followed over several time points (0, 3, 10, 30, 100, 300 minutes) by native PAGE followed by staining with Coomassie Brilliant Blue. The phosphorylation reaction was terminated after 100 minutes. **C**, The two kinases were subsequently separated by affinity chromatography and reaction yield (~80% phosphorylation) was assessed by native PAGE followed by staining with Coomassie Brilliant Blue. **D**, Phosphorylation of tyrosine 766 was confirmed by LC-MS/MS.

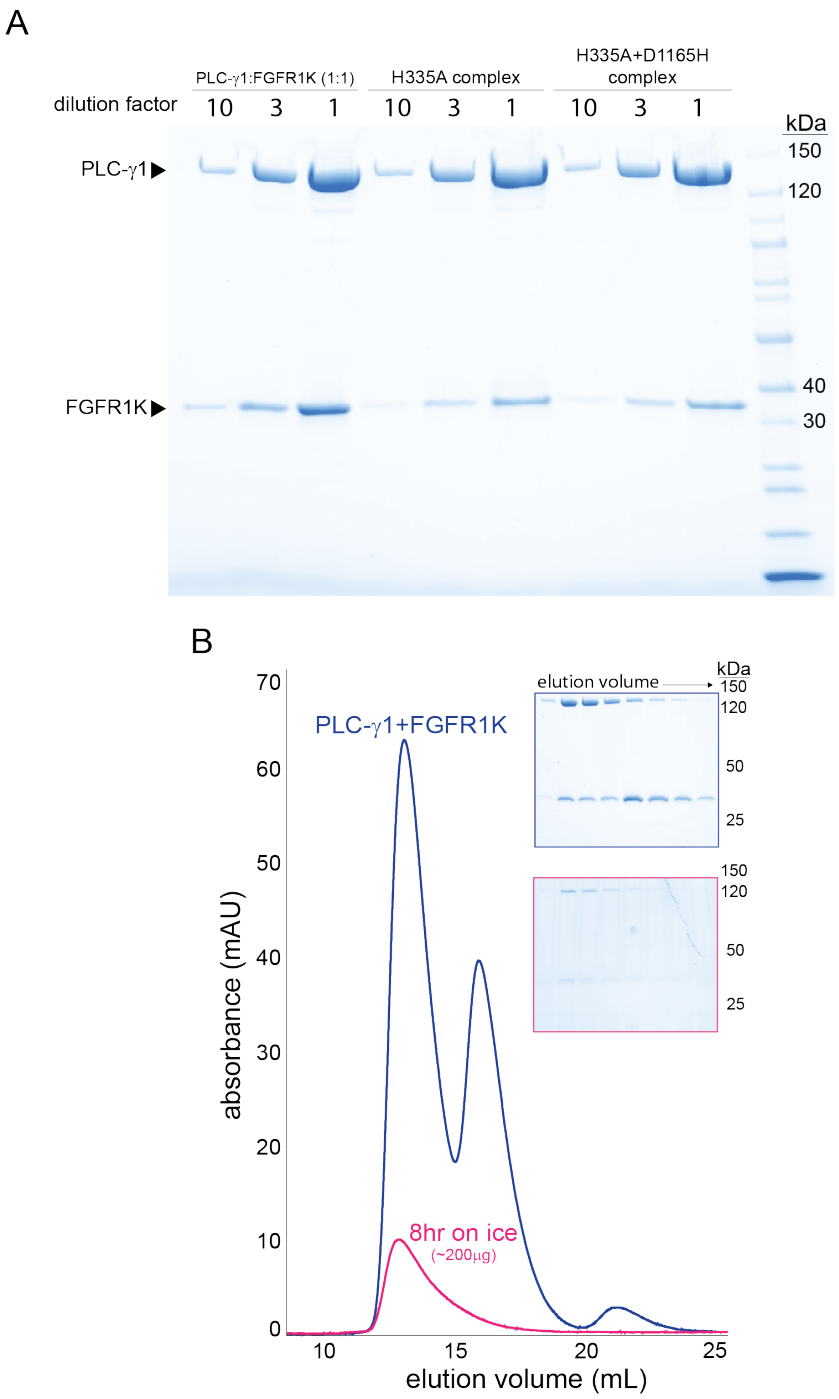

Figure 4.4 – PLC-γ1 and phosphorylated FGFR1K form stable complexes. A, PLC-γ1 (H335A) or PLC-γ1 (H335A+D1165H) were mixed with phosphorylated FGFR1K and isolated by size exclusion chromatography. Isolated complexes were subjected to SDS-PAGE followed by staining with Coomassie Brilliant Blue. For reference, a 1:1 mixture of PLC-γ1 and FGFR1K was treated similarly (left). **B**, Stability of the complexes was assessed by size exclusion chromatography after 8 hours on ice (pink curve). Blue curve and corresponding SDS-PAGE gel are then same as in Figure 1C.

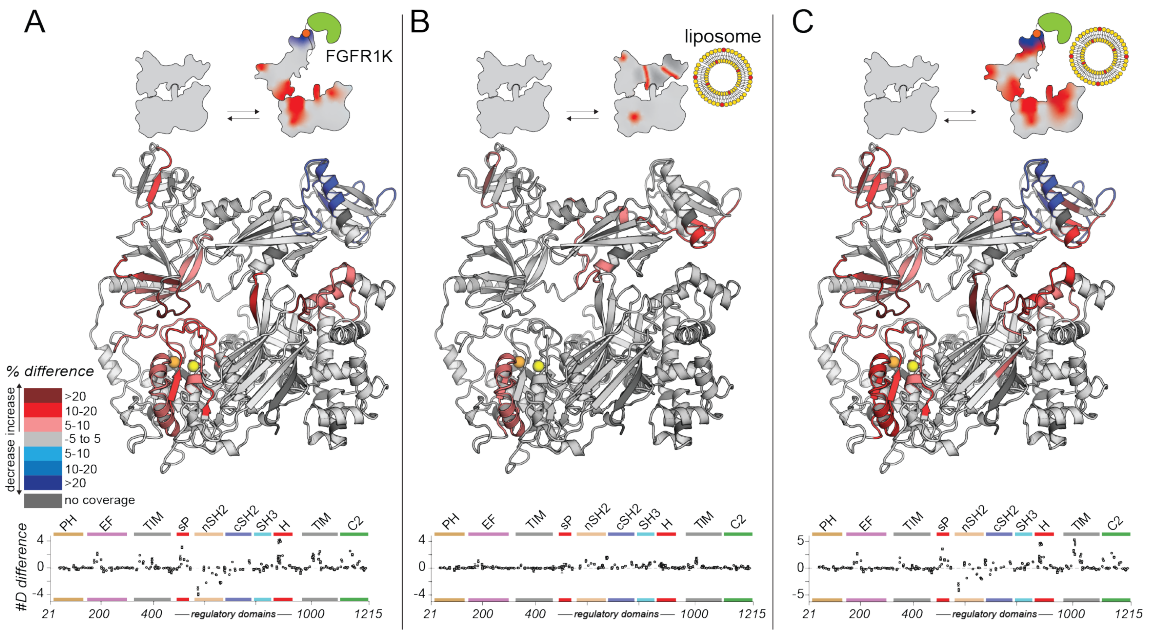

Figure 4.5 – FGFR1K potentially disrupts autoinhibition. Deuterium incorporation was measured for PLC-γ1 (H335A) in three states: bound to phosphorylated FGFR1K (**A**), in the presence of PE:PIP_2 (90:10) liposomes (**B**), or with both kinase and liposomes (**C**). Differences in deuterium incorporation for a series of time points (3, 30, 300, 3000, and 10000 sec) were calculated relative to the phospholipase alone. Peptides that showed H/D exchange differences (by the following criteria: >5% and >0.4 Da difference in exchange at any timepoint, with an unpaired student t-test value <0.01) are mapped onto the structure. For each comparison, the difference in the number of incorporated deuterons was averaged over all time points and shown below the structures as the mean ± SD (n = 3). Each circle represents the central residue of a corresponding peptide.

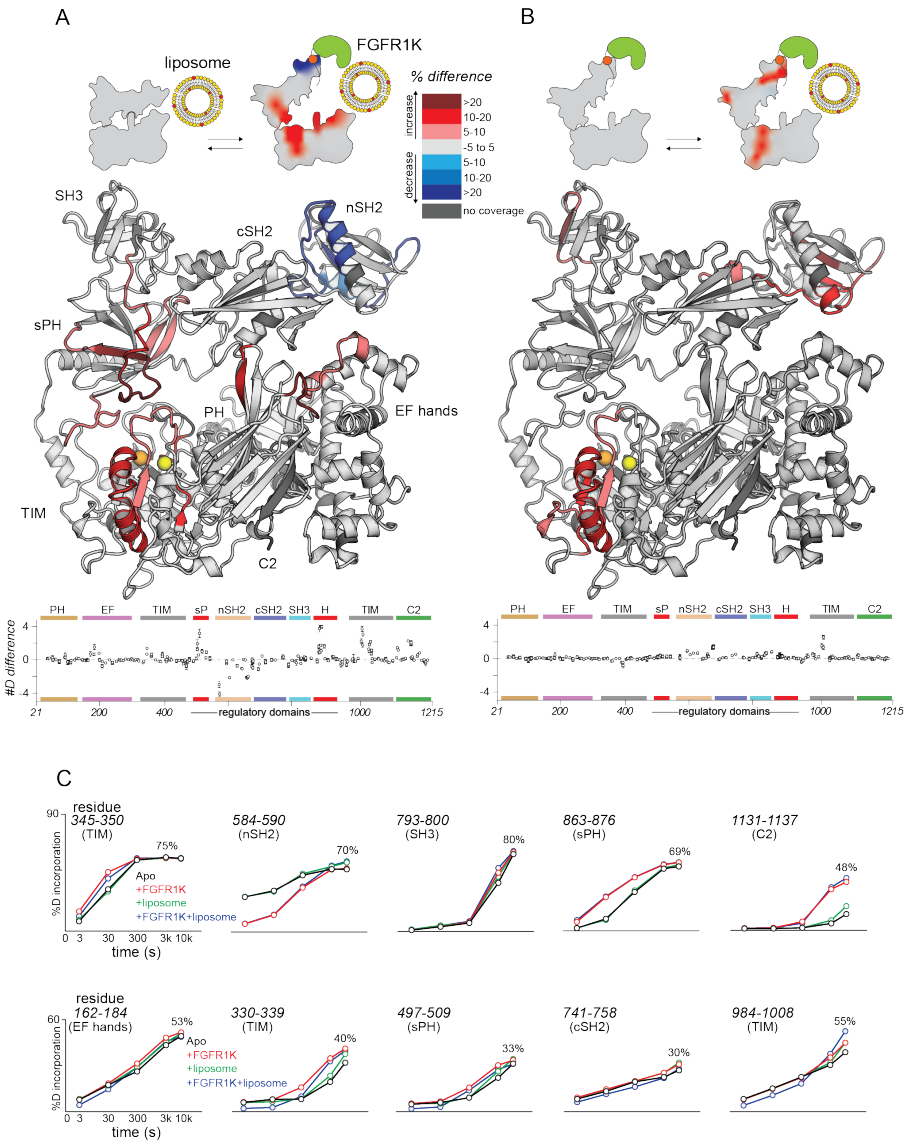

Figure 4.6 – FGFR1K and liposomes act independently. Deuterium incorporation was measured for PLC-γ1 (H335A) bound to FGFR1K and in the presence of PE:PIP_2 (90:10) liposomes. Differences in deuterium incorporation were calculated relative to PLC-γ1 (H335A) in the presence of PE:PIP_2 liposomes (**A**) or to PLC-γ1 (H335A) bound to FGFR1K (**B**). Peptides that showed H/D exchange differences (by the following criteria: >5% and >0.4 Da difference in exchange at any timepoint, with an unpaired student t-test value <0.01) are mapped onto the structure. For each comparison, the difference in the number of incorporated deuterons was averaged over all time points and shown below the structures as the mean ± SD (n = 3). Each circle represents the central residue of a corresponding peptide. **C**, Percent deuterium incorporation for select peptides spanning PLC-γ1 (H335A). Percent deuterium incorporation is for PLC-γ1 (H335A) alone (black line), bound to FGFR1K (red line), in the presence of PE:PIP_2 (90:10) liposomes (green line), and with both kinase and liposomes (blue line) is shown as the mean ± SD (n=3), with most SD smaller than the size of the point. The highest percent of deuterium incorporation is shown above the curves. The Y-axis of the graphs was adjusted to 90% (top row) and 60% (bottom row) deuterium incorporation.

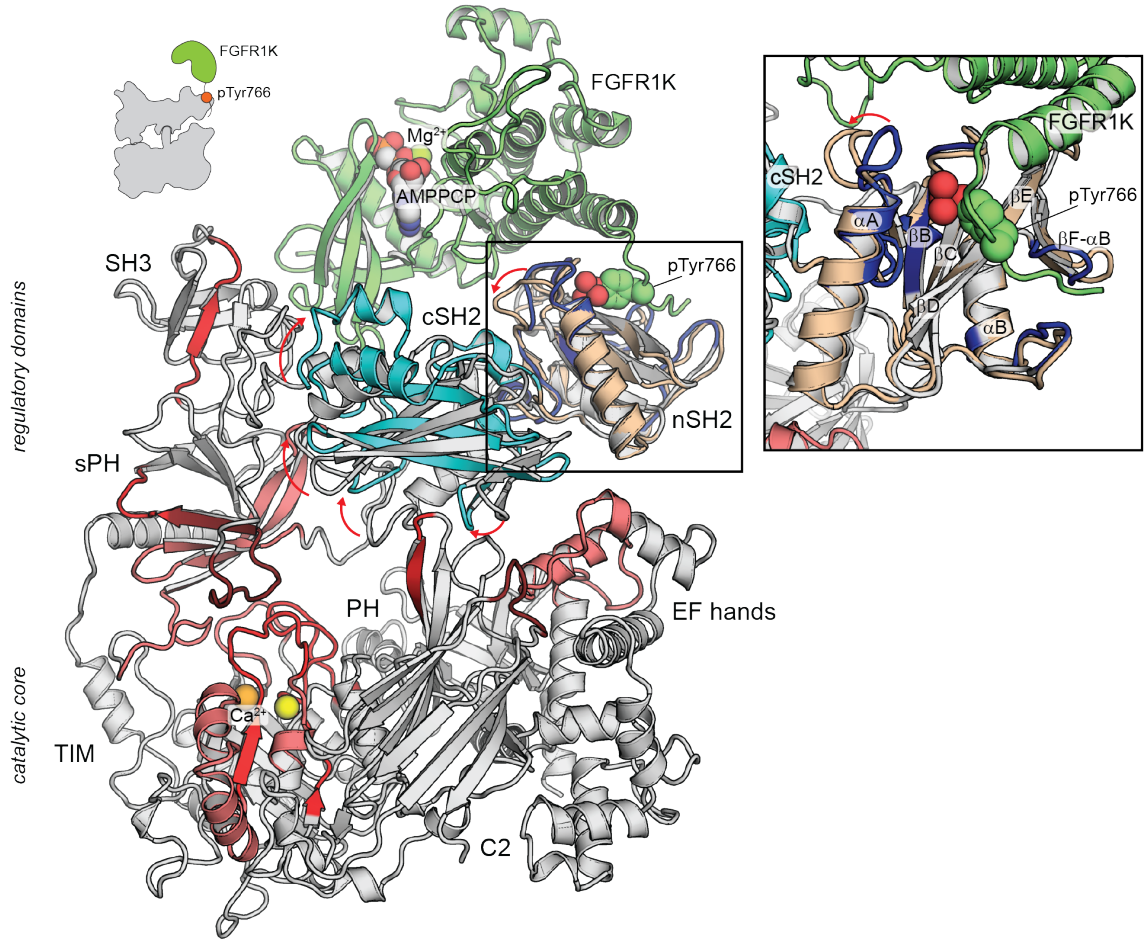

Figure 4.7 – Priming of PLC-γ1 by FGFR1K. Structure alignment of autoinhibited PLC-γ1 (grey, PDB ID: 6PBC) and a structure of the tandem SH2 domains of PLC-γ1 bound to the kinase domain of FGFR1 (nSH2 domain, wheat; cSH2 domain, cyan; FGFR1 kinase domain, green; PDB ID: 3GQ1). Red arrows represent movement of select loops.

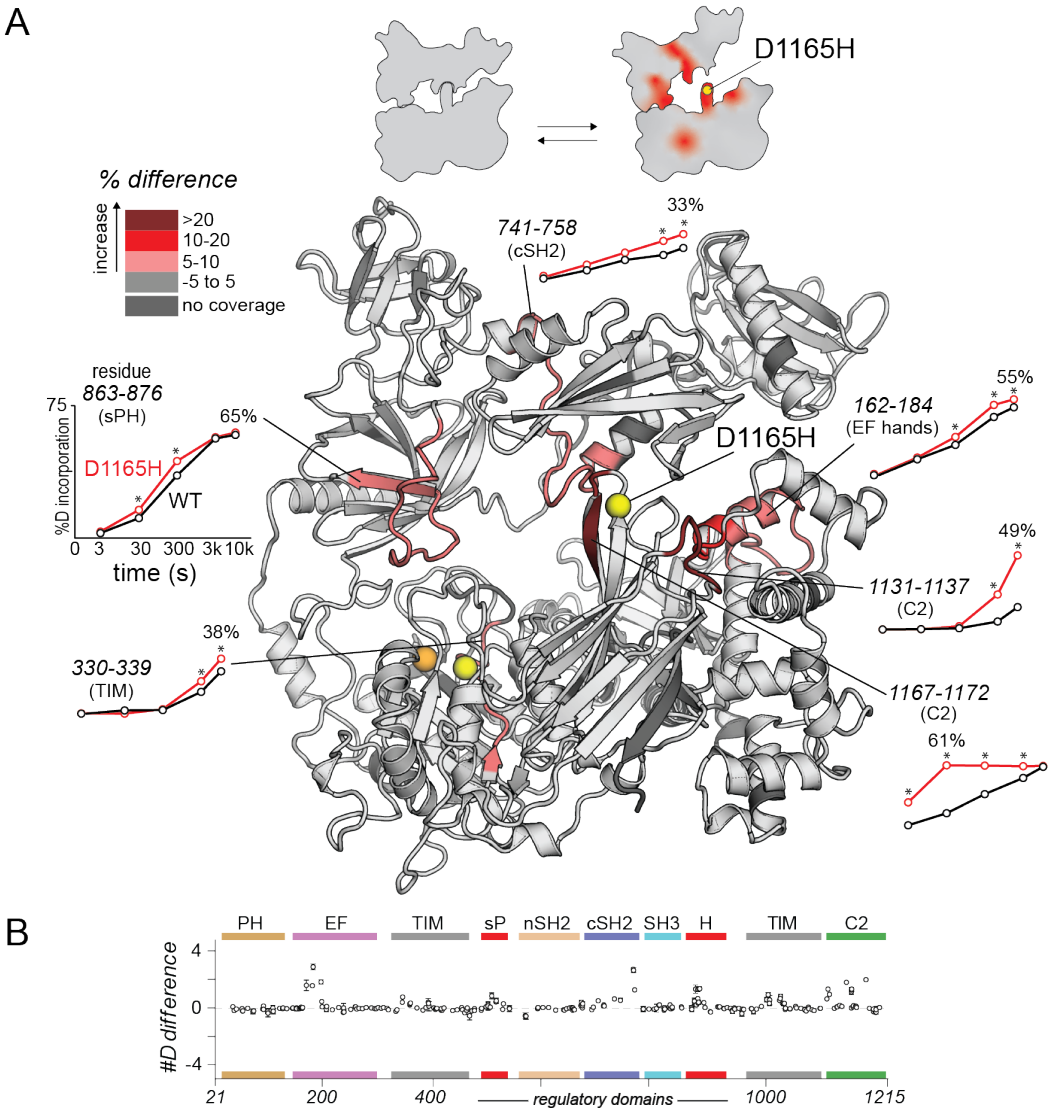

Figure 4.8 – Oncogenic substitution of PLC-γ1 mimics kinase engagement. A, Deuterium incorporation was measured for PLC-γ1 (H335A+D1165H) and differences in deuterium incorporation were calculated relative to PLC-γ1 (H335A). Peptides that showed H/D exchange differences (by the following criteria: >5% and >0.4 Da difference in exchange at any timepoint, with an unpaired student t-test value <0.01) are mapped onto the structure. The percent deuterium incorporation for these regions is graphed over a series of time points (3, 30, 300, 3000, and 10000 sec) and shown around the structure as mean ± SD (n = 3), with most SD smaller than the size of the point. The highest percent of deuterium incorporation is shown above the curves. An asterisk (*) indicates a difference >0.4 Da for the corresponding time point. The range for the Y-axis is the same for all graphs. **B**, The difference in the number of incorporated deuterons was averaged over all time points and shown below the structure as the mean ± SD (n = 3). Each circle represents the central residue of a corresponding peptide.

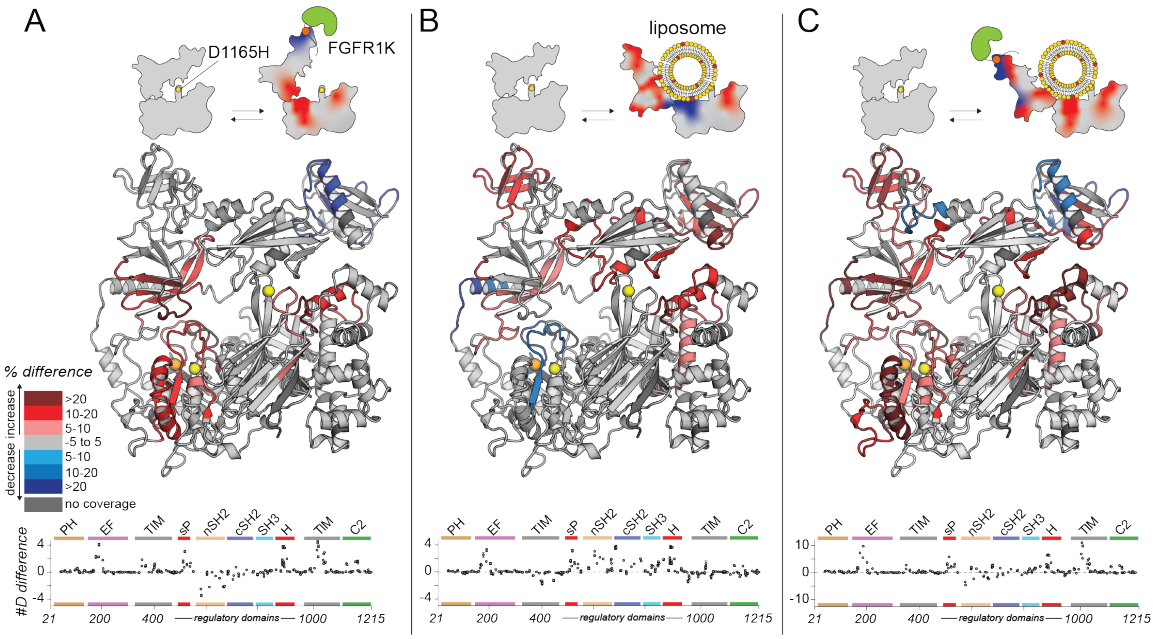

Figure 4.9 – Oncogenic substitution uncovers functional cooperativity. Deuterium incorporation was measured for PLC-γ1 (H335A+D1165H) in three states: bound to phosphorylated FGFR1K (**A**), in the presence of PE:PIP_2 (90:10) liposomes (**B**), or with both kinase and liposomes (**C**). Differences in deuterium exchange for a series of time points (3, 30, 300, 3000, and 10000 sec) were calculated relative to PLC-γ1 (H335A+D1165H) alone. Peptides that showed H/D exchange differences (by the following criteria: >5% and >0.4 Da difference in exchange at any timepoint, with an unpaired student t-test value <0.01) are mapped onto the structure. For each comparison, the difference in the number of incorporated deuterons was averaged over all time points and shown below the structures as the mean ± SD (n = 3). Each circle represents the central residue of a corresponding peptide.

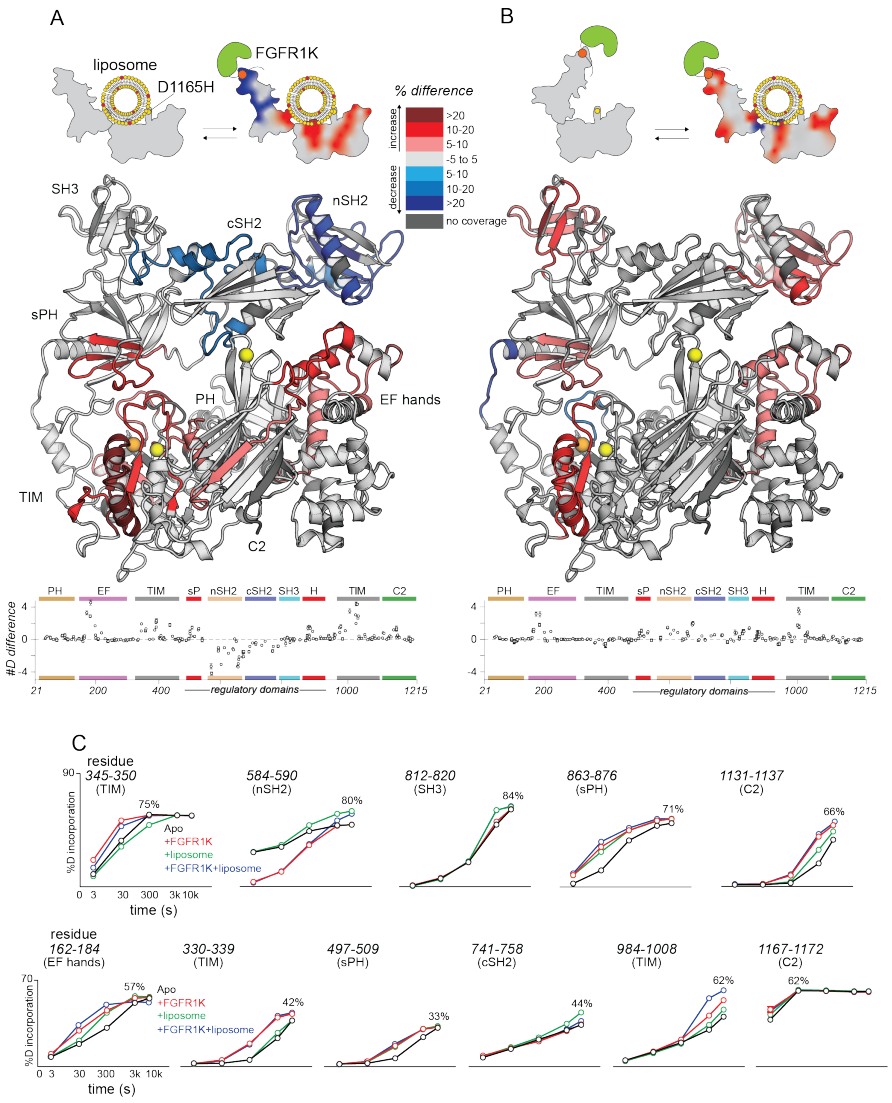

Figure 4.10 – FGFR1K and liposomes affect deuterium exchange. Deuterium incorporation was measured for PLC-γ1 (H335A+D1165H) bound to FGFR1K and in the presence of PE:PIP_2 (90:10) liposomes. Differences in deuterium incorporation were calculated relative to PLC-γ1 (H335A+D1165H) in the presence of PE:PIP_2 liposomes (**A**) or to PLC-γ1 (H335A+D1165H) bound to FGFR1K (**B**). Peptides that showed H/D exchange differences (by the following criteria: >5% and >0.4 Da difference in exchange at any timepoint, with an unpaired student t-test value <0.01) are mapped onto the structure. For each comparison, the difference in the number of incorporated deuterons was averaged over all time points and shown below the structures as the mean ± SD (n = 3). Each circle represents the central residue of a corresponding peptide. **C**, Percent deuterium incorporation for select peptides spanning PLC-γ1 (H335A+D1165H). Percent deuterium incorporation for PLC-γ1 (H335A+D1165H) alone (black line), bound to FGFR1K (red line), in the presence of PE:PIP_2 (90:10) liposomes (green line), and with both kinase and liposomes (blue line) is shown as the mean ± SD (n=3), with most SD smaller than the size of the point. The highest percent of deuterium incorporation is shown above the curves. The Y-axis of the graphs was adjusted to 90% (top row) and 70% (bottom row) deuterium incorporation.

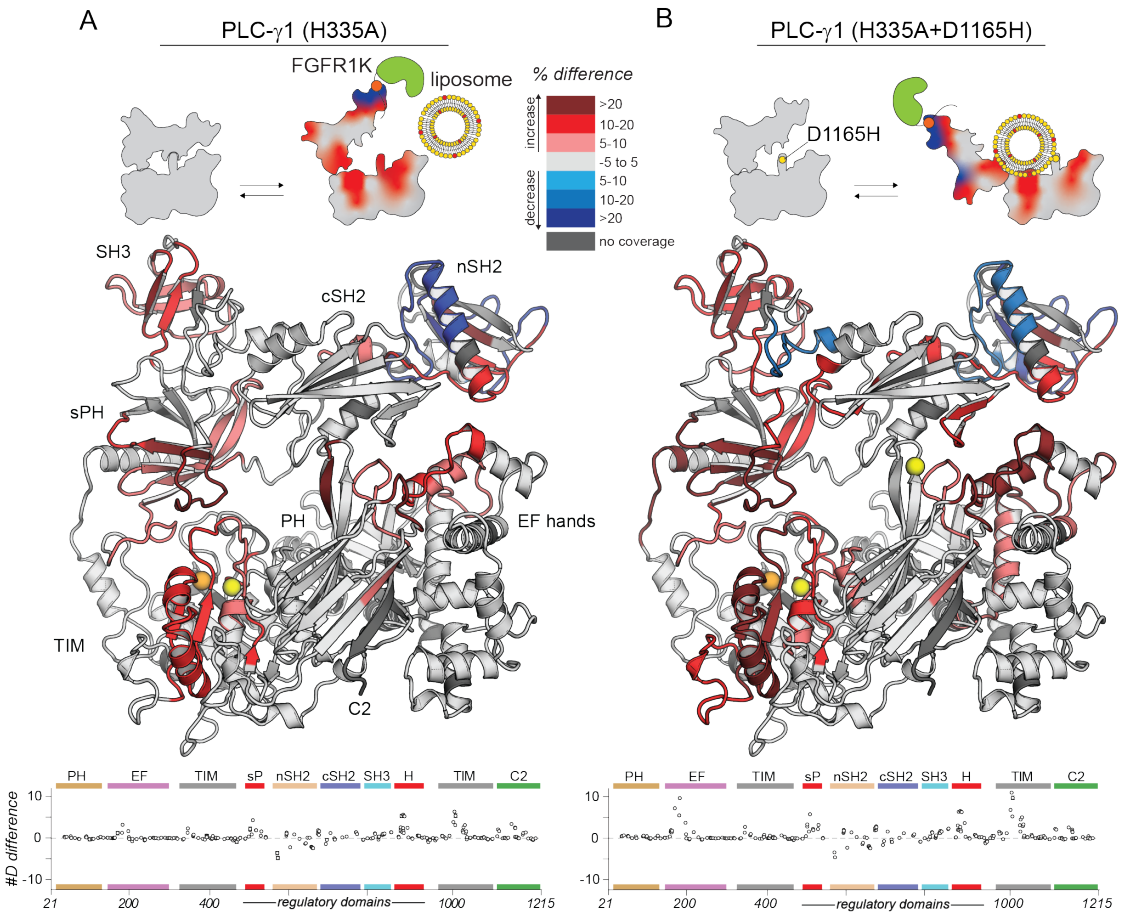

Figure 4.11 – Functional cooperativity in PLC-γ1 (D1165H). Deuterium incorporation was measured for PLC-γ1 (H335A) and PLC-γ1 (H335A+D1165H) with both kinase and liposomes. Differences in deuterium incorporation were calculated relative to PLC-γ1 (H335A) alone (**A**) or to PLC-γ1 (H335A+D1165H) alone (**B**). Peptides that showed H/D exchange differences (by the following criteria: >5% and >0.4 Da difference in exchange at any timepoint, with an unpaired student t-test value <0.01) are mapped onto the structure. For each comparison, the difference in the number of incorporated deuterons was averaged over all time points and shown below the structures as the mean ± SD (n = 3). Each circle represents the central residue of a corresponding peptide.

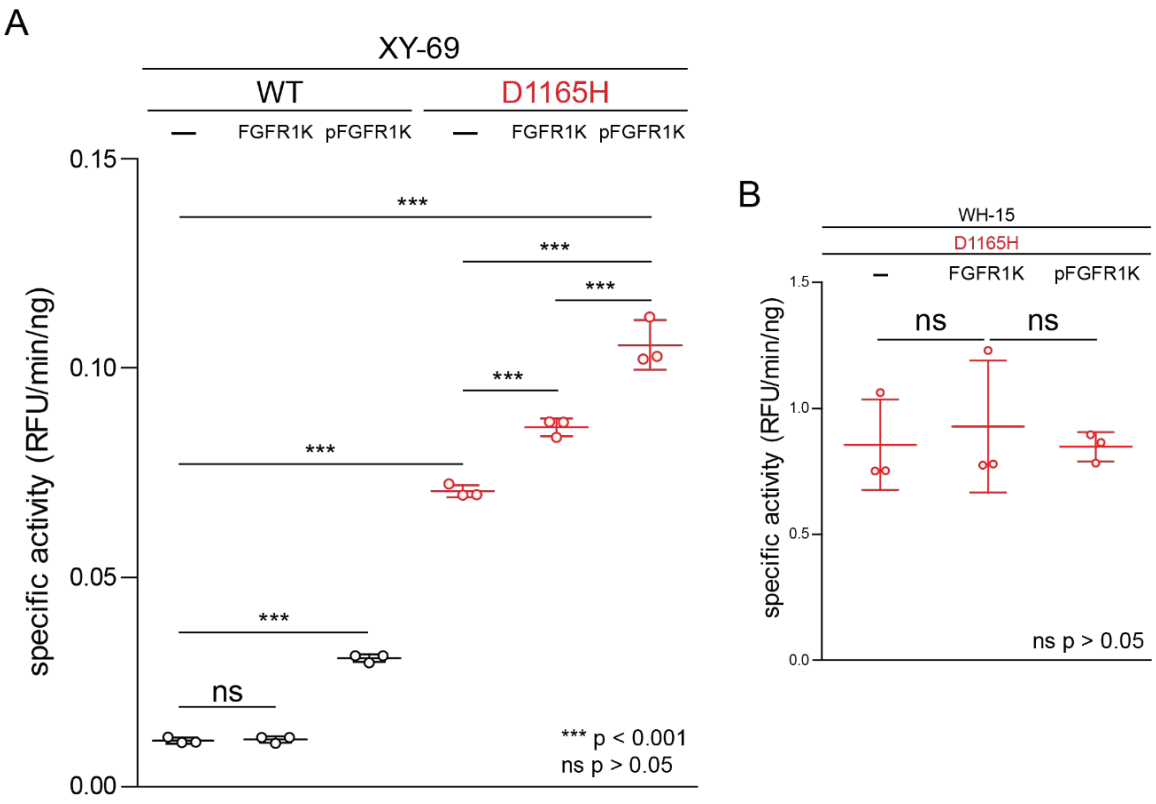

Figure 4.12 – Phosphorylated FGFR1K increases PLC-γ1 specific activity. A, Specific activities measured with the membrane-embedded substrate XY-69. XY-69 (0.5μM) was incorporated into PE:PIP_2 (80:20) liposomes prior to addition of indicated variants of PLC-γ1 (10nM WT; 0.3nM D1165H). The specific activity was calculated for three states: unbound (—), and in the presence of a two-fold molar excess of unphosphorylated FGFR1K (FGFR1K) or phosphorylated FGFR1K (pFGFR1K) relative to PLC-γ1. Phospholipase activity was determined by quantifying XY-69 hydrolysis in real-time and presented as the mean ± SD of three independent experiments (n=3), each with three or more technical replicates. Statistical significance was determined with a one-way ANOVA followed by Tukey's post-hoc test and represented as *** p > 0.001. **B**, Specific activities measured with the soluble substrate WH-15 (5 μM). The specific activity of PLC-γ1 (D1165H) was calculated in three states: unbound (—), and in the presence of a two-fold molar excess of unphosphorylated FGFR1K (FGFR1K) or phosphorylated FGFR1K (pFGFR1K) relative to PLC-γ1. Bars represent the mean ± SD of three independent experiments (n=3), each with three or more technical replicates. Statistical significance was determined with a one-way ANOVA followed by Tukey's post-hoc test and represented as *** p > 0.001.

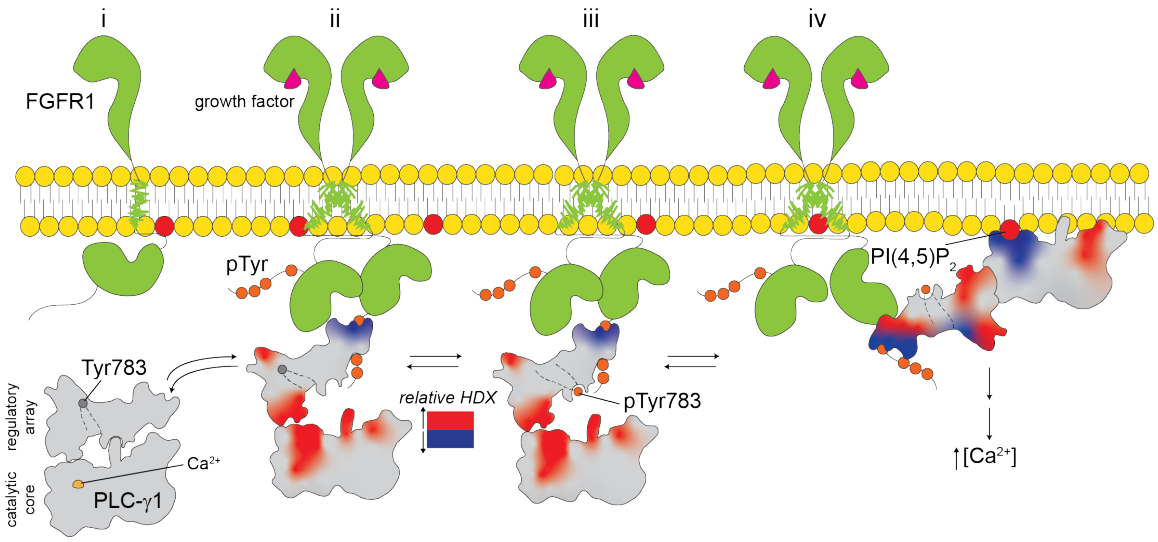

Figure 4.13 – Dynamic activation of PLC-γ1. Model of PLC-γ1 activation. (**i**) PLC-γ1 is basally autoinhibited and cytosolic. (**ii**) It is recruited to membranes through interaction of its nSH2 domain with an active FGFR1. Complex formation reduces deuterium exchange within the nSH2 while simultaneously leading to increased deuterium exchange throughout the interface between the catalytic core and the regulatory domains of PLC-γ1. (**iii**) FGFR1 subsequently phosphorylates Tyr783 of PLC-γ1 and pTyr783 then binds to the cSH2 domain of PLC-γ1 to reinforce the disruption of the interface between regulatory and catalytic domains. (**iv**) This disruption favors a fully open form of PLC-γ1 capable of productively engaging membranes with a concomitant decrease in the deuterium exchange of the catalytic TIM barrel.

REFERENCES

1. Newton, A. C., Bootman, M. D., and Scott, J. D. (2016) Second Messengers. *Cold Spring Harb. Perspect. Biol.* **8**(8), a005926 (10.1101/cshperspect.a005926)

2. Rhee, S. G. (2001) Regulation of phosphoinositide-specific phospholipase C. *Annu. Rev. Biochem.* **70**, 281-312 (10.1146/annurev.biochem.70.1.281)

3. Kadamur, G., and Ross, E. M. (2013) Mammalian Phospholipase C. *Annu. Rev. Physiol.* **75**, 127-154 (10.1146/annurev-physiol-030212-183750)

4. Hicks, S. N., Jezyk, M. R., Gershburg, S., Seifert, J. P., Harden, T. K., and Sondek, J. (2008) General and versatile autoinhibition of PLC isozymes. *Mol. Cell.* **31**(3), 383–394 (10.1016/j.molcel.2008.06.018)

5. Gresset, A., Sondek, J., and Harden, T. K. (2012) The Phospholipase C Isozymes and Their Regulation. *Subcell. Biochem.* **58**, 61-94 (10.1007/978-94-007-3012-0_3)

6. Wahl, M. I., Nishibe, S., Kim, J. W., Kim, H., Rhee, S. G., and Carpenter, G. (1990) Identification of two epidermal growth factor-sensitive tyrosine phosphorylation sites of phospholipase C-γ in intact HSC-1 cells. *J. Biol. Chem.* **265**, 3944–3948

7. Kim, H. K., Kim, J. W., Zilberstein, A., Margolis, B., Kim, J. G., Schlessinger, J., and Rhee, S. G. (1991) PDGF stimulation of inositol phospholipid hydrolysis requires PLC-γ 1 phosphorylation on tyrosine residues 783 and 1254. *Cell* **65**, 435–441 (10.1016/0092-8674(91)90461-7)

8. Serrano, C. J., Graham, L., DeBell, K., Rawat, R., Veri, M. C., Bonvini, E., Rellahan, B. L., and Reischl, I. G. (2005) A New Tyrosine Phosphorylation Site in PLCγ1: The Role of Tyrosine 775 in Immune Receptor Signaling. *J. Immunol.* **174**, 6233–6237 (10.4049/jimmunol.174.10.6233)

9. Gresset, A., Hicks, S. N., Harden, T. K., and Sondek, J. (2010) Mechanism of Phosphorylation-Induced Activation of Phospholipase C-γ Isozymes. *J. Biol. Chem.* **285**, 35836-35847 (10.1074/jbc.M110.166512)

10. Yang, Y. R., Choi, J. H., Chang, J., Kwon, H. M., Jang, H., Ryu, S. H., and Suh, P. (2012) Diverse cellular and physiological roles of phospholipase C-γ1. *Adv. Enzyme Regul.* **52**, 138-151 (10.1016/j.advenzreg.2011.09.017)

11. Arteaga, C. L., Johnson, M. D., Todderud, G., Coffey, R. J., Carpenter, G., and Page, D. L. (1991) Elevated content of the tyrosine kinase substrate phospholipase C-γ1 in primary human breast carcinomas. *Proc. Natl. Acad. Sci.* **88**, 10435-10439 (10.1073/pnas.88.23.10435)

12. Shepard, C. R., Kassis, J., Whaley, D. L., Kim, H. G., and Wells, A. (2007) PLCγ contributes to metastasis of in situ-occurring mammary and prostate tumors. *Oncogene* **26**, 3020-3026 (10.1038/sj.onc.1210115)

13. Park, J., Lee, Y. H., Kim, S. S., Park, K. J., Noh, D., Ryu, S. H., and Suh, P. (1994) Overexpression of Phospholipase C-γ1 in Familial Adenomatous Polyposis. *Cancer Res*. **54**, 2240-2244.

14. Nomoto, K., Tomita, N., Miyake, M., Xhu, D., LoGerfo, P. R., and Weinstein, I. B. (1995) Expression of Phospholipases γ1, β1, δ1 in Primary Human Colon Carcinomas and Colon Carcinoma Cell Lines. *Mol. Carcinogen.* **12**, 146-152 (10.1002/mc.2940120306)

15. Kataoka, K., Nagata, Y., Kitanaka, A., Shiraishi, Y., Shimamura, T., Yasunaga, J., Totoki, Y., Chiba, K., Sato-Otsubo, A., Nagae, G., Ishii, R., Muto, S., Kotani, S., Watatani, Y., Takeda, J., Sanada, M., Tanaka, H., Suzuki, H., Sato, Y., Shiozawa, Y., Yoshizato, T., Yoshida, K., Makishima, H., Iwanaga, M., Ma, G., Nosaka, K., Hishizawa, M., Itonaga, H., Imaizumi, Y., Munakata, W., Ogasaware, H., Sato, Y., Sasai, K., Muramoto, K., Penova, M., Kawaguchi, T., Nakamura, H., Hama, N., Shide, K., Kubuki, Y., Hidaka, T., Kameda, T., Nakamaki, T., Ishiyama, K., Miyawaki, S., Yoon, S., Tobinai, K., Miyazaki, Y., Takaori-Kondo, A., Matsuda, F., Takeuchi, K., Nureki, O., Aburatani, H., Watanabe, T., Shibata, T., Matsuoka, M., Miyano, S., Shimoda, K., and Ogawa, S. (2015) Integrated molecular analysis of adult T cell leukemia/lymphoma. *Nat. Genet.* **47**(11):1304-1315. (10.1038/ng.3415)

16. Landau, D. A., Sun, C., Rosebrock, D., Herman, S. E. M., Fein, J., Sivina, M., Underbayev, C., Liu, D., Hoellenriegel, J., Ravichandran, S., Farooqui, M. Z. H., Xhang, W., Cibuluskis, C., Zviran, A., Neuberg, D. S., Livitz, D., Bozic, I., Leshchiner, I., Getz, G., Burger, J. A., Wiestner, A., and Wu, C. J. (2017) The evolutionary landscape of chronic lymphocytic leukemia treated with ibrutinib targeted therapy. *Nat. Commun.* **8**(1), 2185 (10.1038/s41467-017-02329-y)

17. Hajicek, N., Keith, N. C., Siraliev-Perez, E., Temple, B. R. S., Huang, W., Zhang, Q., Harden, T. K., and Sondek, J. (2019) Structural basis for the activation of PLC-γ isozymes by phosphorylation and cancer-associated mutations. eLife **8**, e51700 (10.7554/eLife.51700)

18. Hajicek, N., Charpentier, T. H., Rush, J. R., Harden, T. K., and Sondek, J. (2013) Autoinhibition and Phosphorylation-induced Activation of Phospholipase C-γ isozymes. *Biochemistry* **52**, 4810-4819

19. Burke, J. E., Perisic, O., Masson, G. R., Vadas, O., and Williams, R. L. (2012) Oncogenic mutations mimic and enhance dynamic events in the natural activation of phosphoinositide 3-kinase p110α (PIK3CA). *Proc. Natl. Acad. Sci.* 109(38): 15259-15264 (10.1073/pnas.1205508109)

20. Burke, J. E., and Williams, R. L. (2012) Dynamic steps in receptor tyrosine kinase mediated activation of class IA phosphoinositide 3-kinases (PI3K) captured by H/D exchange (HDX-MS). *Adv. Biol. Regul.* **53**, 97-110 (10.1016/j.jbior.2012.09.005)

21. Burke, J. E., Vadas, O., Berndt, A., Finegan, T., Perisic, O., and Williams, R. L. (2011) Dynamics of the Phosphoinositide 3-Kinase p110δ Interaction with p85α and Membranes Reveals Aspects of Regulation Distinct from p110α. *Structure* **19**(8), 1127-1137 (10.1016/j.str.2011.06.003)

22. Bae, J. H., Lew, E. D., Yuzawa, S., Tome, F., Lax, I., and Schlessinger, J. (2009) The Selectivity of Receptor Tyrosine Kinase Signaling Is Controlled by a Secondary SH2 Domain Binding Site. *Cell* **138**, 514-524 (10.1016/j.cell.2009.05.028)

23. Essen, L., Perisic, O., Cheung, R., Katan, M., and Williams, R. L. (1996). Crystal structure of a mammalian phosphoinositide-specific phospholipase Cδ. *Nature* **380**, 595-602

24. Huang, W., Wang, X., Endo-Streeter, S., Barrett, M., Waybright, J., Wohlfeld, C., Hajiek, N., Harden, T. K., Sondek, J., and Zhang, Q. (2017) A membrane-associated, fluorogenic reporter for mammalian phospholipase C isozymes. *J. Biol. Chem.* **293**(5), 1728-1735 (10.1074/jbc.RA117.000926)

25. Wang, X., Barrett, M., Sondek, J., Harden, T. K., and Zhang, W. (2012) Fluorescent Phosphatidylinositol 4,5-Bisphosphate Derivatives with Modified 6-Hydroxy Group as Novel Substrates for Phospholipase C. *Biochemistry* **51**, 5300-5306

26. Charpentier, T. H., Waldo, G. L., Barrett, M. O., Huang, W., Zhang, Q., Harden, T. K., and Sondek, J. (2014) Membrane-induced Allosteric Control of Phospholipase C-β Isozymes. *J. Biol. Chem.* **289**, 29545-29557 (10.1074/jbc.M114.586784)

27. Aslanidis, C., and de Jong, P. J. (1990) Ligation-independent cloning of PCR products (LIC-PCR). *Nucleic Acids Res.* **18**(20):6069–6074 (10.1093/nar/18.20.6069)

CHAPTER V: CONCLUSIONS AND FUTURE DIRECTIONS

Conclusions

This work describes biochemical, structural, and dynamical insights into the regulated activation of the PLC-γ isozymes. First, we developed a biochemical assay to quantify phospholipase activity using the membrane-embedded substrate, XY-69 (1). This assay can be modified to determine phospholipase activity of PLC variants with cancer-associated substitutions and in different contexts including the presence of kinases, effectors, peptides, and small molecules. Together with the soluble substrate, WH-15 (2), these biochemical assays are the foundation for drug discovery efforts to target aberrant PLC-γ isozyme signaling.

Second, the crystal structure of essentially full-length PLC-γ1 (3), together with biochemical data, illustrate a model for membrane-dependent activation. The structure describes how the catalytic core is prevented from accessing membranes via an array of regulatory domains that sterically occlude access to the active site. Notably, these domains are arranged to integrate autoinhibition, phosphorylation-dependent activation, and inputs from scaffolding proteins to regulate PLC-γ isozyme activation at signaling hubs. The model also explains how cancer-associated substitutions adorn the interface between the catalytic core and the regulatory domains to disrupt autoinhibition causing a spectrum of elevated activities.

Lastly, we have proven that structural studies and HDX-MS are complementary for the description of dynamical changes in PLC-γ isozymes in response to binding to other proteins and membranes. Using HDX-MS, we showed that the phosphorylated kinase

domain of FGFR1 likely disrupts autoinhibition as measured by an increase in deuterium incorporation at the interface between the catalytic core and the regulatory domains. Moreover, we showed that kinases and liposomes can act in concert to stabilize the ensemble of active PLC-γ1 at membranes. These structural studies are supported with biochemical data that suggest that phosphorylated kinases act as allosteric activators of PLC-γ1 activity.

Future directions

The structure of autoinhibited PLC-γ1 in conjunction with dynamical changes associated with kinase binding and membrane association provide mechanistic details about the regulated activation of the PLC-γ isozymes. These data, together with fluorogenic probes to asses PLC activity *in vitro*, provide new avenues for the study of PLC-γ isozymes. The following section provides an overview of the future directions of this work.

Drug discovery

The PLC-γ isozymes are important clinical targets as they are frequently and recurrently mutated in human diseases. To date, there are no selective and potent modulators of PLC-γ isozyme activity. With the development of fluorogenic probes to monitor PLC activity, and the establishment of protocols to quantify PLC-γ isozyme activity in different contexts, we are equipped to commence drug development efforts.

We previously described the soluble substrate WH-15 (2) for monitoring PLC activity in real-time. Experiments with PLC-β isozymes showed that WH-15-containing mixed micelles failed to recapitulate the activating effects of heterotrimeric G proteins (4). These results suggest that WH-15 will be useful for identifying orthosteric modulators, that is, modulators than bind to the active site. In contrast, the fluorogenic substrate XY-69 (1)

was designed for continuous and high-throughput monitoring. Conducting the same experiment with PLC-β isozymes showed that XY-69-containing phospholipid vesicles recapitulate the activating effects of heterotrimeric G proteins (4) suggesting that XY-69 is useful for the identification of both orthosteric and allosteric modulators.

Using these two fluorogenic substrates, we will conduct high-throughput screening with several chemical libraries to identify chemical leads for the development of drugs to treat aberrant PLC-γ isozyme signaling.

Structural studies

We have proven that HDX-MS, together with structural information, is a viable technique to study dynamical changes in the PLC-γ isozymes associated with kinase binding and membrane association to provide mechanistic details about the regulated activation of the PLC-γ isozymes. According to our studies, binding of phosphorylated FGFR1K to the nSH2 domain of PLC-γ1 is sufficient to disrupt autoinhibition as detected by an increase in deuterium incorporation throughout the interface between the catalytic core and the regulatory domains. Several questions arise from this work, including: How are conformational changes relayed from the nSH2 domain to the rest of the protein? What is the orientation of the kinase when bound to PLC-γ1? Does the kinase contact domains in PLC-γ1 other than the nSH2 domain? These questions could be addressed by using the complex of PLC-γ1 bound to phosphorylated FGFR1K that is described in this work for structural characterization by either X-ray crystallography or cryogenic electron microscopy.

In cells, numerous tyrosines of PLC-γ1 are phosphorylated. However, only the phosphorylation of Tyr783 is absolutely required for phosphorylation-dependent activation *in vitro* and in cells. How phosphorylation impacts the dynamics and overall structure of PLC-γ1 remains to be elucidated. Specifically, we are interested in describing the

arrangement of the regulatory domains relative to the catalytic core in the active, open state. We plan to address this question by conducting structural studies with PLC-γ1 phosphorylated on Tyr783. To achieve this goal, we must eliminate most sites of phosphorylation (186, 472, 481, 771, 775, 959, 977) within the truncated form of PLC-γ1 (residues 21-1215) to ensure stoichiometric phosphorylation of Tyr783. Subsequently, this variant of PLC-γ1 will be incubated with an active kinase and phosphorylation of Tyr783 confirmed via native-PAGE and intact protein mass spectrometry. A similar approach can be applied to study more nuanced and context-specific phosphorylation states. For example, the role of phosphorylated Tyr771 and Tyr775 in PLC-γ1 function, protein structure, and protein dynamics remains a standing question in the field. Studies with phosphorylated PLC-γ1 can be extended to assess dynamical changes in phosphorylated PLC-γ1 when it binds to kinase and in the presence of PIP_2-containing liposomes using HDX-MS.

Our biochemical data suggests that kinases act as allosteric activators. That is, binding of active kinases to PLC-γ1 is sufficient to elevate phospholipase activity. This allosteric effect may be amplified for a kinase that is properly embedded in a lipid bilayer. This idea can be tested more directly with a complex of PLC-γ1 bound to an active receptor tyrosine kinase, e.g. FGFR1, embedded in a lipid bilayer. The creation of such complex would be a demanding task that, if successful, would be useful for the assessment of PLC activities biochemically as well as structural characterization using cryogenic electron microscopy.

REFERENCES

1. Huang, W., Wang, X., Endo-Streeter, S., Barrett, M., Waybright, J., Wohlfeld, C., Hajicek, N., Harden, T.K., Sondek, J., and Zhang, Q. (2018). A membrane-associated, fluorogenic reporter for mammalian phospholipase C isozymes. *J. Biol. Chem.* **293**, 1728-1735.

2. Wang, X., Barrett, M., Sondek, J., Harden, T. K., and Zhang, Q. (2012) Fluorescent Phosphatidylinositol 4,5-Bisphosphate Derivatives with Modified 6-Hydroxy Group as Novel Substrates for Phospholipase C. *Biochemistry* **51**(26), 5300-5306 (10.1021/bi300637h)

3. Hajicek, N., Keith, N. C., Siraliev-Perez, E., Temple, B. R. S., Huang, W., Zhang, Q., Harden, T. K., and Sondek, J. (2019) Structural basis for the activation of PLC-γ isozymes by phosphorylation and cancer-associated mutations. eLife **8**, e51700 (10.7554/eLife.51700)

4. Charpentier, T. H., Waldo, G. L., Barrett, M. O., Huang, W., Zhang, Q., Harden, T. K., and Sondek, J. (2014) Membrane-induced Allosteric Control of Phospholipase C-β Isozymes. *J. Biol. Chem.* **289**, 29545-29557 (10.1074/jbc.M114.586784)